Photodegradation of Organic Photochromic Dyes Incorporated in Ormosil Matrices

A Thesis

Submitted to the Faculty

of the

Worcester Polytechnic Institute

in partial fulfillment of the requirements for the

Degree of Master of Science

in

Chemistry

by

Karsten J. Koppetsch

Date: May 3, 2000

Approved:

Professor W. Grant McGimpsey, Advisor

Professor James P. Dittami, Department Head

Abstract

Ormosils (Organically Modified Silicates) have been used in the past as hosts for various organic molecules. In this work, seven different photochromic dyes most of which belong to the spirooxazine / merocyanine family were doped into thin films that were prepared using several increasingly inorganic Ormosil formulations. These dyes were either physically incorporated into the pores of the film or covalently bound to the matrix via a siloxane substituent. The dyes, which undergo a reversible color change upon irradiation, are relatively stable, although they will ultimately degrade after prolonged exposure to ultraviolet irradiation.

This work focuses on identifying the variables that influence the rate of dye degradation, including rigidity of the Ormosil matrix, wavelength of irradiation, and the presence of oxygen. The silylated dyes, which are generally regarded as having reduced mobility within the pores of the Ormosil, degraded more slowly, suggesting a link between stability and rotational and translational freedom. Irradiation wavelength also affected dye stability in that limiting exposure to wavelengths in the near UV (and eliminating visible light) causes the least degradation. This is attributed to the photostability of the photomerocyanine isomer. Finally, the presence of oxygen was shown to cause dramatic enhancement in degradation. The mechanisms of each of these effects are discussed.

Acknowledgements

It is difficult to know where to begin to thank all of the people whose help would not have made this work possible. Their assistance spans two years worth of work as well as two continents.

I should, of course, start by thanking Professor McGimpsey who has acted as my advisor, both as an undergraduate for my MQP and now as graduate student. I owe him a great deal for his support and guidance over the last two years. I would also like to thank Professor Robert Thompson who is largely responsible for making the Ormosil project and the relationship we have with the Fraunhofer-Institut possible, for his interest in the progress of my work, and for suggestions that were scientifically encouraging. Many of the experiments conducted here at WPI would have been considerably more difficult without the talents of Jack Ferraro, who expertly built a number of devices which saved me a great deal of time and aggravation. I would also like to thank my colleagues in GH05A, past and present (Lie Chen, Redina Kote, David Ferguson, John Benco, Chris Cooper, and Dafei Kang), for their friendship and support. Last, but certainly not least, Matt Powell for helping to make a 12-week stay in Germany a pleasant one.

I must also thank my parents, Bruno and Edith Koppetsch, for their support during my six years at WPI. My thanks also go to my sister, Birgit, for helping me get my thesis printed out (*finally!*).

I would also like to thank the ORMOCER department of the Fraunhofer-Institut für Silicatforschung (Würzburg, Germany) under the direction of Dr. Karl-Heinz Haas for participating in this venture and providing accommodations and materials used in this

work. In particular, I would like to thank Drs. Gerhard Schottner and Uwe Posset, who proposed this course of research and were invaluable as a source of information. My thanks also go to Angela Amthor, Katja Skrajewsky, and Nicole Müller who were gracious enough to let me work in their lab area and to offer their assistance when I needed it. I also wish to mention the following, for their friendship and kindness during my stay: Karl-Joachim Deichman, Matthias Heinrich, Sigrid Beuschlein, Ralf Schwert, Haymo Katschorek, Ulrike Weber, Katja Lehmann, Anette Burger, Anette Rauch, and Dr. Johanna Kron. *Vielen Dank für Ihre Hilfe welche Sie mir entgegen brachten!* ☺

Table of Contents

List of Tables

List of Figures

1. Introduction

The use of solid inorganic matrices as hosts for organic compounds has gained a great deal of attention in recent years. Much of this work has been directed towards the incorporation of photochemically active compounds into the matrix. By isolating individual molecules within the pores of the matrix, inorganic hosts provide numerous advantages over solvent media since the range of motion is more limited, thereby reducing the chances of the deactivation of an excited state by collision or the formation of a dimer.[1,2] With each dopant molecule isolated in its own pore, the concentration will be limited only by the pore density of the matrix. Since the pores prevent aggregation of the dye molecules, the dye concentration can theoretically exceed the concentrations possible in solution.[1] Pores also limit rotational freedom, thus reducing nonradiative internal conversion of an excited state.[1,2] Should the dopant be contaminated or have any impurities, these molecules will be isolated from dopant molecules in individual pores. This can be beneficial if the impurity adversely affects the behavior of the dye (e.g. acting as an excited state quencher).[1] Any degradation products of the dopant will be also isolated in the same manner.[1] Inorganic matrices are often preferable over other matrices such as polymers and plastics, as they are generally more thermally and photochemically stable and can transmit light at shorter wavelengths in the ultraviolet than polymers.[1]

Inorganic matrices such as glasses may in theory be more advantageous, but the high temperatures associated with curing glasses have made the incorporation of organic compounds nearly impossible. Polymers have their own disadvantages, as they must

undergo ultraviolet curing or ionic reactions for synthesis that may also be detrimental to a prospective guest molecule.[3] For these reasons, Ormocers (Organically Modified Ceramics) and Ormosils (Organically Modified Silicates) have been explored as a possible alternative for inorganic matrices. They are prepared via the sol-gel process, which involves the hydrolysis and condensation of metal alkoxides to form a three-dimensional matrix.[4,5] Ormocers and Ormosils can be synthesized using relatively low temperatures (generally less than 200° C and sometimes as low as room temperature) and in the absence of ultraviolet irradiation. Additionally, they may possess a wide range of properties depending on the alkoxide and the reaction conditions. Physical properties range from glass-like to rubbery; optically, they may be transparent or opaque. They may also be cast in a mold or coated on a substrate. For these reasons, numerous applications have been proposed for doped sol-gel matrices. Plates doped with a fluorescent dye may be used as luminescent solar concentrators (LSCs), which generate fluorescence upon exposure to sunlight, trapping it by internal reflection where it is collected at the edges of the plate.[6] Doped sol-gel matrices have been used to develop solid-state tunable dye lasers[2,7] and have shown to have applications in non-linear optics[6]. Kaufman *et al.* were the first to investigate the incorporation of photochromic dyes into sol-gel matrices[8], which will be the focus of this work.

Photochromic dyes are compounds that undergo a reversible change in color upon the absorption of a photon. This new colored species reverts back to the original dye either photochemically (by the absorption of a longer wavelength photon) or thermally. Such dyes incorporated within a sol-gel matrix can have several practical applications, such as optical switches[9-11] (if the reversal is very fast) and optical storage for computer

memory[11-13] (if the reverse color change is not possible at room temperature). Sol-gel materials doped with photochromic dyes have also been investigated as fiber optic delay generators[14], fiber optic shutters[15], and in photomasking and photoresist materials[16]. Sol-gel based coatings may also be used for ophthalmic lenses such as scratch resistant coatings on sunglasses.

A number of papers describing a diverse array of sol-gel syntheses using organic dyes with differing photochromic behavior have been described. The silica glasses prepared by Kaufman *et al.* were doped with Aberchrome-670.[8] Others have produced photochromic glasses using methylviologen that retained its colored form for months after irradiation. The authors attribute the stability of the photochemically produced methylviologen cation radical to poor oxygen diffusion through the matrix.[17] Dithienylethene derivatives incorporated in Ormosil matrices produced films that retain color until irradiation with visible light.[18] Photochromic silica-alumina matrices using the photoinduced enol-keto tautomerization of anthrone to 9-anthrol have also been described.[19] Among the most widely used photochromic dyes in Ormosil matrices are spiropyrans[9,20-23] and spirooxazines[9,11,22-28]. Both types of dyes convert back to their original form thermally.

1.1. Ormosils

Ormosils and Ormocers begin with inorganic silica or metal oxide backbones that are bonded to organic functional groups. An Ormosil represents a specific type of Ormocer, in that the inorganic backbone is composed entirely of silica. Ormocers may be composed of silica, aluminum, titanium, zirconium, etc. or any combination of these. As

mentioned earlier, Ormosils are synthesized via a sol-gel process that permits the manufacture of materials at relatively low temperatures.

Sol-gel prepared materials can be synthesized using one of three routes: (1) the gelation of a solution of colloidal powders, (2) the hydrolysis and condensation of siloxane precursors followed by hypercritical drying of the gels, and (3) the hydrolysis and condensation of siloxanes followed by aging and drying under ambient atmosphere.[29] Ormosil samples created for this work were prepared via the third synthetic route using a variety of siloxane monomers.

The siloxane monomers used in the synthesis of an Ormosil can be described as network formers or network modifiers depending upon the number of reactive alkoxy groups in the molecule.[30] Each alkoxy group represents a site where two siloxanes may react to form a Si-O-Si bond. Network formers, such as tetraethyl orthosilicate (TEOS) or tetramethyl orthosilicate (TMOS) have four reactive sites (tetrafunctional) and can form bonds to four neighboring siloxanes. Network modifiers substitute alkoxy groups with other organic groups that cannot be hydrolyzed, usually an alkyl or aryl group. These groups are what give the Ormosil its organic character. Monofuntional siloxanes have only one reactive site and terminate the network. Difunctional siloxanes linearly bridge two other molecules. Trifunctional siloxanes act as "endcappers".[30]

In the first step of Ormosil synthesis, the siloxanes are hydrolyzed either in the presence or absence of an acid or base catalyst,[29] although Ormosil syntheses done in this work utilized a base catalyst. Siloxanes and water are generally immiscible and a mutual solvent, such as an alcohol, is used.[31] Hydrolysis follows an S_N2 type mechanism with the formation of a pentavalent species that has been described as either a transition state[32]

or as an intermediate[33,34]. In acid catalysis, one of the alkoxy groups is protonated making the Si atom more susceptible to nucleophilic attack by water to form the pentavalent species. (Figure 1.1a) In base catalysis, the hydroxyl ion attacks the silicon atom directly. (Figure 1.1b) In both cases, an alcohol is eliminated as a hydroxy group replaces an alkoxy group. In general, smaller alkoxy groups are more readily hydrolyzed than bulkier groups.

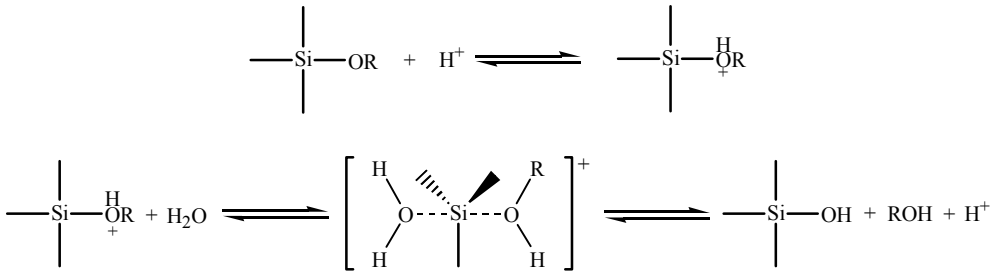

Figure 1.1a. Acid catalyzed hydrolysis

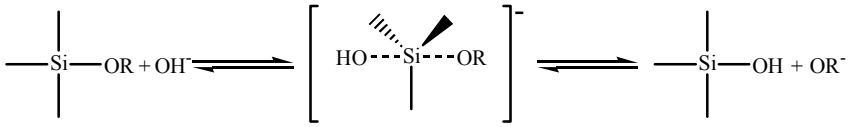

Figure 1.1b. Base catalyzed hydrolysis

Once hydrolyzed, siloxane monomers are free to bond via a condensation reaction, accompanied by either the elimination of an alcohol or water. Water condensation takes place between two silanols and forms a Si-O-Si linkage with the elimination of water.[29] (Figure 1.2a) Alcohol condensation occurs between a silanol and a siloxane and eliminates an alcohol to form the same linkage.[29] (Figure 1.2b) Under high temperatures, it is possible for two unhydrolyzed siloxanes to undergo condensation with the elimination of an ether[35], but the temperatures used for hydrolysis in this work should not favor this process. Repeated hydrolysis and condensation reactions generate

interconnected three-dimensional networks in the form of microscopic particulates suspended in the liquid, referred to as a "sol". The sol can then be cast into a

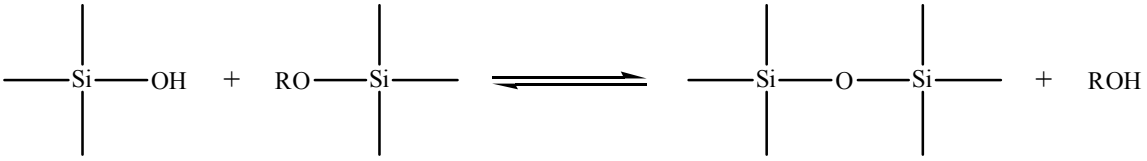

Figure 1.2a. Alcohol condensation

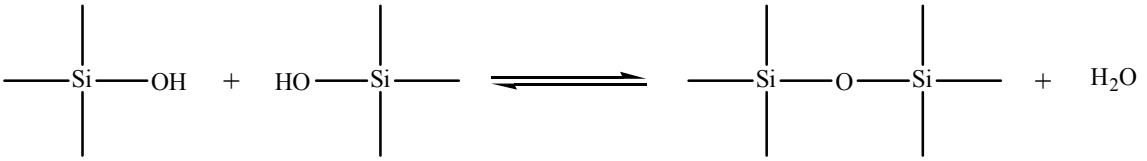

Figure 1.2b. Water condensation

mold or coated onto a substrate. Over time, the individual particles of the sol link to one another and form an interconnected rigid network called a "gel".[29] The monolith at this point has pores in the submicrometer range as well as polymeric chains longer than a micrometer. Aging the gel increases the strength of the matrix and reduces the likelihood of fracture during drying. To accomplish this, the gel is immersed in a liquid during the aging process to prevent the premature evaporation of solvents. The porosity decreases and the density increases as the gel is given time to continue condensation reactions.[29] The final step is drying, where all solvents and excess water are eliminated by evaporation. This process generates high stresses within the pores that can cause fracturing of the monolith. This may be resolved either by careful control of the reaction conditions to obtain monodisperse pore sizes[29] or by the addition of a surfactant[29,36].

The siloxanes used for this work were 3-glycidoxypropyltrimethoxysilane (GPTMS, Figure 1.3a) and dihydro-3-(3-(triethoxysilyl)propyl)-2,5-furandione (Wacker

GF 20, Figure 1.3b). To some Ormosil samples, TMOS was added in varying concentrations to increase the matrix rigidity. Also used were colloidal silica particles in the form of Ludox® TM-50 (50% w/w SiO_2 in water). TM-50 adds inorganic silica particles thus performing the same function as the TMOS. For the hydrolysis step, water was always used in a half-stoichiometric amount. That is, the number of moles of water used was always one-half the number of moles required for complete hydrolysis of the siloxanes. This is to ensure that no water is remaining upon completion of hydrolysis and condensation. For every two hydrolysis reactions consuming two moles of water, one mole of water is returned in the condensation reaction. Using a half-stoichiometric amount insures that there is zero net water formation and no water remaining after the gel process. This makes the removal of the more volatile solvents easier.

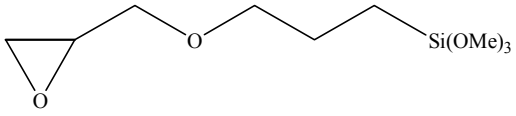

Figure 1.3a. GPTMS

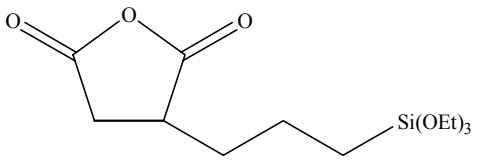

Figure 1.3b. GF 20

Hydrolysis of GPTMS and GF 20 was done under basic conditions using 1-methylimidazole (MI) as a catalyst. MI served a secondary function by inducing a reaction between the organic groups of the two siloxanes. MI can act as a Lewis base and open the epoxy ring of the GPTMS. The oxide ion on the opened ring can then continue to react by opening another epoxy ring or an anhydride. (Figure 1.4) This process continues indefinitely contributing additional organic cross-linking to the existing silica framework.

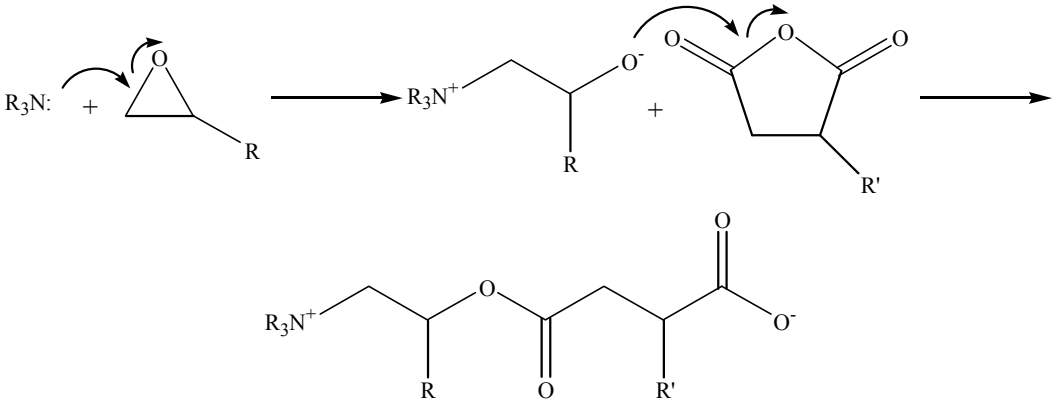

Figure 1.4. Cross-linking of the siloxane organic groups

1.2. Spirooxazines

As mentioned earlier, a photochromic dye is a compound that undergoes a reversible color change upon the absorption of a photon, resulting from the isomerization of the dye. The newly formed species absorbs light at wavelengths different from the parent molecule, which produces the change in color. Spiro compounds (Figure 1.5) such as spiropyrans (X = CH) and spirooxazines (X = N) represent a class of such compounds and both have been extensively studied, although the research into spirooxazines is more recent. The use of spirooxazines in sol-gel matrices for commercial applications is preferred as they generally have a higher resistance to degradation after long-term exposure to ultraviolet light.[37]

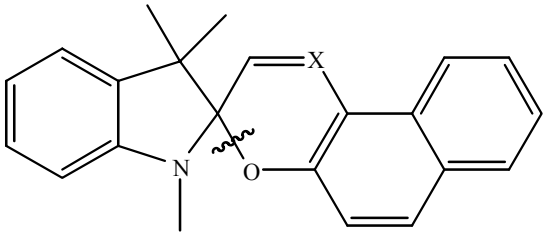

Figure 1.5. Spiro compound

The mechanisms behind the photochromism of spirooxazines and spiropyrans are fairly similar, due to their closely related structures. (Figure 1.6) Both compounds absorb almost exclusively in the ultraviolet. Upon the absorption of a photon in this range, the

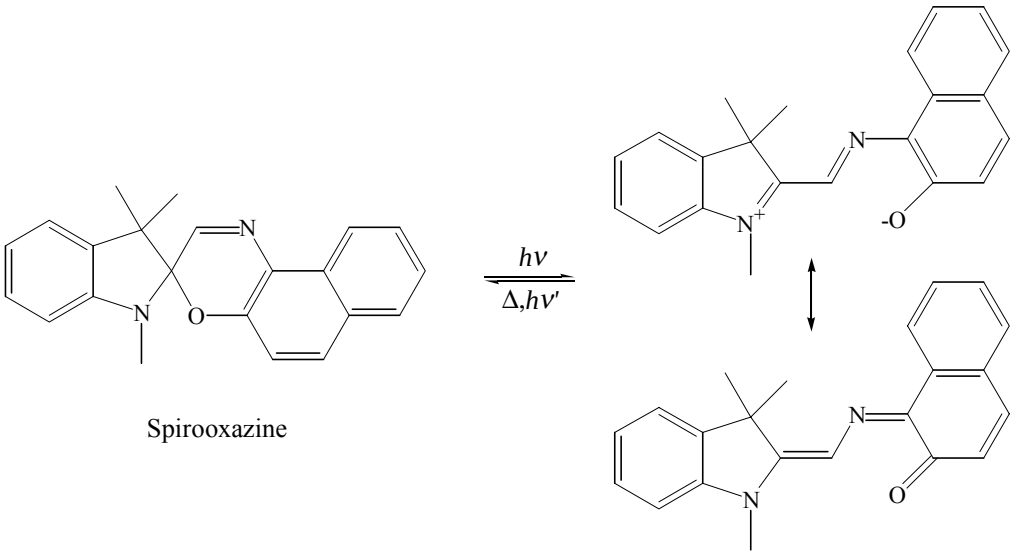

Spirooxazine

Photomerocyanine

Figure 1.6. Photoconversion of a spirooxazine

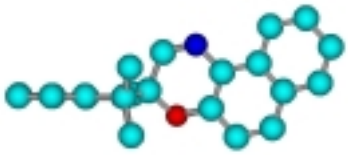

Figure 1.7a. Geometry of spirooxazine

Figure 1.7b. Geometry of photomerocyanine

C-O bond may undergo heterolytic cleavage.[38,39] The rate of bond cleavage is very fast and has been reported to be approximately 700 fs^{-1}.[40] Once cleaved, the spirooxazine is believed to pass through a non-planar, short-lived intermediate "X"[39-41], the lifetime of which has been reported as 470 fs[40]. This intermediate isomerizes to form one of several planar isomers.[42] In the spiro form, the two halves of the molecule are orthogonal to one another with no interaction of the π systems.[43] (Figure 1.7a and 1.7b) In the planar form of the photomerocyanine, the π system is more extensively conjugated and absorbs at longer wavelengths (around 600 nm for most spirooxazines). The reconversion of the photomerocyanine to spirooxazine requires the rotation of the merocyanine to bring the C and O back into proximity with one another. This process has a low probability and proceeds slowly, which accounts for the relatively long lifetime of the photomerocyanine.[38] The photomerocyanine of spirooxazine may last for under 1 second in solution at room temperature, and may last several seconds to minutes in a solid matrix. Conversion of the photomerocyanine to the spirooxazine may be facilitated either thermally[37] or photochemically by the absorption of a long wavelength photon[44,45].

Photomerocyanine formation of the spirooxazine in Figure 1.5 occurs exclusively within the first excited singlet state[46], although photochromic behavior may be induced through a triplet state via triplet-triplet energy transfer from a sensitizer[47-49]. The triplet energy has been measured to be 200±5 $kJ \cdot mol^{-1}$.[50] The quantum yield of conversion to the photomerocyanine under ultraviolet irradiation is relatively low, approximately 0.2 with little dependence on the solvent.[46] Spirooxazines do not demonstrate any observable fluorescence[51], suggesting that the remaining energy is wasted from either the internal conversion of the excited state, or from the closure of the C-O bond immediately after

opening.[46] The photomerocyanine can take quinoidal or zwitterionic resonance forms. However, the absorption spectrum exhibits a bathochromatic shift, suggesting a generally non-polar ground state[46] and therefore it is likely it is the quinoidal form that dominates.

Spirooxazines demonstrate good resistance to photochemical degradation after prolonged ultraviolet irradiation[52]; however, they will ultimately irreversibly fade over time. Analysis of the primary degradation products of spirooxazines appears to indicate that oxidation is a major factor in the degradation.[53] The precise role of oxygen, however, is a matter of speculation. Malatesta *et al.*, for example, have explored the possibility of the role of singlet oxygen as a possible cause.[54] However, their experiments found no evidence for the formation of singlet oxygen upon the irradiation of spirooxazines or by the irradiation of the photomerocyanine.[54] Their findings were corroborated by Eloy and Jardon, who determined the quantum yield of singlet oxygen formation to be less than 0.005.[55] Furthermore, experiments conducted by Malatesta *et al.* and Firth *et al.* using known singlet oxygen sensitizers show that spirooxazines will efficiently quench singlet oxygen without suffering any adverse affects.[54,56] Since an excited oxygen species most likely is responsible for the observed degradation, they have suggested a mechanism involving a superoxide anion radical. Their proposed mechanism involves an electron transfer between molecular oxygen and the excited triplet state of the photomerocyanine. The superoxide anion radical can then attack the photomerocyanine, leading to the observed degradation.[54] (Figure 1.8) This electron transfer mechanism is supported by the observation that electron acceptors such as Fe^{3+} and Cu^{2+} can promote degradation even in the absence of oxygen.[54,57]

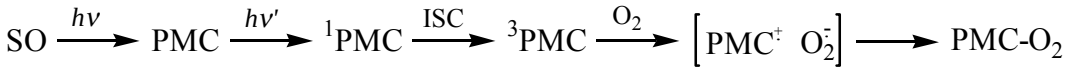

SO = spirooxazine

PMC = photomerocyanine

Figure 1.8. Proposed degradation reaction scheme[54]

Despite the evidence against singlet oxygen involvement, other authors continue to invoke this species in their mechanisms for degradation. Salemi *et al.*, for example, believe that degradation occurs through two separate channels: a reaction of the photomerocyanine with singlet oxygen and a reaction of a photomerocyanine biradical with molecular oxygen.[58] Their work is based on the use of 1,4-diazabicyclo[2.2.2]octane (DABCO), a known quencher of singlet oxygen. Solutions of spirooxazine containing DABCO showed a significant reduction in the rate of degradation as well as a significant change in the degradation product distribution. Hindered amine light stabilizers (HALS), such as di(2,2,6,6-tetramethyl-4-piperidyl) sebacate (Tinuvin® 770DF), which also act as singlet oxygen quenchers also demonstrated the same behavior.[59] This would seem to suggest that singlet oxygen plays at least some role in spirooxazine degradation. The authors make no mention of the work done by Malatesta and others, and so have not yet addressed the findings regarding singlet oxygen formation.[52]

1.3. Incorporation of Photochromic Dyes

Sol-gel derived matrices generally possess a suitable environment for the incorporation of photochromic dyes such as spirooxazines; however, there are a number of factors that must still be considered. For example, the use of an acid catalyst for Ormosil synthesis may be detrimental to the photochromism of a spirooxazine dye. It has

been reported that an acid may protonate the N on the indoline half of the spirooxazine.[60] This greatly affects the spectral characteristics of the dye due to the formation of a new species that absorbs strongly in the blue region and exhibits different photochromic behavior than that of the spirooxazine. This has been described as "acidichromism" by the authors. Experiments conducted in this laboratory suggest that the presence of acid may also degrade the dye. Another concern is the effect of the matrix on the photomerocyanine. The photomerocyanine is more polar than the spirooxazine form and may be stabilized by a polar matrix. Thus, the matrix may be permanently blue until it is irradiated. This "reversed photochromism" has been observed for some spiropyrans in silica gel.[61] As mentioned earlier, electron acceptors such as Cu^{2+} and Fe^{3+} may promote degradation in the presence or absence of oxygen. These are often used as catalysts in polymeric films and may inadvertently be detrimental to the dye.

The structure of the seven photochromic dyes used (5 spirooxazines and 2 chromenes) is shown in Figure 1.9. Physically incorporated dyes (unsilylated) were added to the Ormosil "lacquer" (the formulation in the sol phase) before curing. The Ormosil formulation must be basic as spirooxazines can be protonated in acidic media and undergo degradation. Silylated dyes covalently bind to the Ormosil matrix itself. These dyes posses a siloxane group and undergo hydrolysis and condensation reactions in the same way as the other siloxanes.

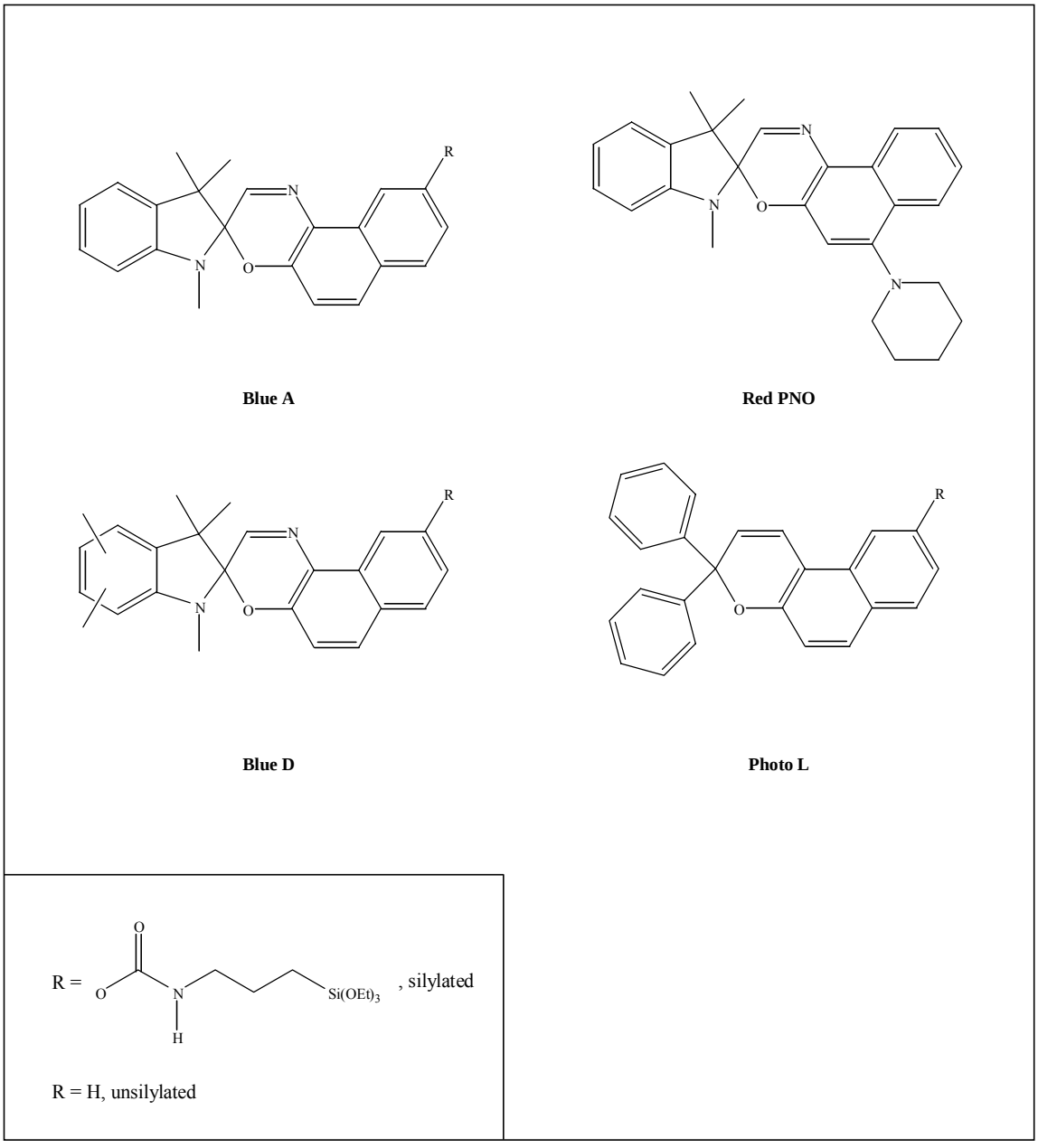

Figure 1.9. Photochromic dyes used

2. Experimental

2.1. Materials

All siloxanes, reagents, and solvents were obtained from Fluka unless otherwise indicated and were used as received. The siloxanes used in this work were 3-Glycidoxypropyltrimethoxysilane (GPTMS), tetramethyl orthosilicate (TMOS), and tetraethyl orthosilicate (TEOS). 1-Methylimidazole (MI), tetrahydrofuran (THF), and *n*-propanol were of reagent grade. Dihydro-3-(3-(triethoxysilyl)propyl)-2,5-furandione (GF 20) was obtained from Wacker Chemie. Ludox™ TM-50 (50% w/w colloidal silica) was obtained from DuPont. The silylated and unsilylated forms of the dyes Blue A, Blue D, and Photo L were obtained from Great Lakes Chemical Italia. Red PNO was also obtained from Great Lakes. The dye Photosol® 7-49 was provided by PPG. A mar and slip additive, BYK-301, was also used as received from BYK Chemie.

2.2. Ormosil Syntheses

Five Ormosil systems were investigated. Four of these are described by the mole percentage of TMOS versus GPTMS (25% TMOS is 1:3 TMOS:GPTMS). The fifth system used the TM-50 silica particles and is described simply as the Silica Particle system.

2.2.1. 0% TMOS

In a round bottom flask, GPTMS (8.86 g, 37.5 mmol) was stirred and cooled to between 15° C and 18°C. To this, MI was added at a 1:20 ratio (0.15 g, 1.38 mmol) as well as a 1.5:1 ratio of H_2O (1.01 g, 56.25 mmol). The temperature and the stirring of the reaction mixture were maintained for 3 hrs. For approximately 2 hrs the mixture

appeared slightly cloudy. The mixture was then cooled to below 10° C and a total of 3.75 g of solvent (50% THF and 50% *n*-propanol) was added. GF 20 was added drop wise at a 1:2 ratio with respect to the GPTMS (5.71 g, 18.75 mmol). The mixture was then allowed to react for an additional hour. The finished lacquer could then be refrigerated for storage.

2.2.2. 10% TMOS

GPTMS (21.27 g, 90 mmol) was stirred and cooled as described above. TMOS (2.08 g, 10 mmol) was added later in the synthesis. MI was added at 1:20 with respect to the total siloxanes (0.41 g, 5 mmol). Water (2.79 g, 155 mmol) was added at 1.5:1 with respect to the GPTMS and 2:1 with respect to the TMOS. The reaction mixture was stirred for 1.5 hrs and appeared cloudy for approximately 1 hr. At this point, the TMOS was added drop wise and stirring continued for an additional 1.5 hrs. As described earlier, the mixture was cooled to below 10° C and 10 g of solvent was added. GF 20 was added drop wise at 1:2 with respect to the GPTMS (13.70 g, 45 mmol) and the reaction was allowed to continue for 1 hr.

2.2.3. 25% and 40% TMOS

The syntheses for the 25% and 40% TMOS system followed the scheme described above for the 10% TMOS system. In each case, the water used was half the stoichiometric amount required to completely hydrolyze the TMOS and GPTMS, MI was always 1:20 with respect to the total siloxanes, and GF 20 was 1:2 with respect to the GPTMS alone. In the case of the 40% TMOS system, it was observed that in the 40% TMOS system, the absence of sufficient solvent resulted in premature gelation of the sol.

For this reason, solvents were added 45 minutes after the addition of the TMOS, instead of immediately after the addition of GF 20.

2.2.4. Silica Particle System

The synthesis involving the use of TM50 silica particles differs from the other syntheses in that the reaction mixture is not cooled to avoid precipitation of the particles. The water in the suspension provided the necessary water for the reaction and therefore no water was added. In a round bottom flask, a quantity of GPTMS (17.73 g, 75 mmol) was added and was stirred. TMOS (3.81 g, 25 mmol) was added later in the procedure. MI was added at a 1:20 ratio with respect to the total siloxanes (0.41 g, 5 mmol). TM50 (13.91 g) was added at a ratio of 1.1875:1 to the total siloxanes (given that 50% of the weight of the suspension was SiO_2). This was stirred for approximately 20 minutes, during which time the silica particles briefly came out of the suspension and the mixture appeared cloudy. Once the mixture regained clarity, TMOS was slowly added. This was stirred for an additional 45 minutes. At this point, 10 g of the solvents were added as well as GF 20 at a 1:2 ratio with respect to the GPTMS (11.42 g, 37.5 mmol). The final lacquer could not be refrigerated and gelled completely at room temperature within a few days after synthesis.

2.2.5. Dye Incorporation

All unsilylated dyes were added based on a percentage of the solids content of the Ormosil lacquer. The solids content of the lacquer was determined as the net mass of the sample when subjected to 200° C for 2 hrs. Blue A and Blue D were both added at 8% in each matrix. Photo L was added at 4%, Red PNO was added at 1%, and Photosol® 7-49 was added at 1.5%. Dyes were added after the synthesis of a stock lacquer. First, the

appropriate amount of dye was dissolved in 3 g THF. The solution was added to 10 g of lacquer and stirred. A 1 μm filter was used to eliminate any particulates. Silylated dyes (Blue A, Blue D, and Photo L) were added as equal molar quantities as their unsilylated counterparts. These dyes are chemically incorporated into the Ormosil matrix, and therefore the synthesis must be modified slightly to enable hydrolysis and condensation. The dye was first dissolved in the amount of THF that was to be used later in the synthesis. This solution was added to the GPTMS, MI, and water mixture at the start of the synthesis. Additionally, 1.5 equivalents of water were added to account for the hydrolysis of the dye.

2.3. Ormosil Coatings

Ormosil lacquers were applied to glass substrates. Uniform coatings were made by spin coating. The glass slide was spun for 30 s at 600 rpm and then for 10 s at 1200 rpm. The Silica Particle lacquer system did not disperse evenly on the substrate. For this reason, a mar and slip additive, BYK-301, was added at 0.3% by weight to the lacquer. Once coated, the samples were cured at 120° C for 1 hr and kept in the dark to prevent photochemical degradation.

2.4. Irradiation

For the degradation studies, the Ormosil samples were irradiated using a Rayonet photochemical reactor lamp with a maximum wavelength of 350 nm. The glass samples were placed with the coating side facing the lamp approximately 2.5 cm away. A number of filters were used to explore the effects of different wavelengths on the dyes. In all cases, wavelengths below 300 nm were filtered either using a cut-off filter or a glass

slide. In some cases, a broad-band filter eliminating wavelengths below 300 nm and above 500 nm (where the photomerocyanine absorbs) was used.

2.5 UV-Visible Spectroscopy / Degradation Measurements

Absorption spectra were measured using a Shimadzu UV-2100U spectrometer. Spectra of the dyes in isotropic solution were recorded using HPLC grade methanol. The Ormosil coated slides were cut into smaller pieces less than 1 cm^2. Once cut, the samples were placed into a holder such that the sample was held fast with a minimum amount of free movement. This holder also fit tightly into the cuvette holder making the position of the sample with respect to the light source reasonably reproducible. The absorption spectra of the Ormosil coated slides were taken against a background of air. No information could be gathered for wavelengths below 300 nm, as the glass slides are opaque in that region.

Measurements to gather data on dye degradation began with the irradiation of an Ormosil coated slide through a 300 nm cut-off filter for approximately 30 s. This irradiation was to produce the colored merocyanine form of the dye. The sample in the holder was placed in the spectrometer with a 5 s delay and the absorption was monitored at the λ_{max} of the dye. The absorption was continuously monitored for the duration that the colored form is present. The change in absorption over this time represents the amount of dye present. (Figure 2.1) The measurement is made five times for the purposes of reproducibility. Once this first value is determined, the sample is exposed to 8 to 12 hr intervals of continuous irradiation. After each period of irradiation, another set of measurements is made as described above. This continues until there is little to no observable merocyanine present within the sample.

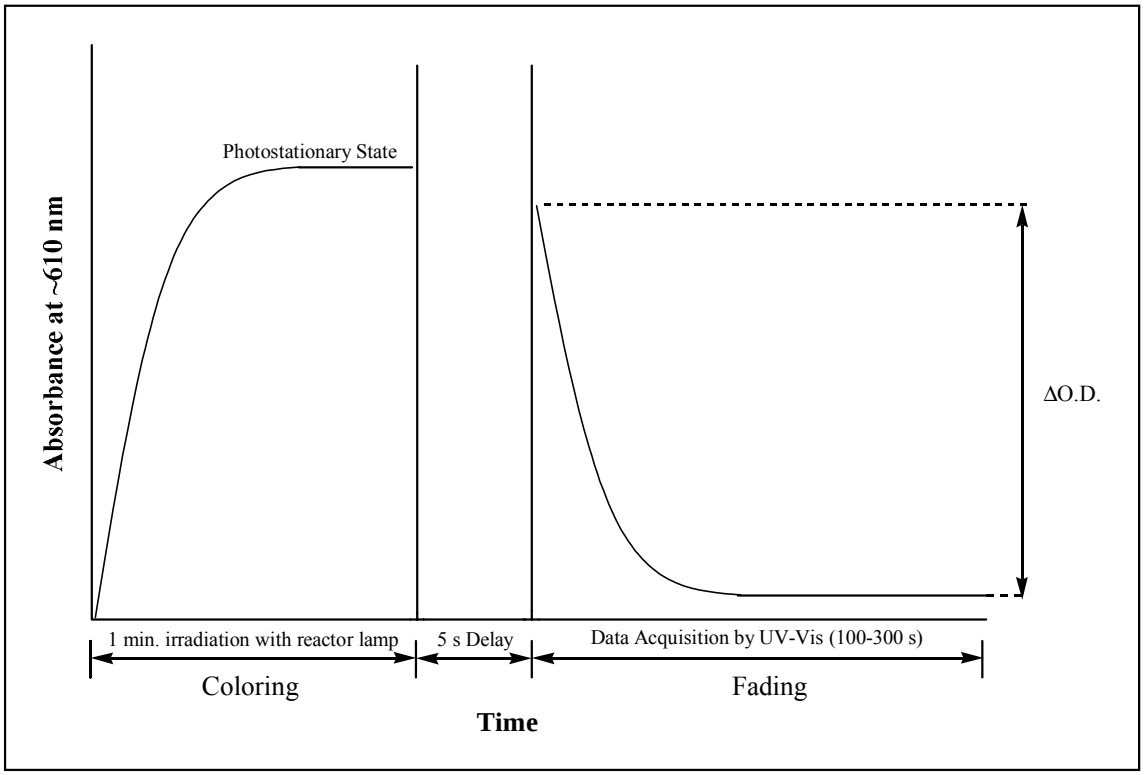

Figure 2.1. Timeline for single measurement in a degradation experiment

Kinetic measurements of the bleaching (the restoration of the spirooxazine from the photomerocyanine) of the dye Blue A were done using the same instrument. Samples were again held in place using the slide holder. To produce the photomerocyanine, samples were irradiated inside the cuvette holder of the UV-vis for 1 minute using a hand-held TLC lamp set at long-wavelength UV. The slits of the instrument were covered for the duration to prevent any damage to the instrument caused by the relatively intense light source. Removing the lamp and the coverings meant that there was a delay of approximately 4 seconds between terminating irradiation and the collection of data. (Figure 2.2) Kinetic plots were taken at 5 C° intervals from 5 to 30° C to obtain rate constants for an Arrhenius plot. Temperature was regulated using a refrigeration unit

attached to the cuvette holders. The temperature of the slide was monitored using a thermocouple.

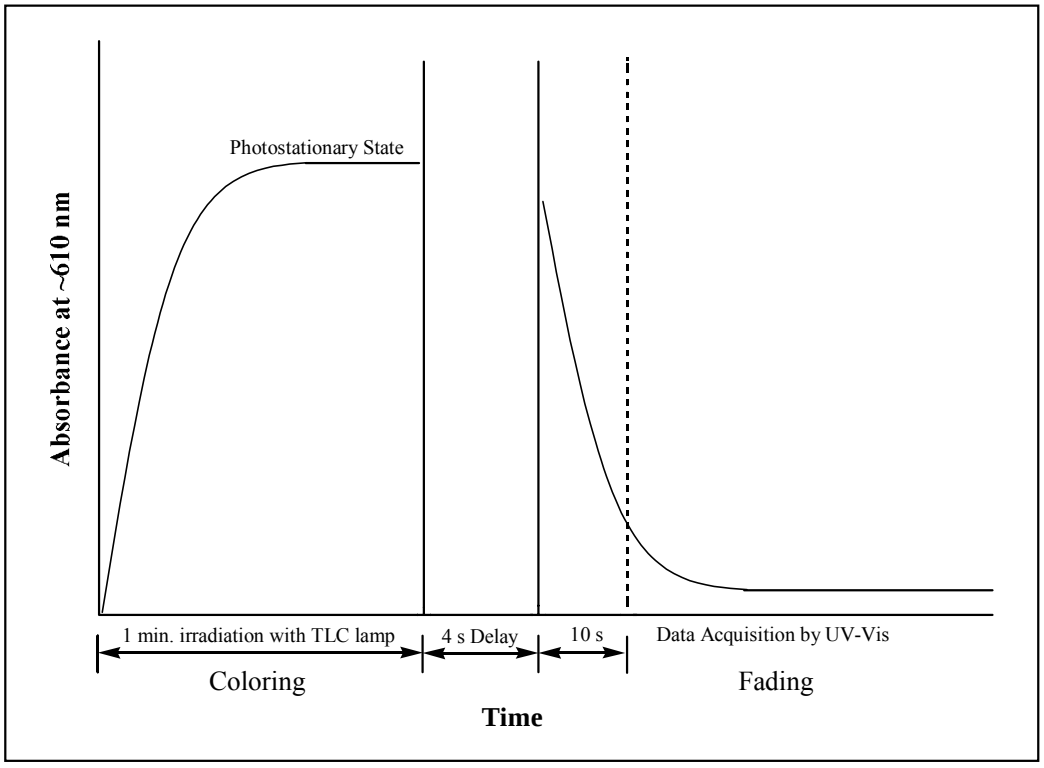

Figure 2.2. Timeline for measurement of kinetics at a single temperature

2.6. Laser Flash Photolysis

Laser flash photolysis experiments conducted in this work used two laser excitation sources. The first was a Lumonics EM510 XeCl excimer laser (308 nm, 20-40 mJ/pulse, 8 ns pulse duration). The second was a Candela SLL 250 flashlamp-pumped dye laser. Rhodamine 590 was used as the dye producing 590 nm wavelength pulses. A 150 W ORIEL xenon lamp producing a continuum from 200 to 900 nm was used as a monitoring source. The detection system was composed of an Acton Research Corp.

microprocessor-controlled 27.5 cm focal length monochrometer. Attached to the exit slit was a Burle 4840 photomultiplier.

The data collected from the photomultiplier was converted into digital form with a Tektronix 7912HB transient digitizer. This was comprised of a Tektronix 7A29P vertical amplifier plug-in module for voltage, a Tektronix 7B90P horizontal plug-in module for time, and the 7912 mainframe. The I_0 values were recorded with an automatic baseline compensator. The monitoring lamp, digitizer, lasers, and baseline compensator were triggered by a DG535 Stanford Research System Digital Delay Pulse Generator. A Sciemetric Labmate Intelligent Lab Interface was used as an interface between the computer and the other devices. Data was stored on an 80486 PC using FORTRAN and QuickBasic programs written by Prof. W.G. McGimpsey.

In a typical experiment, the computer signals the interface to open the laser and lamp shutters. The lamp power supply is triggered and the lamp is flashed. The light passes through the sample, the wavelengths are separated by the monochrometer, and the single wavelength reaches the photomultiplier. This signal goes to the baseline compensator and the value recorded at t=0 is I_0. The digitizer is activated and begins recording light intensity as a function of time. The laser fires and the data are transferred to the computer. In experiments using the dye laser in conjunction with the excimer laser, the dye laser fired 1-2 μs after the first.

Ormosil samples were placed in the cell holder facing the monitoring lamp to maximize the intensity of the signal. This mandated the use of mirrors to orient both lasers parallel to the light from the lamp.

2.7. Raman Spectroscopy

Raman spectra were taken using a Bruker RFS100 Raman spectrometer. Raman spectra were taken of finished lacquers as well as after the addition of a reagent (e.g. TMOS) and at several time intervals afterwards.

2.8. Hardness Measurements

A Fischerscope H100V-HCU using a Berkovich indentor was used to measure the hardness of finished Ormosil coatings. The instrument functions by forcing the indentor down onto the surface of the sample. On its way down (loading), the depth of the indentor (P) is recorded at various points and the opposing force (F) is measured. The indentor is then withdrawn (unloading) and again the opposing force is recorded at several depths. The microhardness is calculated by this F/P curve. The elasticity can also be calculated from this curve by comparing the opposing force during loading and unloading. A rubbery sample (with elasticity approaching 100%) would have nearly identical loading and unloading curves, as the opposing force would be the same at each depth no matter which direction the indentor moves.

3. Results and Discussion

3.1. Ormosil Syntheses

Ormosil films synthesized in this work measured approximately 15 μm in thickness. Despite the apparent thinness of the films, all doped formulations absorbed sufficiently at the λ_{max} value of the particular photochromic dye in order to exhibit a noticeable color change upon irradiation as the spirooxazine form converts to the photomerocyanine form (ΔO.D. of 0.1-0.2 at room temperature). In total, 20 formulation/dye combinations were investigated. Blue A, Photosol® 7-49, and Red PNO were incorporated in each of the five matrix types. The silylated form of Photo L was also successfully incorporated into the 0% TMOS, 10% TMOS, and Silica Particle systems and the silylated form of Blue D was incorporated in the 0% TMOS and Silica Particle systems. Syntheses involving the remaining matrices failed due to precipitation of the dyes out of the lacquer.

3.2. Film Properties

Table 3.1 shows the hardness and elasticity data of the 0% TMOS matrices at several different curing temperatures. Increasing the curing temperature shows a dramatic increase in the hardness of the matrix from 3.69 at 90° C for 15 minutes to 91.06 $N \cdot mm^{-2}$ at 120° C for 1 hour. This is consistent with reports that curing the gel at higher temperatures increases the density of the matrix.[29] The increased density of the matrix also affects its elasticity. The data for the 0% TMOS matrix shows a high degree of elasticity, decreasing as the curing temperature increases. The elasticity does not

appear to decrease below ~90% elasticity, suggesting that this may be the limit achievable for this particular matrix under any curing conditions.

Curing conditions	Hardness ($N \cdot mm^{-2}$)	Elasticity (%)
90° C, 15 min.	3.69	96.81
100° C, 15 min.	7.74	95.24
110° C, 15 min.	16.97	89.38
120° C, 1 hr.	91.06	89.75

Table 3.1. Hardness data for 0% TMOS formulation

Since one possible application for such matrices is scratch resistant coatings, matrices with a high hardness value are desirable and therefore a high curing temperature and time (120° C for 1 hr) was chosen for all syntheses. Table 3.2 shows the hardness and elasticity data for all five formulations used in this work and illustrates the variety of properties that can be achieved by varying the matrix formulation. Increasing the inorganic component of the matrix (the amount of TMOS or silica particles) increases the matrix rigidity as well as decreases the elasticity.

Matrix	Hardness ($N \cdot mm^{-2}$)	Elasticity (%)
0% TMOS	91.06	96.81
10% TMOS	106.7	86.99
25% TMOS	109.5	86.26
40% TMOS	145.0	80.83
Silica Particle	193.2	76.34

Table 3.2. Hardness data for matrices cured at 120° C for 1 hr.

3.3. Photochromic Behavior

In this work, the influences of several variables that affect photodegradation of the dyes were explored. These included the effects of curing conditions, oxygen, and the wavelength range of the irradiation source. Of particular interest were the effects of the matrix upon the rate of degradation.

3.3.1. Curing Conditions

It was observed in the 0% TMOS samples, that higher curing temperatures resulted in an observable reduction of the color produced upon irradiation, implying that the dye degrades thermally. To test this, samples containing Blue A were subjected to 120° C for extended periods of time and the change in the amount of photomerocyanine produced upon irradiation was recorded. (Figure 3.1) The results show a significant decrease in color produced with time. By fitting the decay to first-order kinetics, the dye under these high temperature conditions has a half-life of approximately 59 hrs. Thus, the increased hardness offered by higher curing temperatures, which will be beneficial for some applications, must be balanced by the desire to maximize the colorability of the films. It should be noted that using first-order kinetic analysis does not imply that the degradation follows strictly first-order behavior (*vide infra*). Rather, we are applying first-order kinetics in an attempt to obtain half-lives for comparative purposes.

Figure 3.1. Blue A in 0% TMOS Matrix; Exposed to 120° C Only (no UV Exposure)

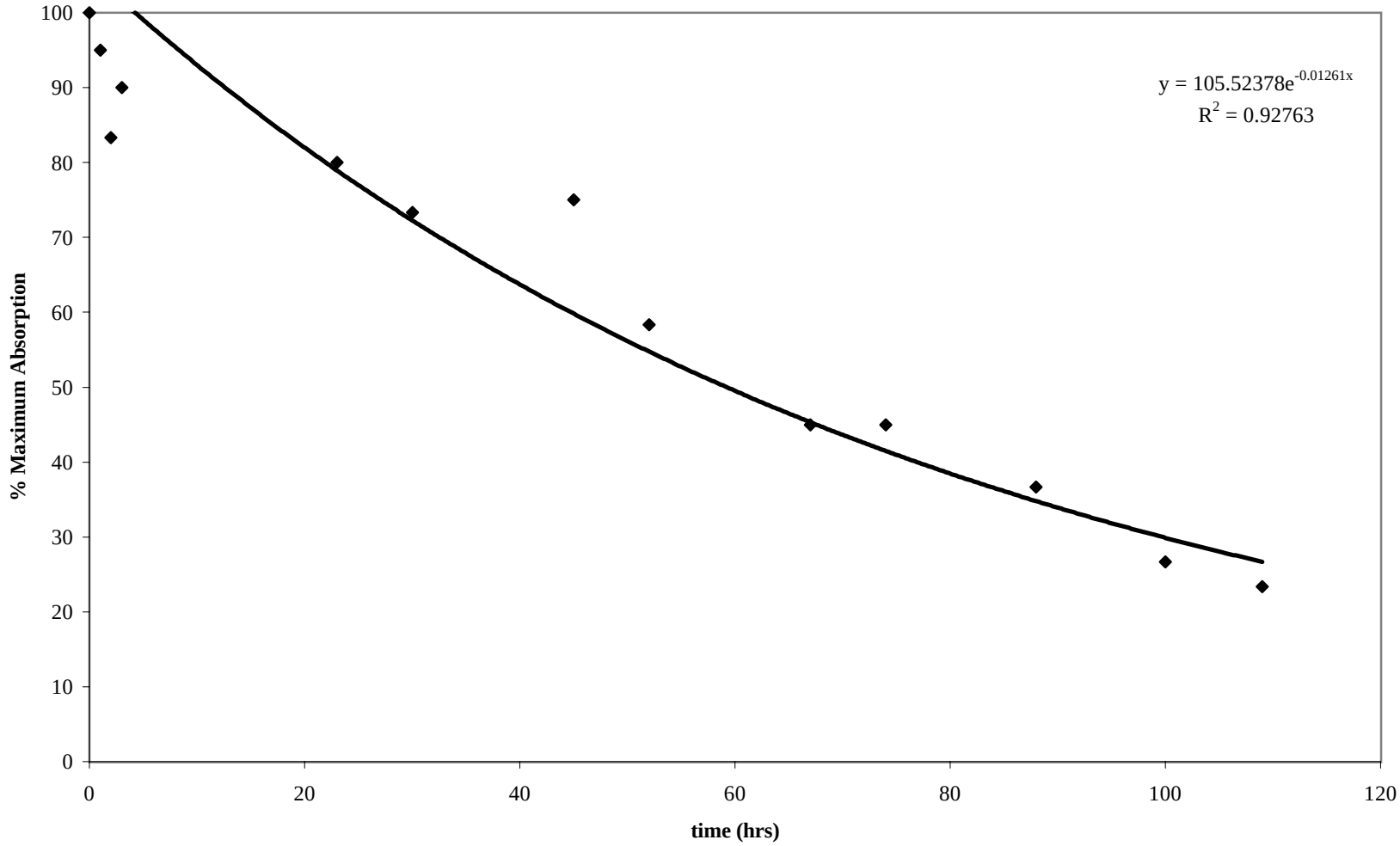

3.3.2. Oxygen Effects

As mentioned previously, it has been shown that photochemical dye degradation occurs primarily through a photochemical reaction in the presence of oxygen.[53] Experiments performed with nitrogen-purged samples of Blue A in a 25% TMOS matrix demonstrated no observable reduction in photomerocyanine formation even after over 120 hours of UV irradiation. Such samples exposed to oxygen would typically be completely degraded over such an interval. (Figure 3.2) Thus, it may be possible to limit degradation with Ormosil matrices that allow for poor diffusion of air. However, it may also be the case that the inherent porosity of Ormosil matrices will always present a poor barrier against diffusion. Nitrogen successfully permeated the 25% TMOS matrix, resulting in the reduction in the degradation of Blue A. It was also observed that photochemical degradation proceeded normally once degassing ceased.

Figure 3.2. Photodegradation of Blue A in 25% TMOS Matrix - Degassed versus Oxygen Present

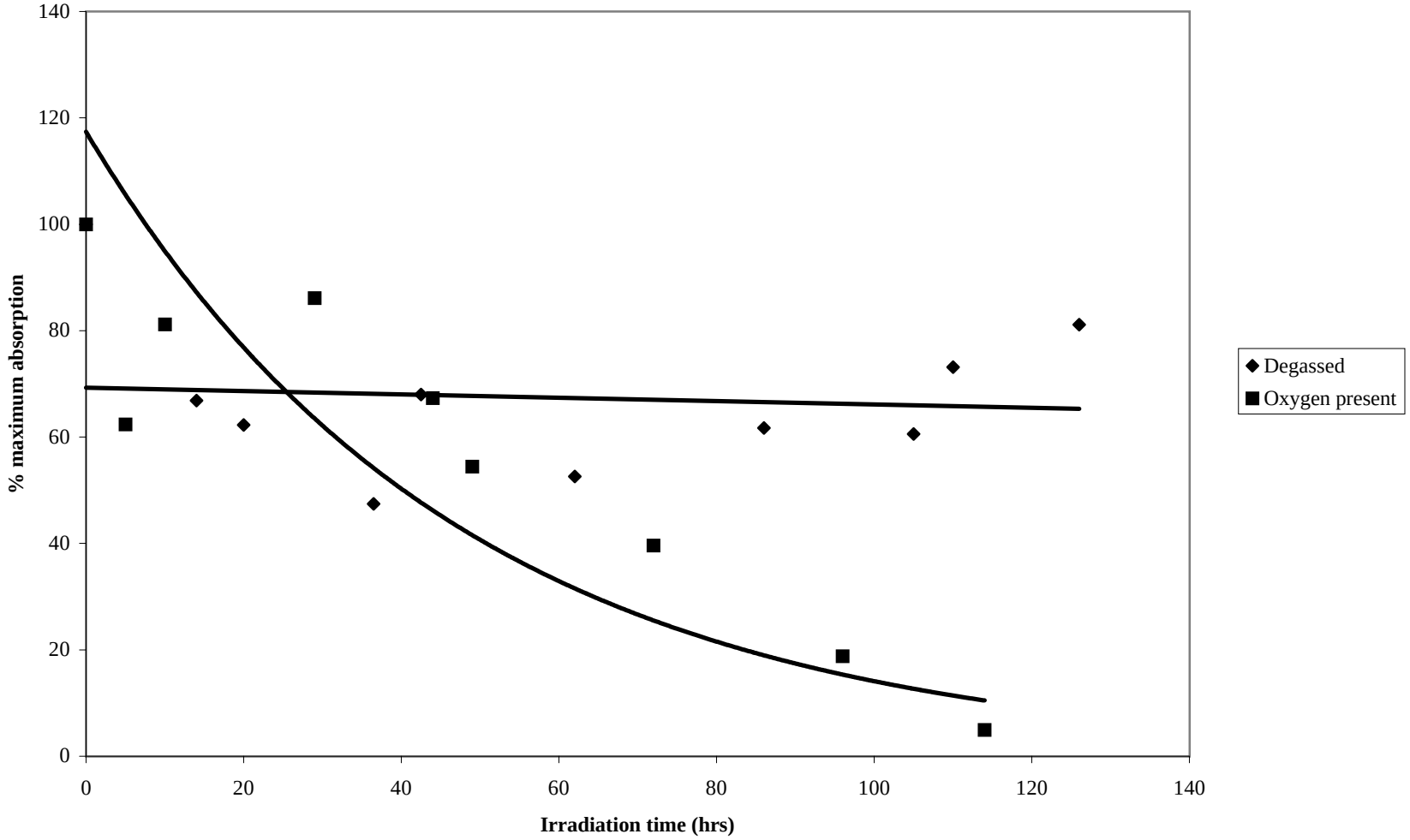

3.3.3. Filter Effects

The effect of different irradiation wavelengths on the degradation of the dyes was probed by the use of several different filters. To limit the amount of energy allowed into the samples and also to more accurately reflect UV conditions found in sunlight (which may reflect the ambient conditions under which the films will be used), a cut-off filter or glass slide was used to eliminate wavelengths below 300 nm. Figure 3.3 shows the degradation of Blue A in a 40% TMOS matrix irradiated through a cut-off filter. The dye is completely degraded after 80 hrs. This is compared to the same matrix irradiated through a broad-band filter. This filter eliminates wavelengths below 300 nm as well as light in the visible region above 550 nm, where the photomerocyanine form of Blue A absorbs. The 40% TMOS samples in Figure 3.3 show the same ΔO.D. at the start of the experiment, yet the sample irradiated through the broad-band filter shows that the color is preserved through an additional 20 hrs of irradiation. Other authors have observed similar behavior when irradiating a sample with monochromatic light versus a continuous spectrum provided by a lamp.[62] The increased degradation of the sample irradiated through the cut-off filter may be a result of a photomerocyanine excited state. The broad-band filter prevents the absorption of light by the photomerocyanine, so this excited state is not generated. Although this result does offer some clues as to the behavior of the dye, exploiting this to reduce degradation is not practical, as it would require a filter having the same color as the dye.

Figure 3.3. Blue A in 25% TMOS Matrix - Degradation Plot Using Two Filters

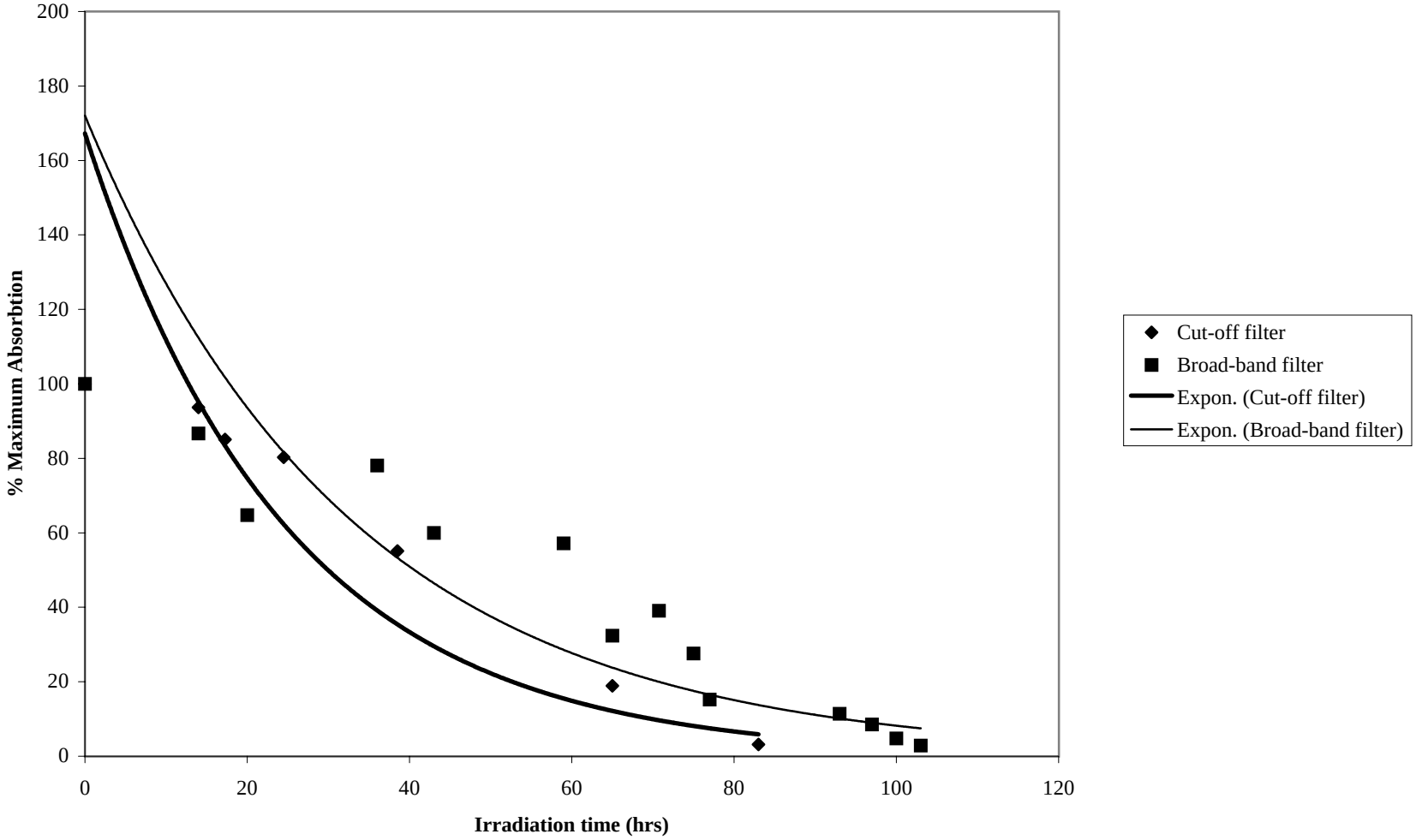

3.4. Photodegradation

The primary focus of this work was to explore the effects of the different Ormosil formulations on the rate of photochemical dye degradation. Degradation plots showing the amount of residual dye as a function of irradiation time were made for each dye/Ormosil combination available. (see Appendix 1) In order to obtain a value for comparison, first-order kinetics were assumed for the samples and the half-lives were calculated. In other work on the degradation of spirooxazines in Ormosils, the authors visually approximated the half-life.[28] Despite the apparent good fit of the plots, the use of first-order kinetics here does not imply that the degradation strictly follows first order kinetics. Rather, it is used only for comparative purposes. Malkin *et al.* have described the kinetics of photodegradation for the structurally related spiropyran class of dyes in solution and have found that the rate of degradation is dependent upon the intensity of the irradiating light, the extinction coefficients of the spiropyran and of the degradation products, and the quantum yield of photodegradation, among other factors.[63,64] The authors note that determining the quantum yield is difficult, as the process by which degradation takes place is not clearly understood (i.e. singlet oxygen, superoxide anion radical, etc.) The effects of the matrix further complicates the kinetics, as one may expect oxygen to diffuse through the matrix at different rates. Also, degradation products absorb in the UV region of the spectrum. Thus, as time progresses, the products will act as a more and more effective filter.

3.4.1. Matrix Effects

Table 3.3 shows the half-lives of the dyes in each of the five matrices. Of interest are the slower degradation rates seen in the more rigid matrices (the 40% TMOS and

Silica Particle). These two matrices have the highest inorganic character and have been shown to have the highest hardness. The high hardness is a result of the increased density of the matrix, which may make the matrix less porous. Poor porosity may reduce the rate of oxygen diffusion through the 40% TMOS and Silica Particle matrices, extending the lifetime of the dye incorporated in the matrix.

	0% TMOS	10% TMOS	25% TMOS	40% TMOS	Silica
Blue A	35.7	63.8	48	44.3	108.7
Red PNO	8.6	16.9	7.1	14.7	17.7
Photosol® 7-49	49.7	68.3	17.5	85.7	68.9
Sil. Blue D	121.0	NA	NA	NA	144.8
Sil. Photo L	88.3	48.7	NA	NA	215.3

Table 3.3. Half-life data for all Ormosil matrices and dyes

Another possible factor that may explain the reduced rate of degradation in the more rigid matrices may be that the dye molecules are more tightly confined within the pores of the matrix, limiting rotational and translational freedom. A mobile molecule, as in solution, will be more likely to encounter an oxygen molecule and undergo degradation. Less freedom, as defined by the restrictive pores of the matrix, may make the dye molecule less likely to react with oxygen.

If matrix rigidity is the primary factor influencing the rate of degradation, the dyes in the 10% TMOS matrix should not show greater resistance to degradation compared to those with higher inorganic character. Yet, the half-lives of Blue A, Red PNO, and Photosol® 7-49 in 10% TMOS are all comparable to the half-lives observed in the 40% TMOS and Silica Particle matrices. This suggests that the restrictive nature of the 10% TMOS matrix is higher than what one would expect based on inorganic character alone.

A possible explanation for the restrictive nature of the matrix may be added organic cross-linking within the matrix. In the case of the 10% TMOS matrix, there may be greater opportunities for the functional groups of the GF 20 and GPTMS to link. Matrices having higher inorganic character may actually "crowd out" the functional groups of GPTMS and GF 20 and prevent cross-linking from occurring. (Figure 3.4) The 0% TMOS matrix may have the opposite effect. When two siloxane monomers form the Si-O-Si bond, it may be difficult from a steric point of view for the two organic functional groups to bond. (Figure 3.5) The 10% matrix may represent a situation where the degree of organic cross-linking is optimal for this process.

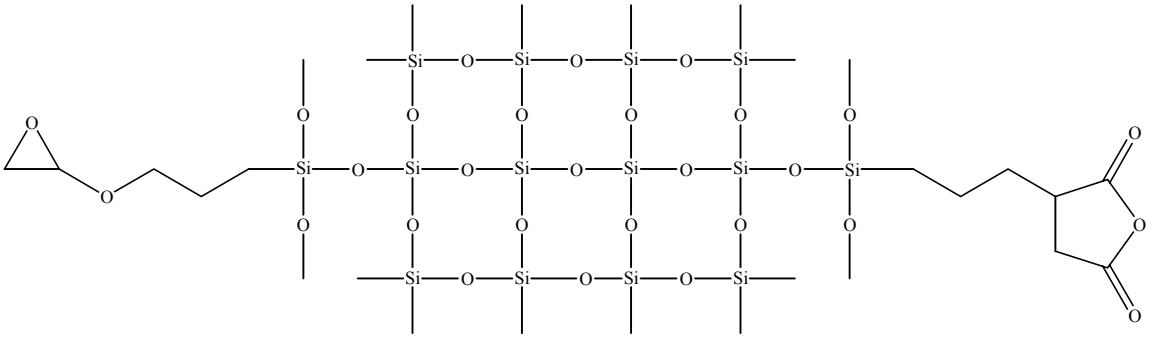

Figure 3.4. A representation of matrix with high inorganic character (e.g. 40% TMOS). The two organic functional groups may have difficulties cross-linking due to interference from large SiO_2 networks.

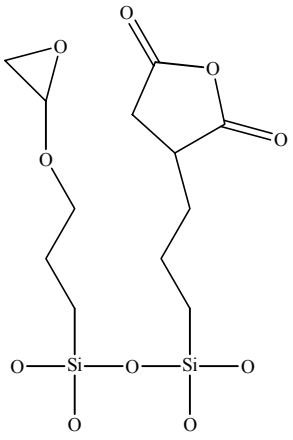

Figure 3.5. The low inorganic character in the 0% TMOS matrix may make cross-linking unfavorable. The wide range of motion the alkyl chains allow may make bonding between the two groups improbable.

3.4.2. Silylated versus Unsilylated Dyes

Table 3.3 also shows a dramatic difference between the half-lives of the silylated dyes compared to the unsilylated dyes. The former show a significant increase in the half-life over their unsilylated counterparts (see Blue A and Silylated Blue D, Figure 3.6). The siloxane substituent of the silylated dyes does not significantly affect the photochemical properties of the dyes, so it is unlikely that the difference in degradation is due to a chemical difference between Blue A and Silylated Blue D. The silylated dyes also would not significantly affect the porosity of the matrix, making a change in the rate of oxygen diffusion unlikely. Here, the reason for the reduced rate of photochemical degradation may again be due to the reduced degrees of freedom that the dye molecule is allowed. Silylated dyes, unlike their counterparts, are covalently bound to the matrix, so their motion is considerably more limited. This effect can be observed in the decay kinetics of the silylated dyes versus the unsilylated dyes. The conversion of the dye from the photomerocyanine back to the spirooxazine is considerably slower than in unsilylated dyes. This, too, is an indication of the more limited degrees of freedom in the matrix.[65] The kinetic behavior of the silylated dye also deviates considerably from first-order (Figure 3.7) due to the heterogeneous nature of the matrix. In the pores of the matrix, individual dye molecules will experience different environments. (Figure 3.8) Dye molecules with more freedom will convert more quickly than those that are more tightly bound.[11]

Figure 3.6. Degradation of Blue A versus Silylated Blue D in 0% TMOS Matrix

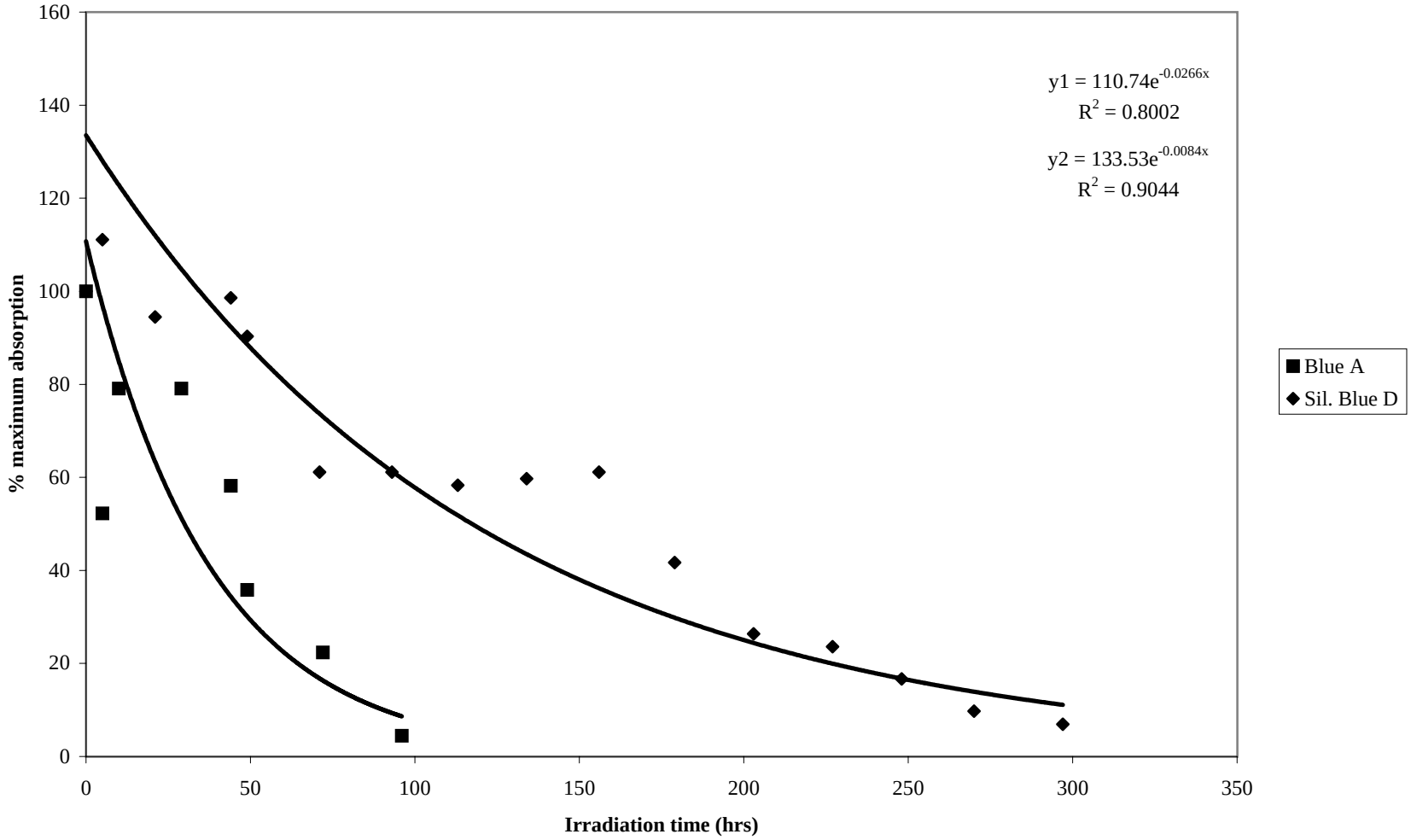

Figure 3.7. First Order Kinetic Plot for Silylated Blue D in 0% TMOS Matrix

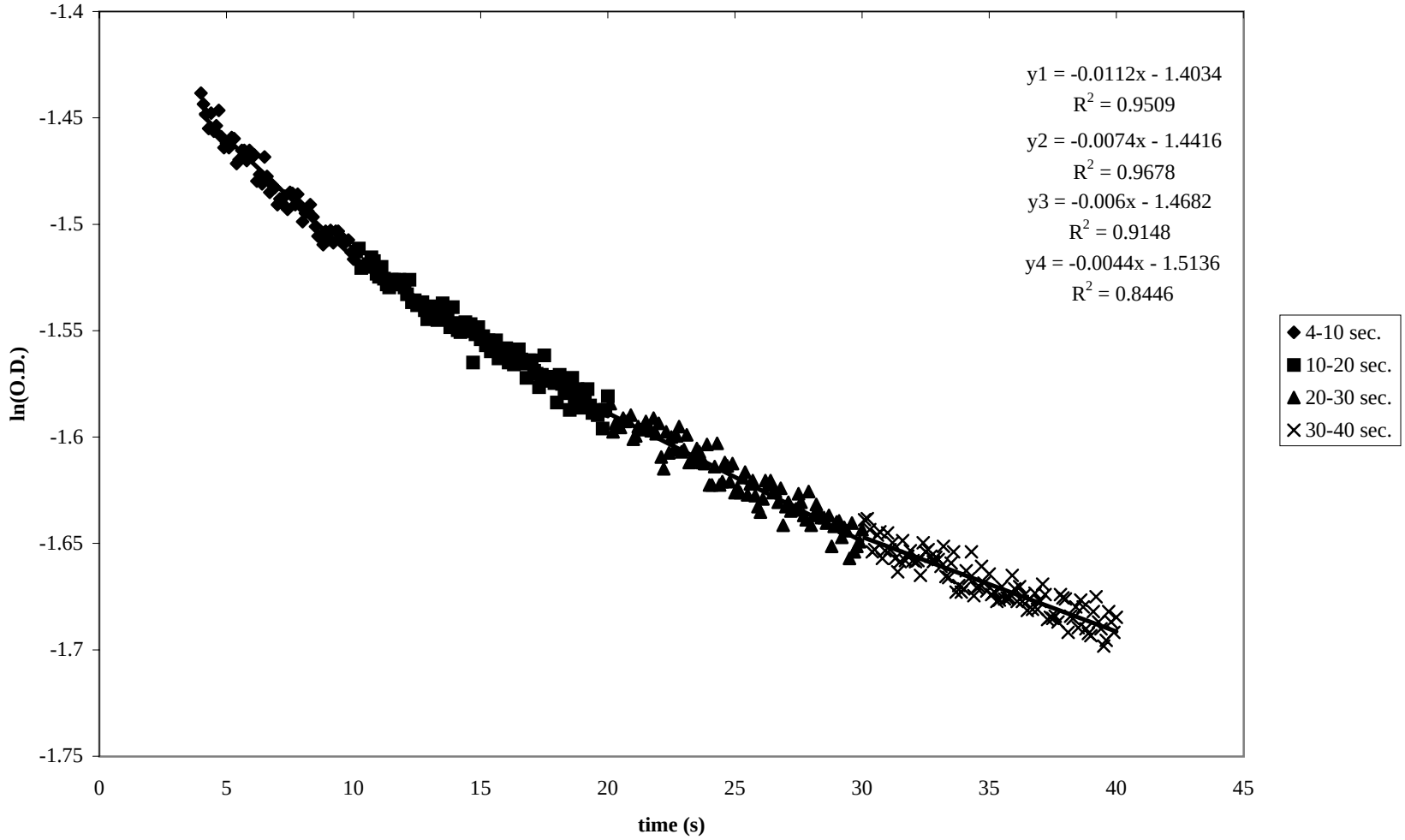

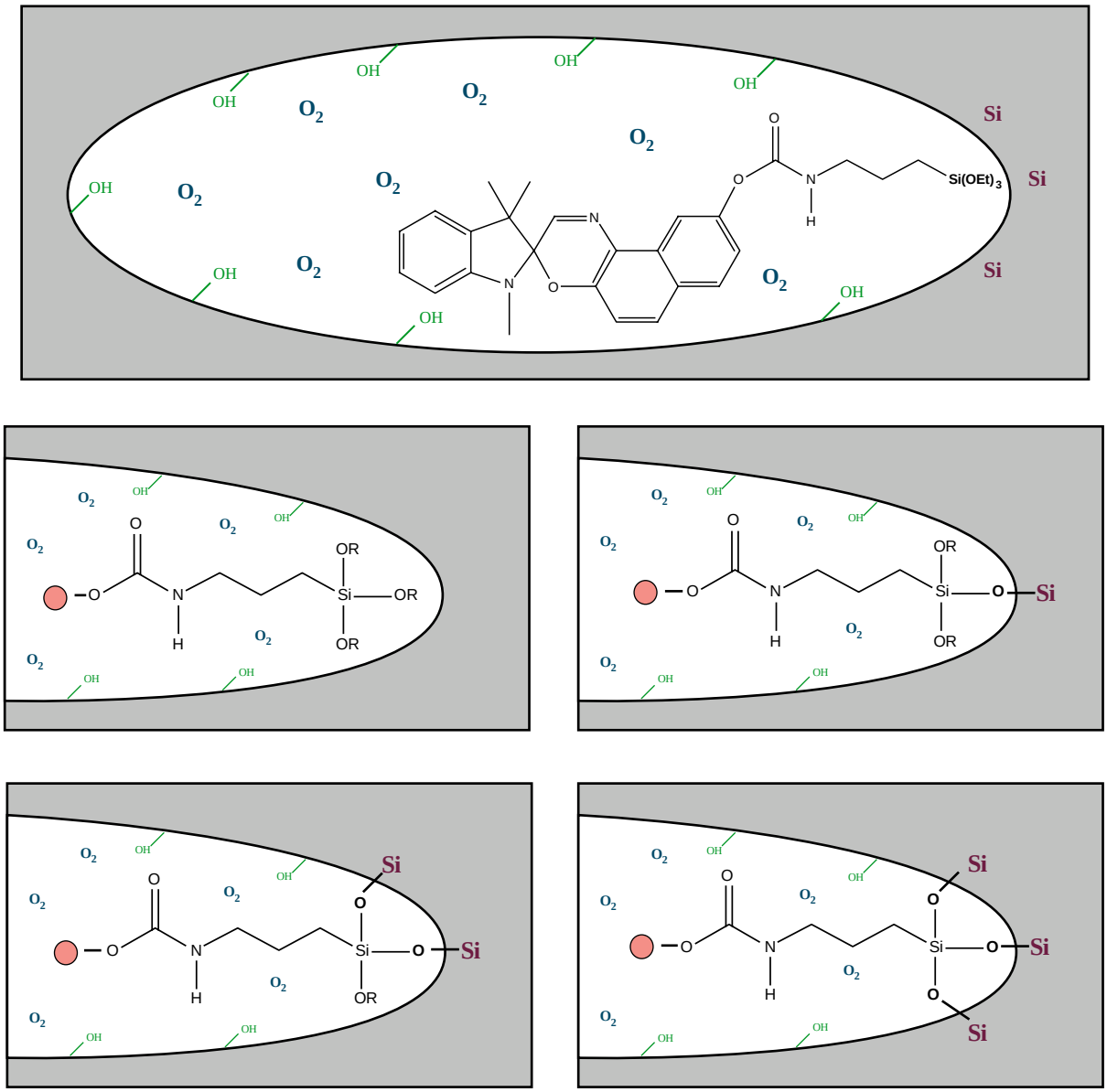

Figure 3.8. Schematic representation of the different connectivity of Silylated Blue A to the Ormosil matrix
Matrix Pore Spirooxazine R = H, CH_3

3.5. Arrhenius Data

We suggest that relaxation of a photomerocyanine molecule to the spirooxazine form in a rigid matrix will be more difficult and thus have a higher activation energy than in solution or a less rigid matrix. Arrhenius plots for Blue A in each of the five matrices were generated in order to attempt to correlate the degradation observations with matrix rigidity. (Figures 3.9-3.13, Appendix 2) Plots were also made for Blue A in methanol (Figure 3.14) as well as a 70% GPTMS / 30% ETES (ethyltriethoxysilane) matrix (Figure 3.15) as described by Hou and Schmidt.[11] The authors reported that the kinetics of the dye in this matrix closely follows first-order behavior and is similar to the dye in solution. In each of the five matrices, there was a considerable deviation from Arrhenius behavior at temperatures higher than 20° C. This deviation has not been observed for spirooxazines in solution[37] or in the ETES matrix[11]. The parabolic shape of the Arrhenius plot implies a negative activation energy at these temperatures, which then reaches a threshold and more closely follows Arrhenius behavior. The reason for this behavior is not entirely clear. The data for the dye in the Ormosil matrices at low temperatures show that the dye does not, in fact, follow first-order behavior. (Figure 3.16) By sampling at different time intervals, it is apparent that the rate constant increases with time much like the silylated dyes. Again, this is most likely an effect of the pores of the matrix as dyes that have the most freedom convert first and, at later time periods, more constrained dye molecules convert. This effect may also serve to explain why there is non-Arrhenius behavior observed.

Furthermore, at high temperatures, less photomerocyanine is produced upon irradiation. With the 4-second delay between irradiation and data acquisition, the data

collected may reflect only the slower, more constrained dyes. The calculated rate constants would then tend to be smaller than the actual rate constants. This could result in the apparent negative energy of activation observed at high temperatures. At lower temperatures, more photomerocyanine is observed and the effect is less noticeable. It should be noted that both in solution and in the ETES matrix, the Arrhenius plots generated in this work are linear, in agreement with literature, and the first order plots of conversion show no deviation at long times.[11,37] However, data could not be obtained above 20° C for the ETES matrix and methanol. At these temperatures, little photomerocyanine was observed due to its rapid decay in these media.

Medium	k (s^{-1})
Methanol	0.240
0% TMOS	0.065
10% TMOS	0.056
25% TMOS	0.060
40% TMOS	0.054
Silica Particle	0.055

Table 3.4. Kinetic data for the conversion of the Photomerocyanine of Blue A to Spirooxazine at 20° C

The non-Arrhenius behavior observed in the matrices makes determining the activation energy impossible. Another possible suitable comparison is between the rate constants at one particular temperature (20° C). Table 3.4 shows the rate constant for Blue A in methanol and each matrix using only the first 6 seconds of data for the calculation (from 4 to 10 seconds after irradiation). The data show that the rate of conversion of the dye is much faster in solution at this temperature than in the Ormosil matrices. More important is the difference between the Ormosil matrices themselves.

The dye in the 10% TMOS, 40% TMOS, and Silica Particle systems show slower kinetics than in the other matrices. It is these same matrices that demonstrate the slowest rate of degradation.

Figure 3.9. Arrhenius Plot for Blue A in 0% TMOS Matrix

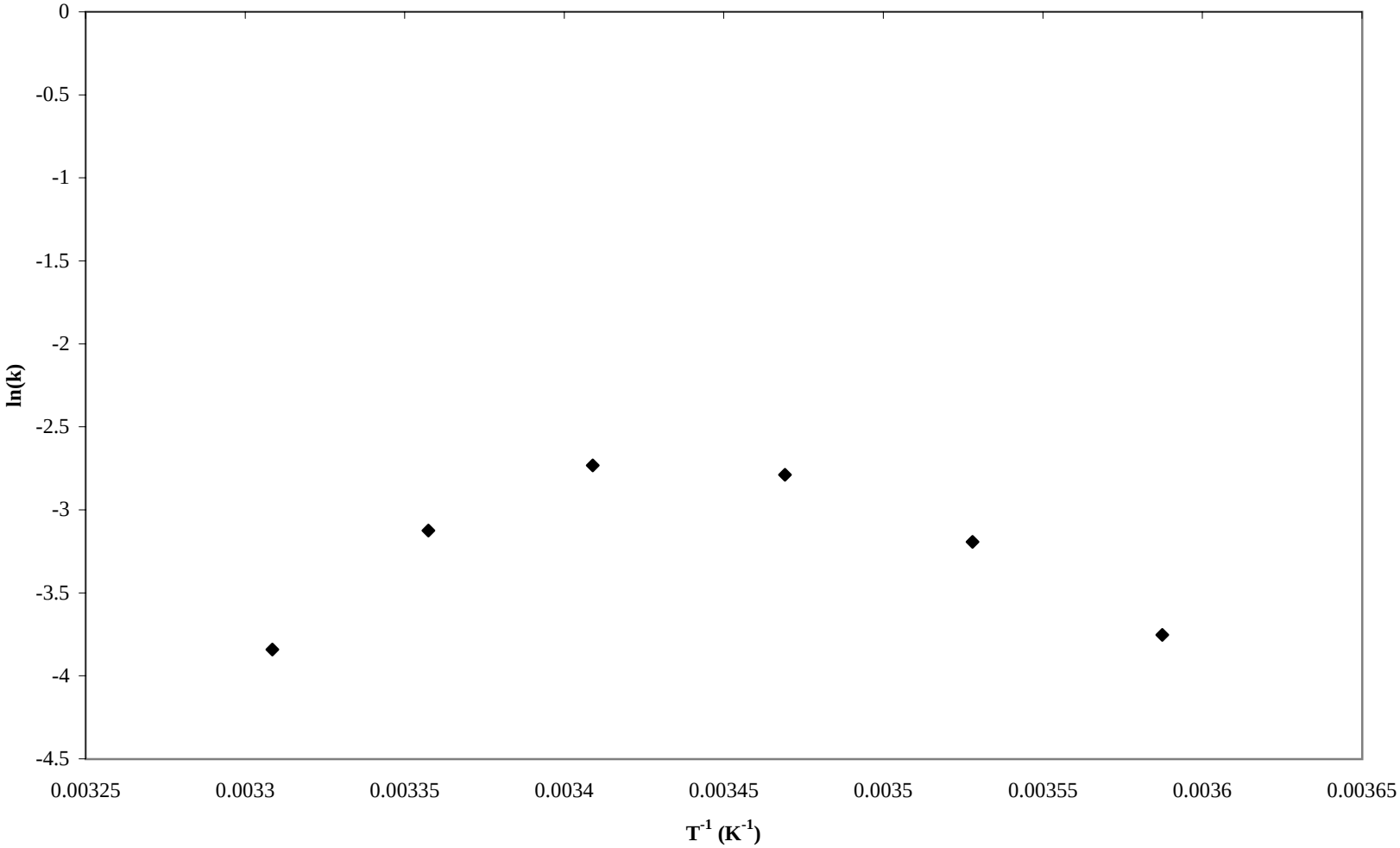

Figure 3.10. Arrhenius Plot for Blue A in 10% TMOS Matrix

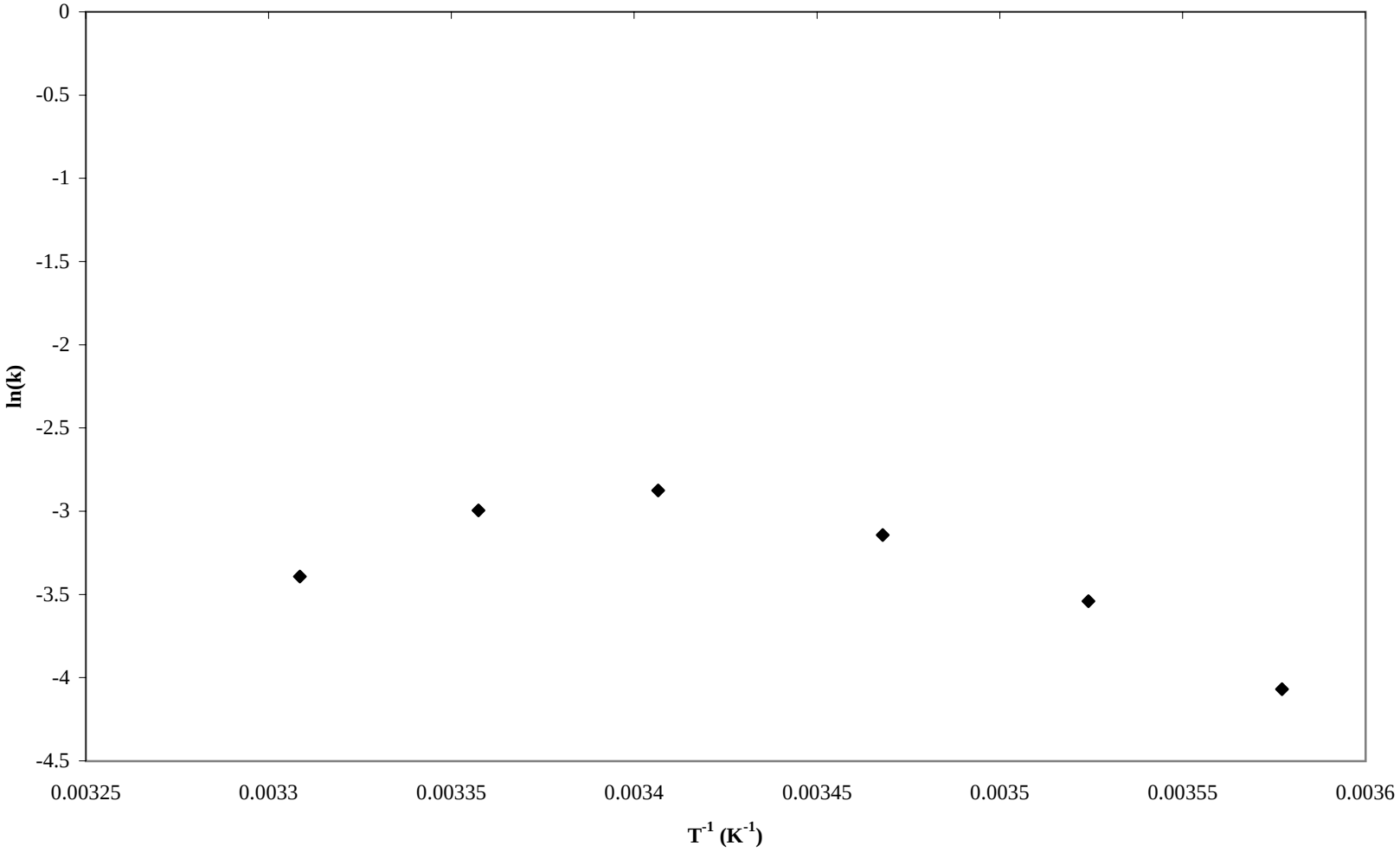

Figure 3.11. Arrhenius Plot for 25% TMOS Matrix

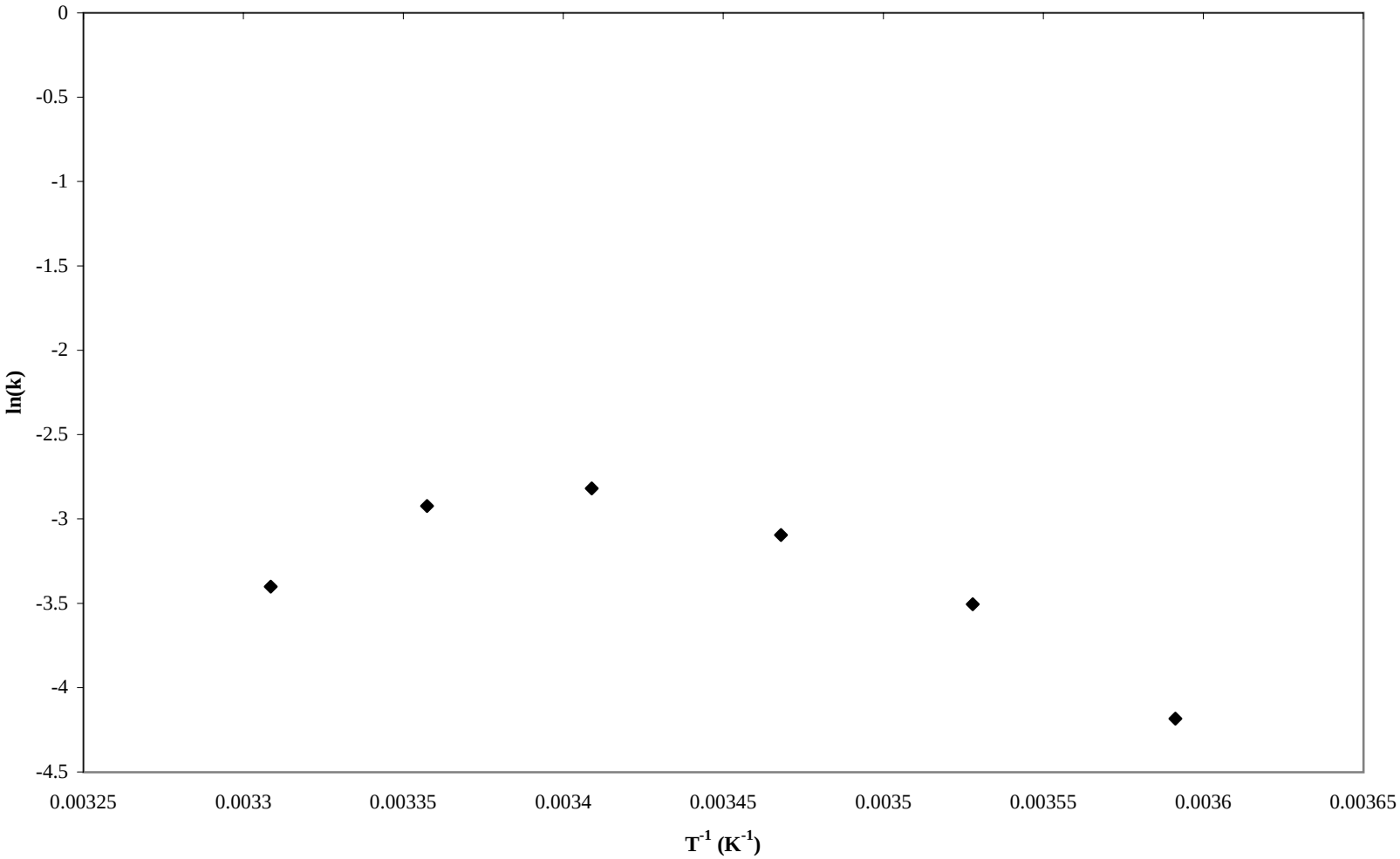

Figure 3.12. Arrhenius Plot for Blue A in 40% TMOS Matrix

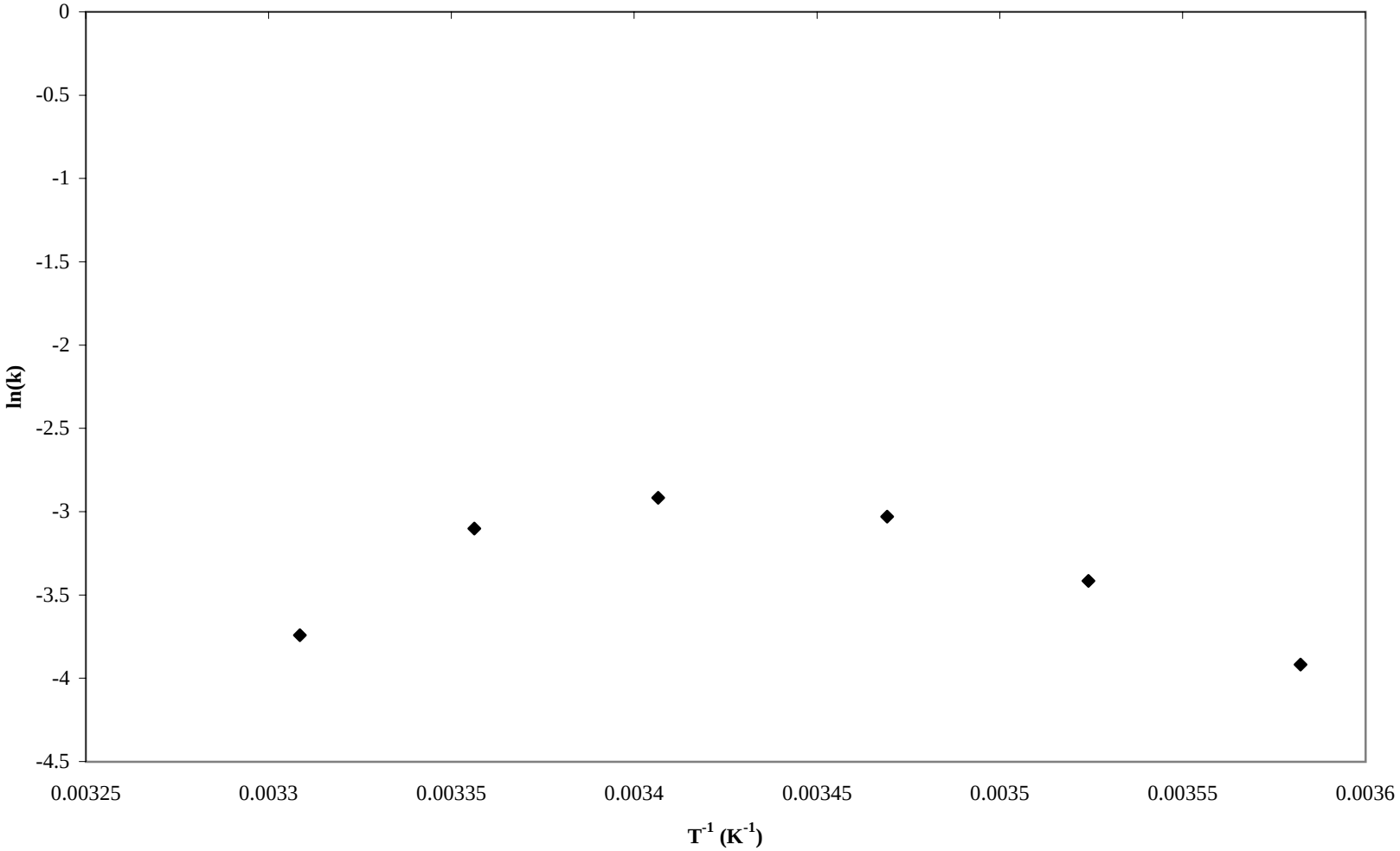

Figure 3.13. Arrhenius Plot for Blue A in Silica Particle Matrix

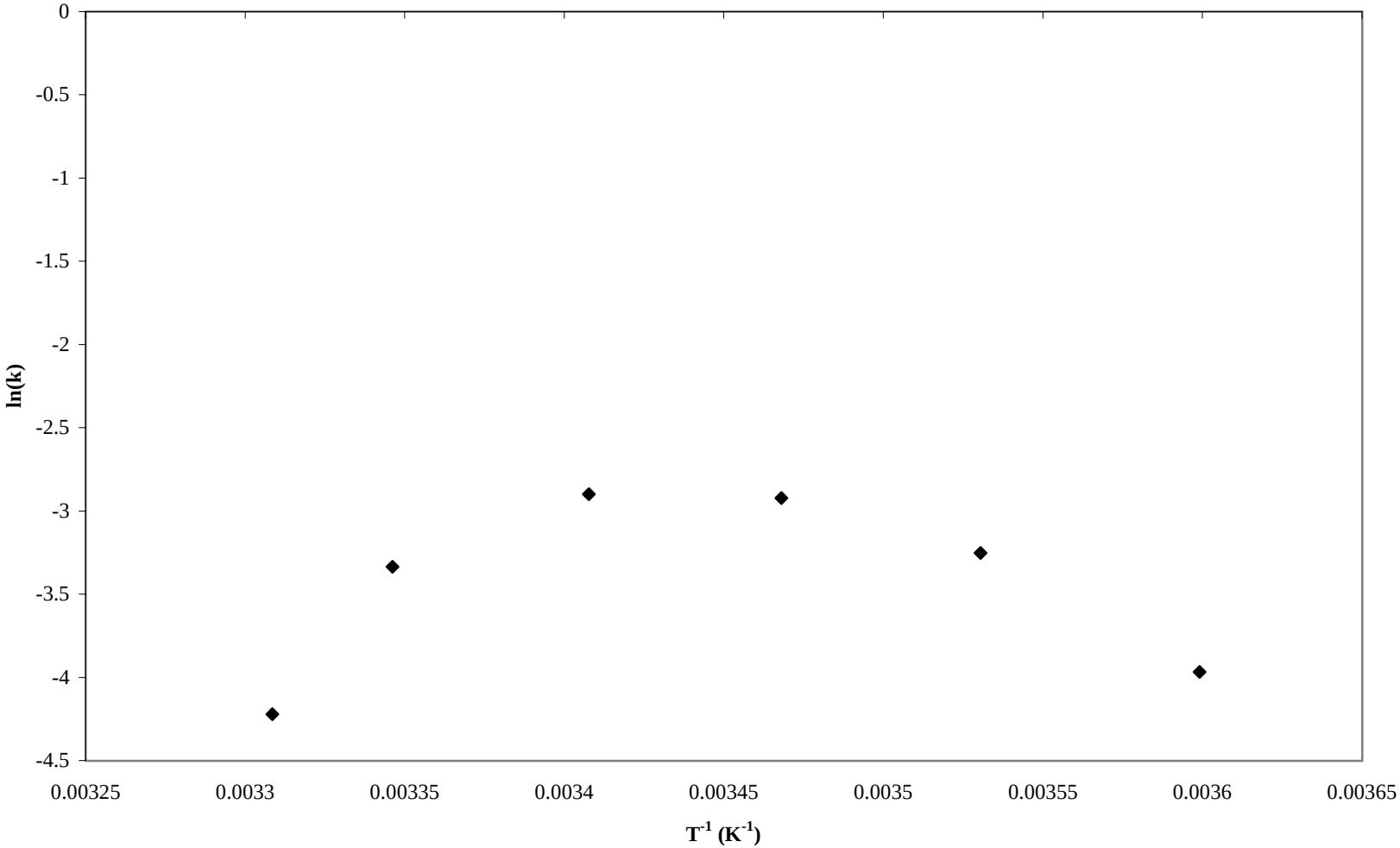

Figure 3.14. Arrhenius Plot for Blue A in Methanol

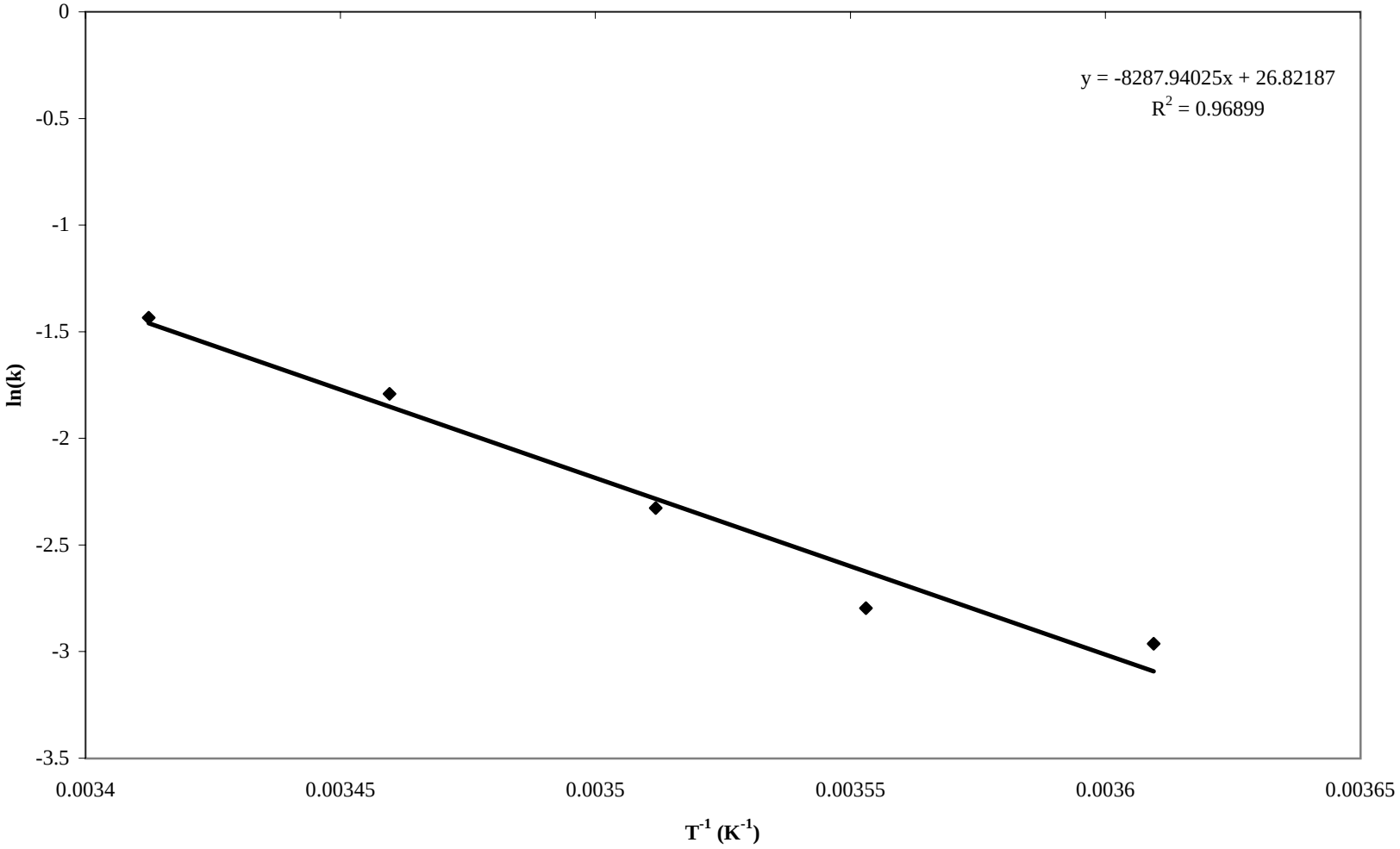

Figure 3.15. Arrhenius Plot for Blue A in 30% ETES / 70% GPTMS Matrix

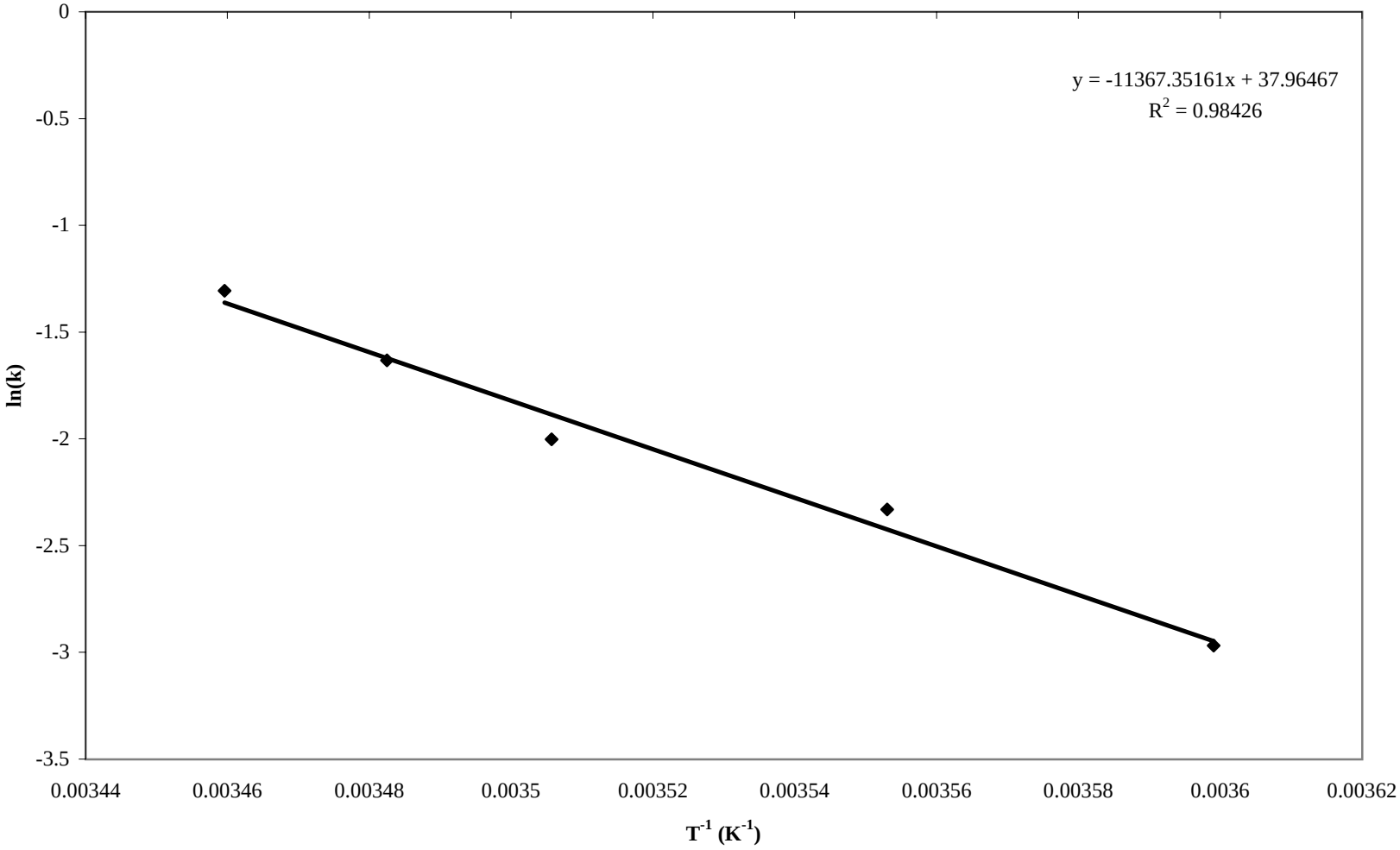

Figure 3.16. Blue A in 10% TMOS Matrix at 6.4° C - First Order Kinetic Plots at Various Time Intervals

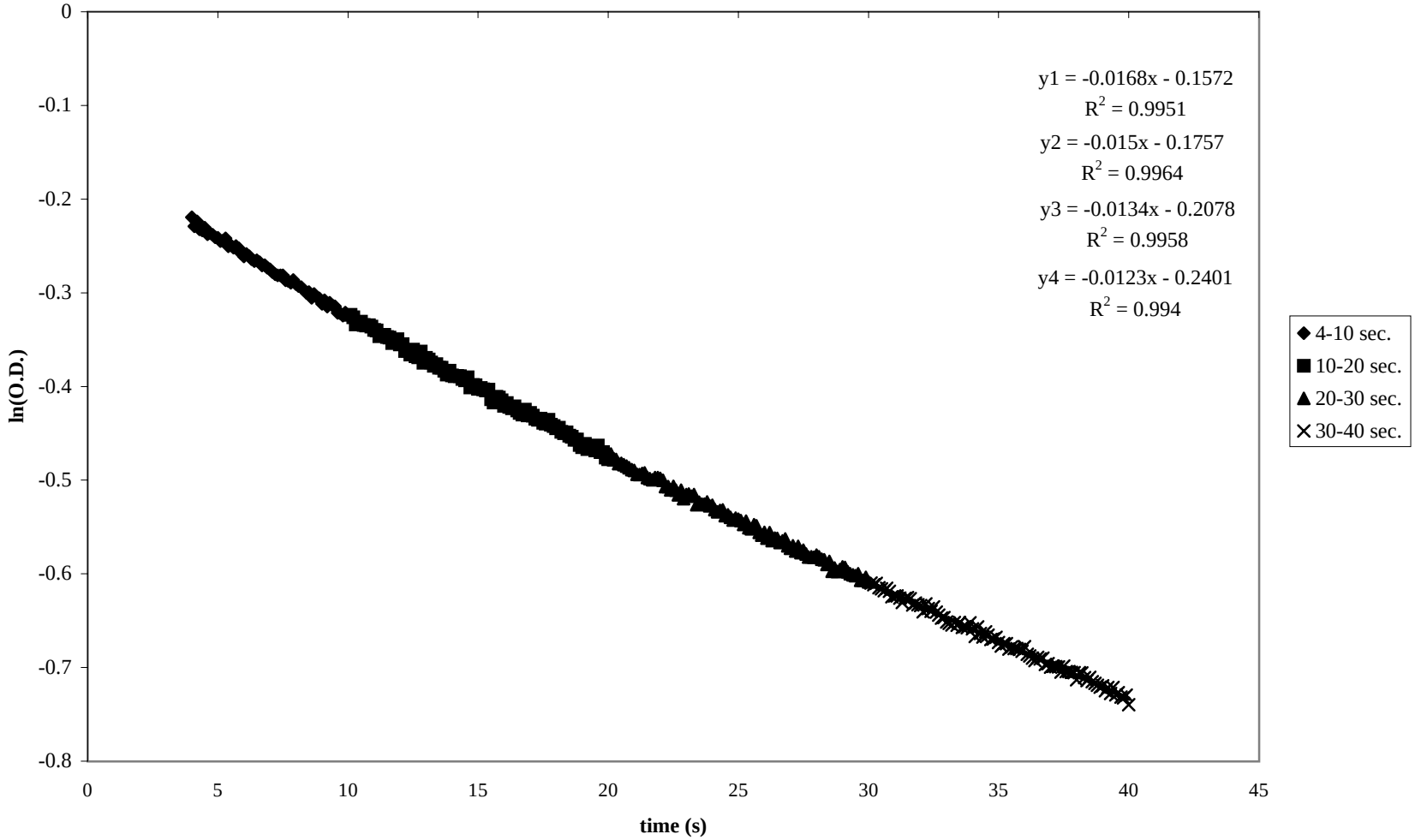

4. Summary of Conclusions

In this work, five Ormosil formulations were synthesized and doped with a number of organic photochromic dyes. Some of these dyes were covalently bound to the Ormosil matrix through a siloxane substituent. The effects of the matrix as well as the effects of silylation on the rate of degradation of each of these dyes were studied.

The first observation to be made was that more rigid matrices (the 40% TMOS and Silica Particle matrices) showed a much slower rate of degradation than their counterparts. This may result from the increased rigidity of these matrices that will slow the rate of oxygen diffusion as well as limit the freedom of the dye making is less likely to react with oxygen. One exception that was noted was the 10% TMOS matrix, which demonstrated a rate of degradation comparable to the 40% TMOS and Silica Particle matrices. If matrix rigidity is related to increased resistance to degradation of the dyes, it may be that the 10% TMOS matrix represents a case where the organic cross-linking of the organic substituents is optimized, and it is this cross-linking that accounts for increased rigidity and thus the slower rate of degradation. This fact would seem to be corroborated by measurements of the rate constants of the photomerocyanine form of the dye returning to the spirooxazine form. The 10% TMOS, 25% TMOS, and Silica Particle matrix all showed the slowest kinetics, indicating that molecular motion of the dye is more restricted in these matrices.

It was also observed that the silylated dyes also show a substantial reduction in the rate of degradation over their unsilylated counterparts. The silylated dyes would not

affect the porosity significantly, but will affect the amount of freedom allowed as they are covalently bound to the Ormosil matrix.

5. References

(1) Avnir, D.; Levy, D.; Reisfeld, R. *J. Phys. Chem.* **1984**, *88*, 5956.
(2) Lin, H.-T.; Bescher, E.; Mackenzie, J. D.; Dai, H.; Stafsudd, O. M. *J. Mater. Sci.* **1992**, *27*, 5523.
(3) Avnir, D.; Kaufman, V. R.; Reisfeld, R. *J. Non-Cryst. Solids* **1985**, *74*, 395.
(4) Yamane, M.; Aso, S.; Sakaino, T. *J. Mater. Sci.* **1978**, *13*, 865.
(5) Dislich, H.; Hussmann, E. *Thin Solid Films* **1981**, *77*, 129.
(6) Reisfeld, R. *J. Non-Cryst. Solids* **1990**, *121*, 254.
(7) Gvishi, R.; Reisfeld, R. *J. Non-Cryst. Solids* **1991**, *128*, 69.
(8) Kaufman, V. R.; Levy, D.; Avnir, D. *J. Non-Cryst. Solids* **1986**, *82*, 103.
(9) Levy, D.; Einhorn, S.; Avnir, D. *J. Non-Cryst. Solids* **1989**, *113*, 137.
(10) Nešpůrek, S. *Int. J. Electronics* **1992**, *73*, 1059.
(11) Hou, L.; Schmidt, H. *J. Mater. Sci.*, **1996**, *31*, 3427.
(12) Tamaoki, N.; Yoshimura, S.; Yamaoka, T. *Thin Solid Films* **1992**, *221*, 132.
(13) Fiksman, G.; Datta, P.; Otón, J. M.; Matías, I. R.; López-Amo, M.; del Monte, F.; Levy, D. *Opt. Eng.* **1997**, *36*, 1766.
(14) Levy, D.; del Monte, F.; López-Amo, M.; Otón, J. M.; Datta, P.; Matías, I. *J. Appl. Phys.* **1995**, *77*, 2804.
(15) Matías, I. R.; López-Amo, M.; Fiksman, G.; Datta, P.; Otón, J. M. *IEEE J. Quantum Elec.* **1997**, *3*, 780.
(16) Levy, D. *J. Non-Cryst. Solids* **1992**, *147&148*, 508.
(17) Dai, S.; Sigman, M. E.; Burch, E. L. *Chem. Mater.* **1995**, *7*, 2054.
(18) Biteau, J.; Tsivgoulis, G. M.; Chaput, F.; Boilot, J.-P.; Gilat, S.; Kawai, S.; Lehn, J.-M.; Darracq, B.; Martin, F.; Levy, Y. *Mol. Cryst. Liq. Cryst.* **1997**, *297*, 65.
(19) Fujii, T.; Kodaira, K.; Kawauchi, O.; Tanaka, N.; Yamashita, H.; Anpo, M. *J. Phys. Chem. B* **1997**, *101*, 10631.
(20) Levy, D.; Avnir, D. *J. Phys. Chem.* **1988**, *92*, 4734.
(21) Preston, D.; Pouxviel, J.-C.; Novinson, T.; Kaska, W. C.; Dunn, B.; Zink, J. I. *J. Phys. Chem.* **1990**, *94*, 4167.
(22) Schaudel, B.; Guermeur, C.; Sanchez, C.; Nakatani, K.; Delaire, J. A. *J. Mater. Chem.* **1997**, *7*, 61.
(23) Sanchez, C.; Ribot, F.; Lebeau, B. *J. Mater. Chem.* **1999**, *9*, 35.
(24) Hou, L.; Hoffmann, B.; Mennig, M.; Schmidt, H. *J. Sol-Gel Sci. Technol.* **1994**, *2*, 635.
(25) Biteau, J.; Chaput, F.; Boilot, J.-P. *J. Phys. Chem.* **1996**, *100*, 9024.
(26) Hou, L.; Schmidt, H. *J. Mater. Sci. Lett.* **1997**, *16*, 435.
(27) Biteau, J.; Chaput, F.; Boilot, J.-P. *Mol. Cryst. Liq. Cryst.* **1997**, *297*, 49.
(28) Mennig, M.; Fries, K.; Lindenstruth, M.; Schmidt, H. *Thin Solid Films* **1999**, *351*, 230.
(29) Hench, L. L.; West, J. K. *Chem. Rev.* **1990**, *90*, 33.
(30) Deng, Q.; Moore, R. B.; Mauritz, K. A. *Chem. Mater.* **1995**, *7*, 2259.

(31) Aelion, R.; Loebel, A.; Eirich, F. *J. Am. Chem. Soc.* **1950**, *72*, 5705.
(32) Zerda, T. W.; Hoang, G. *J. Non-Cryst. Solids* **1989**, *109*, 9.
(33) McNeil, K. J.; DiCaprio, J. A.; Walsh, D. A.; Pratt, R. F. *J. Am. Chem. Soc.* **1980**, *102*, 1859.
(34) Brinker, C. J. *J. Non-Cryst. Solids* **1988**, *100*, 31.
(35) Schmidt, H.; Scholze, H.; Kaiser, A. *J. Non-Cryst. Solids* **1984**, *63*, 1.
(36) Lev, O.; Tsionsky, M.; Rabinovich, L.; Glezer, V.; Sampath, S.; Pankratov, I.; Gun, J. *Anal. Chem.* **1995**, *67*, 22A.
(37) Favaro, G.; Masetti, F.; Mazzucato, U.; Ottavi, G.; Allegrini, P.; Malatesta, V. *J. Chem. Soc., Faraday Trans.* **1994**, *90*, 333.
(38) Heiligman-Rim, R.; Hirschberg, Y.; Fischer, E. *J. Phys. Chem.* **1962**, *66*, 2470.
(39) Schneider, S.; Mindl, A.; Elfinger, G.; Melzig, M. *Ber. Bunsenges. Phys. Chem.* **1987**, *91*, 1222.
(40) Tamai, N.; Masuhara, H. *Chem. Phys. Lett.* **1992**, *191*, 189.
(41) Schneider, S. *Z. Phys. Chem. Neue Folge* **1987**, *154*, 91.
(42) Schneider, S.; Baumann, F.; Klüter, U.; Melzig, M. *Ber. Bunsenges. Phys. Chem.* **1987**, *91*, 1225.
(43) Tyer, N. W., Jr.; Becker, R. S. *J. Am. Chem. Soc.* **1970**, *92*, 1289
(44) Bohne, C.; Fan, M. G.; Li, Z.-J.; Lusztyk, J.; Scaiano, J. C. *J. Chem. Soc., Chem. Commun.* **1990**, 571.
(45) Bohne, C.; Fan, M. G.; Li, Z. J.; Liang, Y. C.; Lusztyk, J.; Scaiano, J. C. *J. Photochem. Photobiol. A: Chem.* **1992**, *66*, 79.
(46) Kellman, A.; Tfibel, F.; Dubest, R.; Levoir, P.; Aubard, J.; Pottier, E.; Guglielmetti, R. *J. Photochem. Photobiol. A: Chem.* **1989**, *49*, 63.
(47) Eloy, D.; Escaffre, P.; Gautron, R.; Jardon, P. *J. Chim. Phys.* **1992**, *89*, 897.
(48) Favaro, G.; Malatesta, V.; Mazzucato, U.; Ottavi, G.; Romani, A. *Mol. Cryst. Liq. Cryst.* **1994**, *246*, 299.
(49) Favaro, G.; Malatesta, V.; Miliani, C.; Romani, A. *J. Photochem. Photobiol. A: Chem.* **1996**, *97*, 45.
(50) Hobley, J.; Wilkinson, F. *J. Chem. Soc., Faraday Trans.* **1996**, *92*, 1323.
(51) Chu, N. Y. C. *Can. J. Chem.* **1983**, *61*, 300.
(52) Malatesta, V. In *Organic Photochromic and Thermochromic Compounds Volume 2: Physicochemical Studies, Biological Applications, and Thermochromism*; Crano, J. C.; Guglielmetti, R. J., Eds.; Kluwer Academic / Plenum: New York, 1999; pp 65-166.
(53) Baillet, G.; Giusti, G.; Guglielmetti, R. *J. Photochem. Photobiol. A: Chem.* **1993**, *70*, 157.
(54) Malatesta, V.; Milosa, M.; Millini R.; Lanzini, L.; Bortolus, P.; Monti, S. *Mol. Cryst. Liq. Cryst.* **1994**, *246*, 303.
(55) Eloy, D.; Jardon, P. *J. Chim. Phys.* **1994**, *91*, 489.
(56) Firth, A. A.; McGarvey, D. J.; Truscott, T. G. *Mol. Cryst. Liq. Cryst.* **1994**, *246*, 295.
(57) Malatesta, V.; Millini, R.; Montanari, L. *J. Am. Chem. Soc.* **1995**, *117*, 6258.

(58) Salemi, C.; Giusti, G.; Guglielmetti, R. *J. Photochem. Photobiol. A: Chem.* **1995**, *86*, 247.
(59) Salemi-Delvaux, C.; Campredon, M.; Giusti, G.; Guglielmetti, R. *Mol. Cryst. Liq. Cryst.* **1997**, *298*, 61.
(60) Fan, M.; Sun, X.; Liang, Y.; Zhao, Y.; Ming, Y.; Knobbe, E. T. *Mol. Cryst. Liq. Cryst.* **1997**, *298*, 29.
(61) Evans, T. R.; Toth, A. F.; Leermakers, P. A. *J. Am. Chem. Soc.* **1967**, *89*, 5060.
(62) Pimienta, V.; Frouté, C.; Deniel, M. H.; Lavabre, D.; Guglielmetti, R.; Micheau, J. C. *J. Photochem. Photobiol. A: Chem.* **1999**, *122*, 199.
(63) Malkin, Y. N.; Krasieva, T. B.; Kuzmin, V. A. *J. Photochem. Photobiol. A: Chem.* **1989**, *49*, 75.
(64) Malkin, Y. N.; Krasieva, T. B.; Kuz'min, V. A. *Izv. Akad. Nauk SSSR, Ser. Khim.* **1990**, 236.
(65) Kryszewski, M.; Nadolski, B.; North, A. M.; Pethrick, R. A. *J. Chem. Soc., Faraday Trans. 2* **1980**, *76*, 351.

Appendix 1

Degradation of Blue A in 0% TMOS Matrix

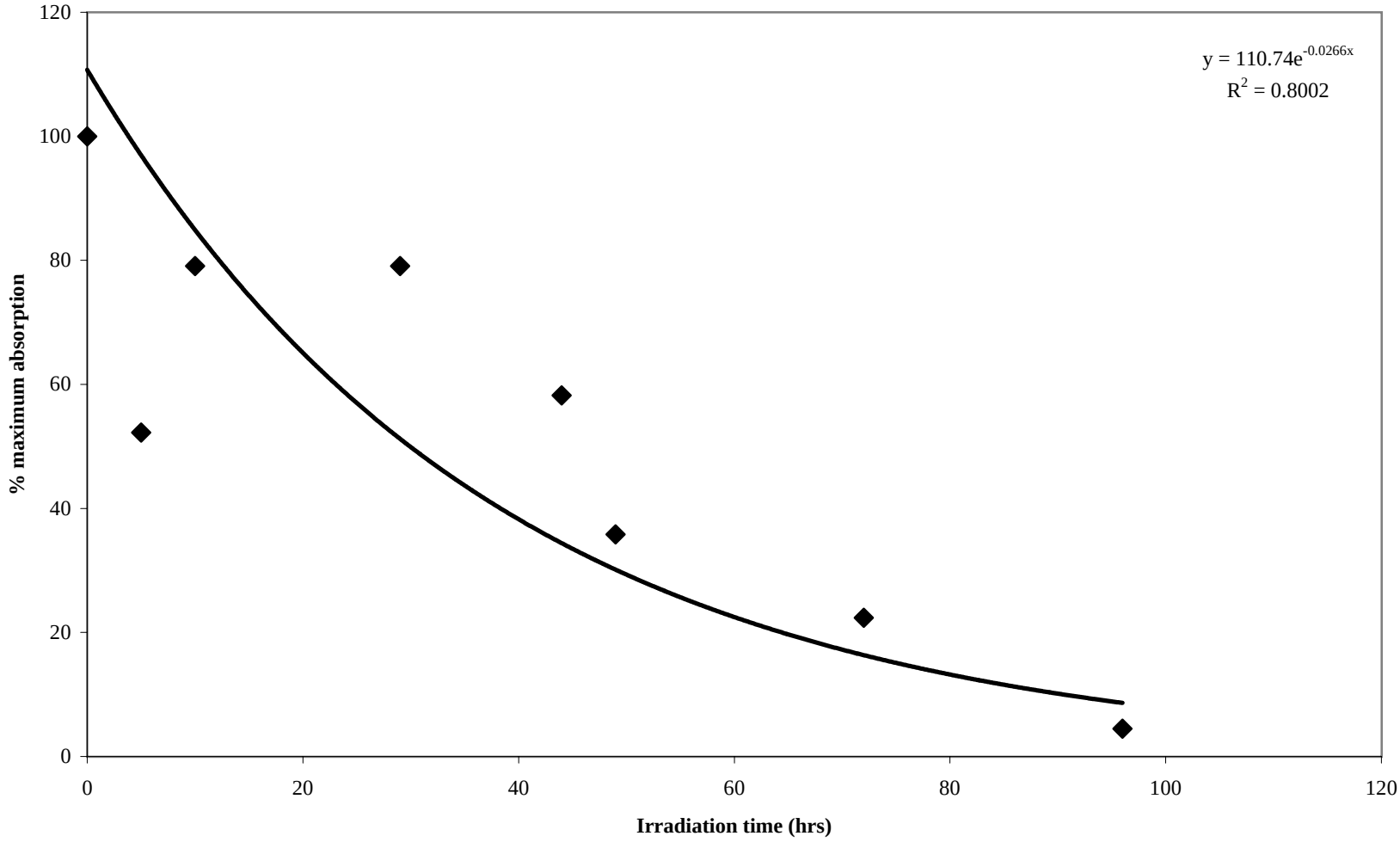

Degradation of Blue A in 10% TMOS Matrix

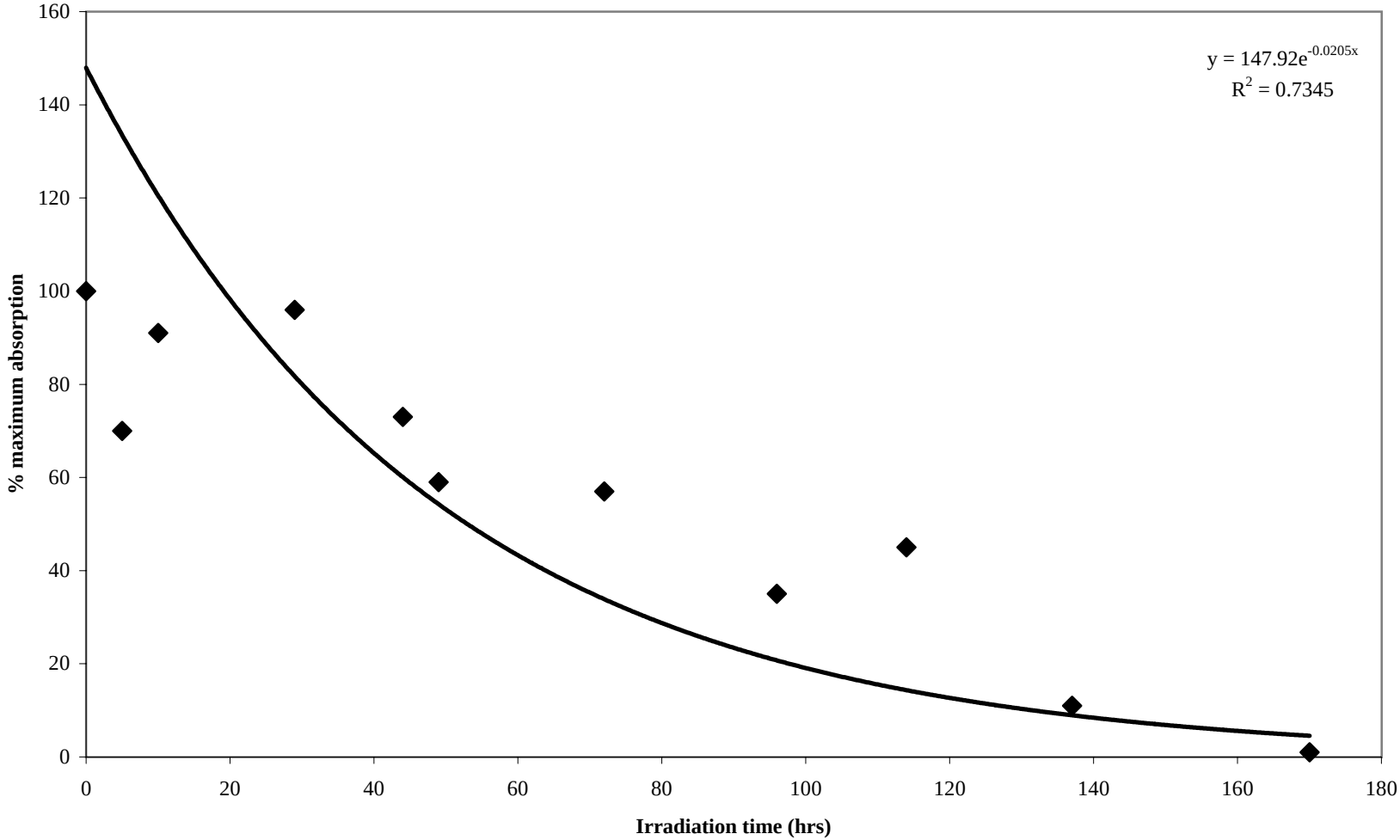

Degradation of Blue A in 25% TMOS Matrix

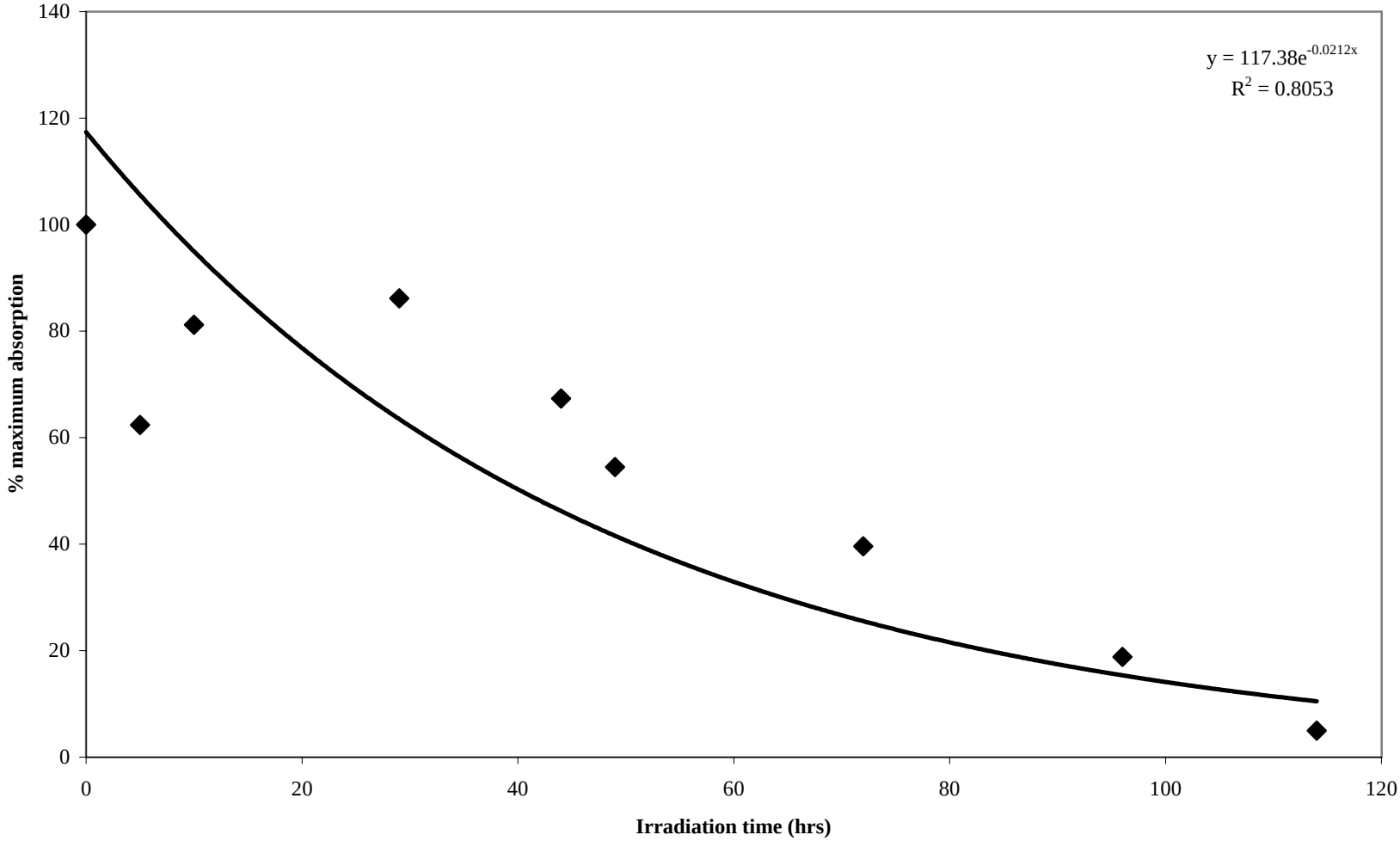

Degradation of Blue A in 40% TMOS Matrix

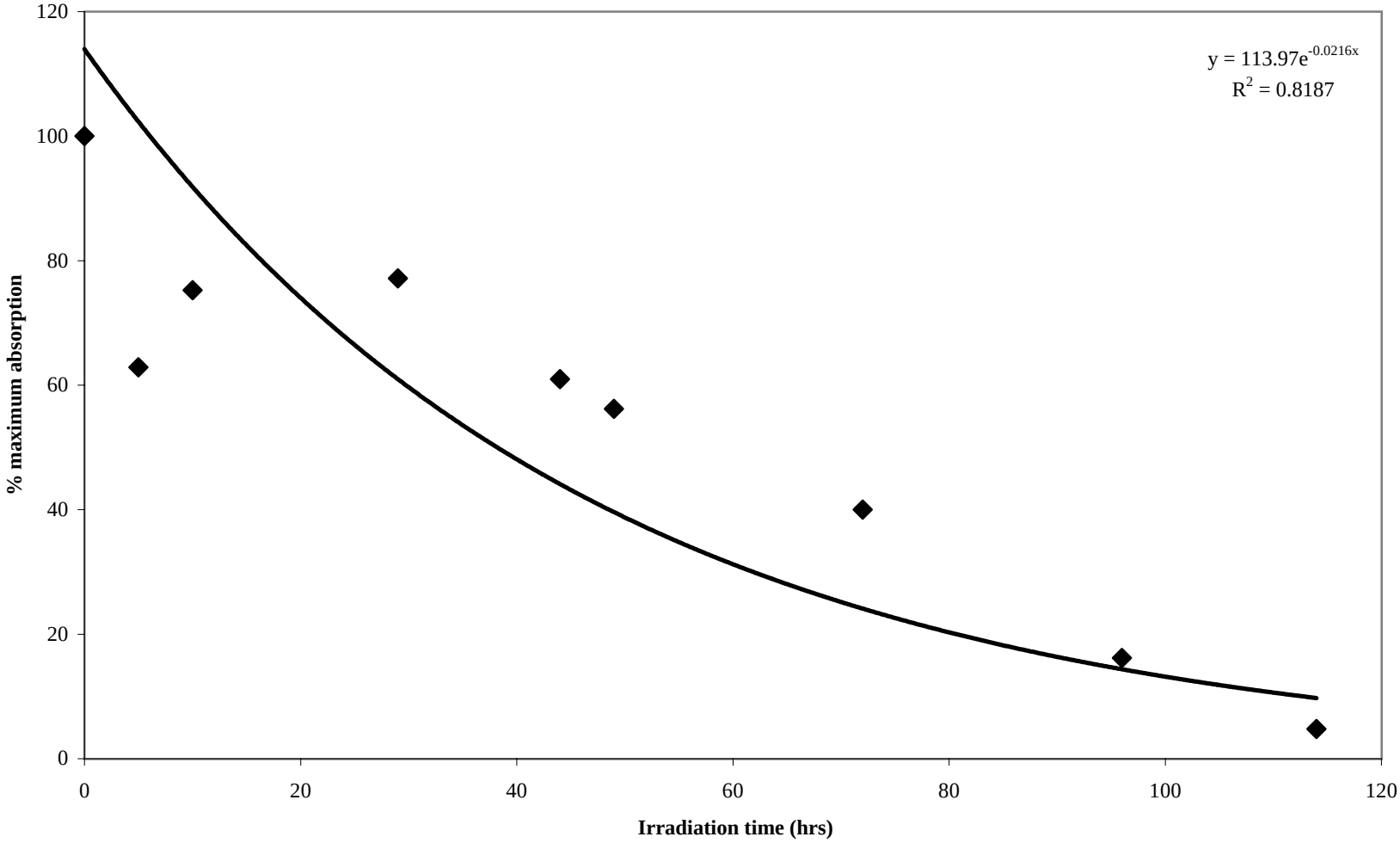

Degradation of Blue A in Silica Particle Matrix

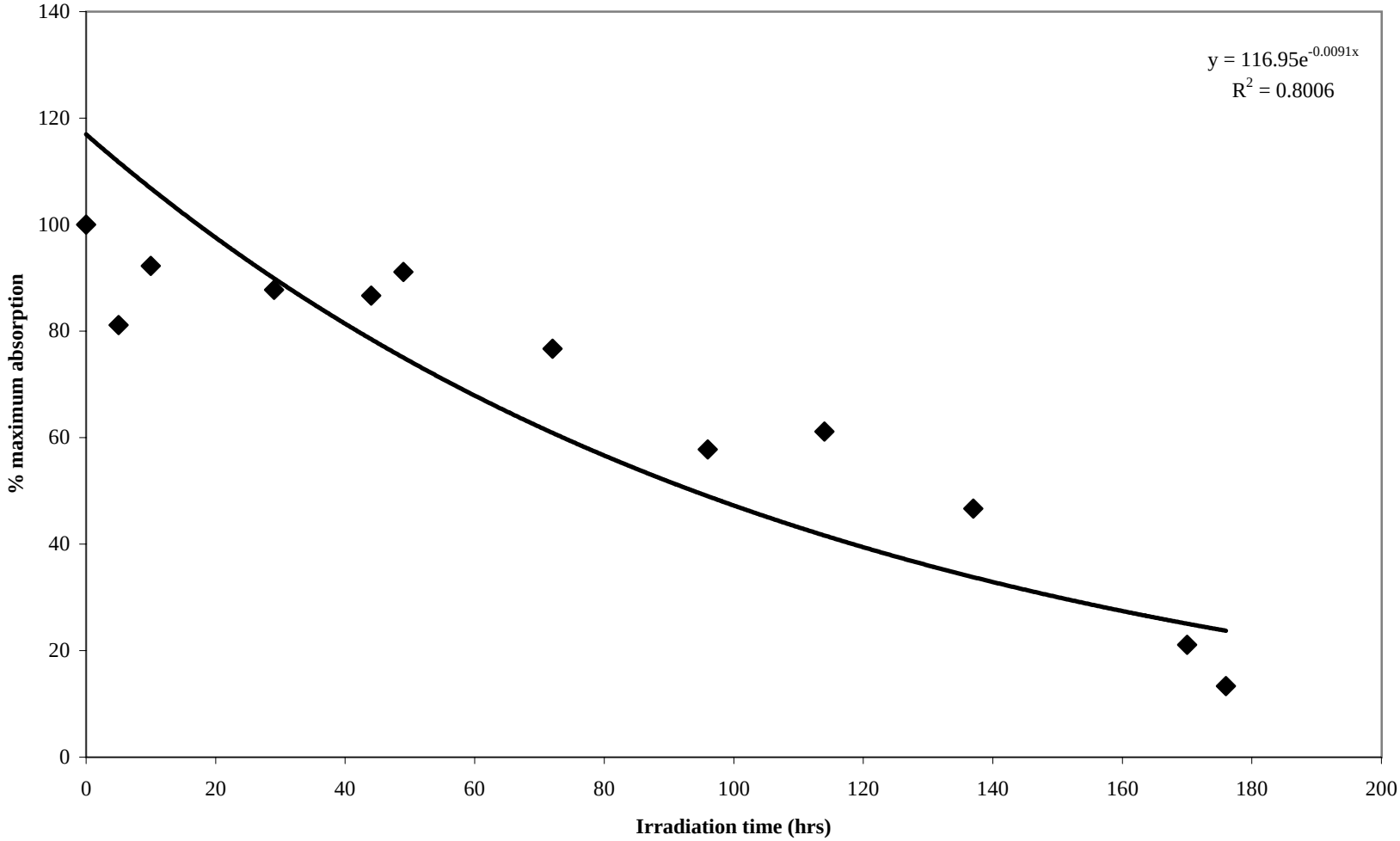

Degradation of Red PNO in 0% TMOS Matrix

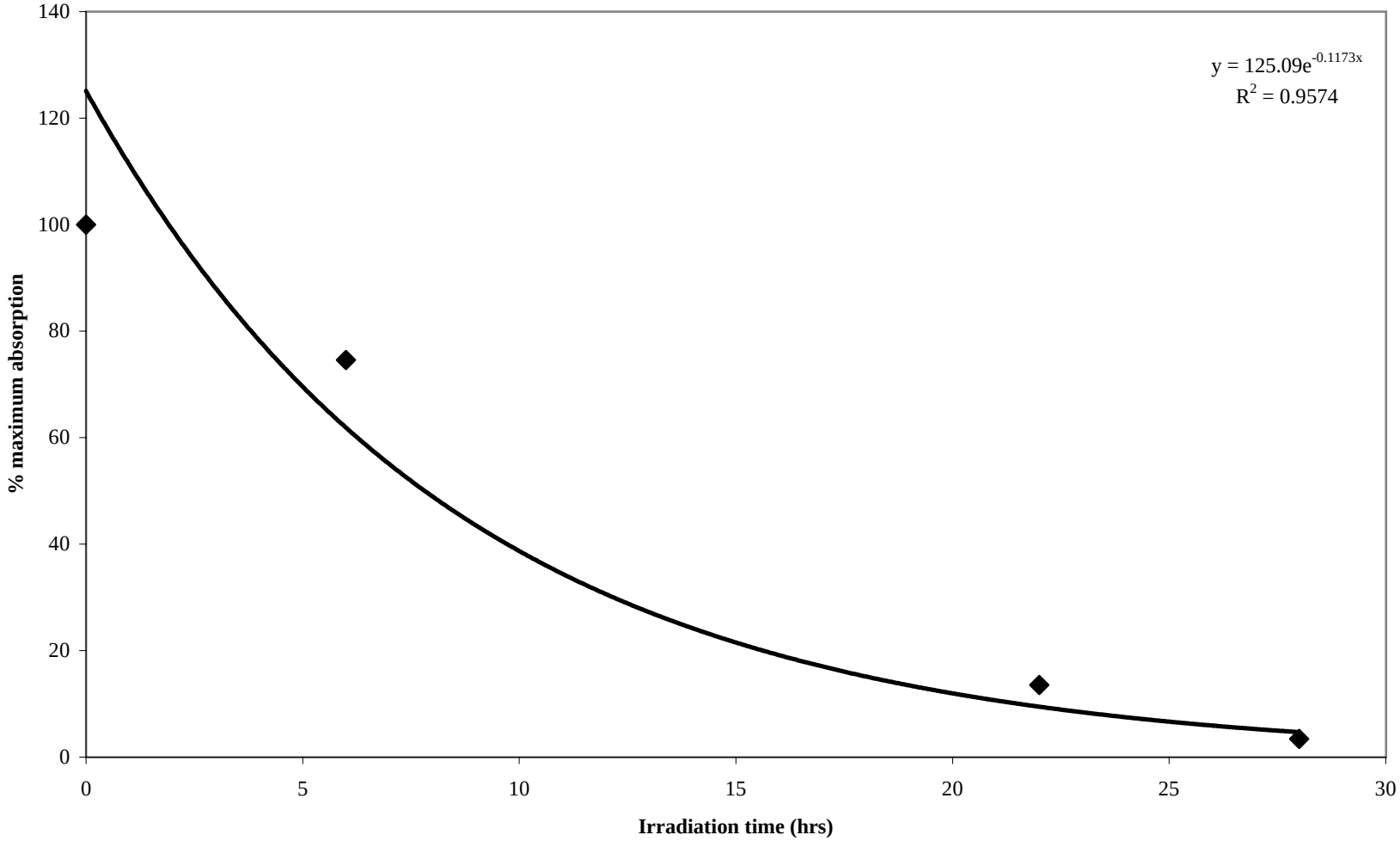

Degradation of Red PNO in 10% TMOS Matrix

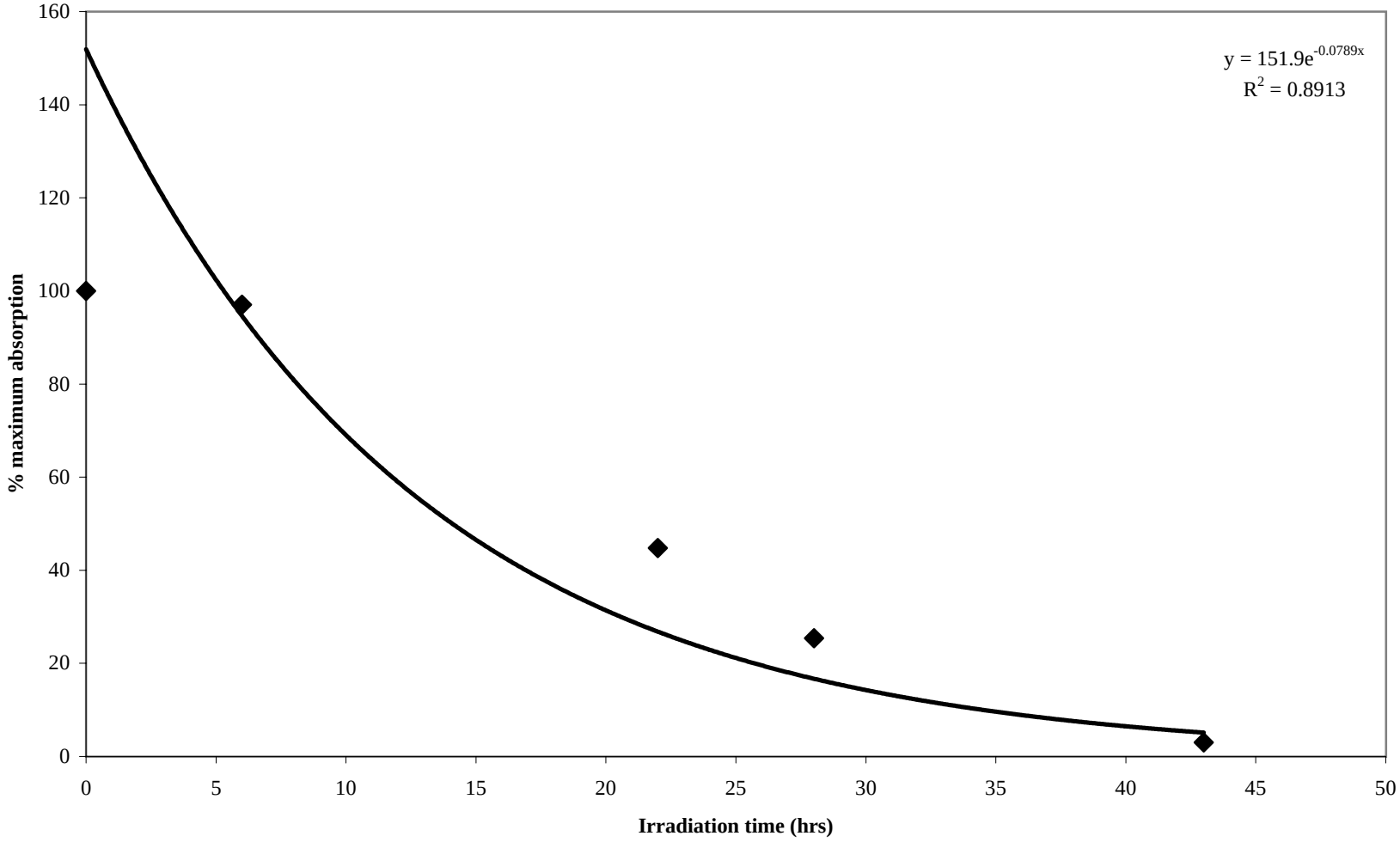

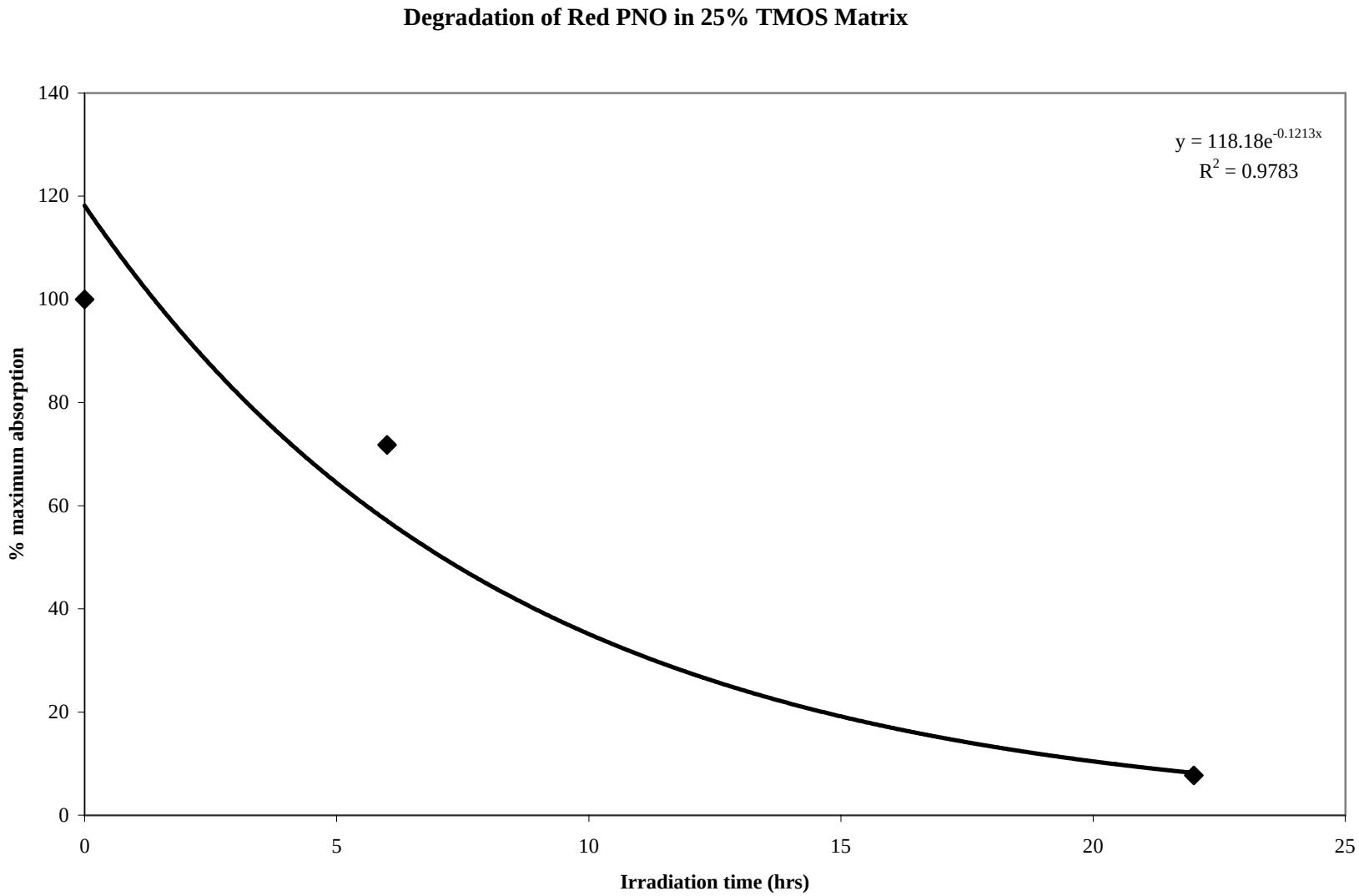
Degradation of Red PNO in 25% TMOS Matrix
y = 118.18e-0.1213x
R2 = 0.9783
% maximum absorption
Irradiation time (hrs)
0
20
40
60
80
100
120
140
0
5
10
15
20
25

Degradation of Red PNO in 40% TMOS Matrix

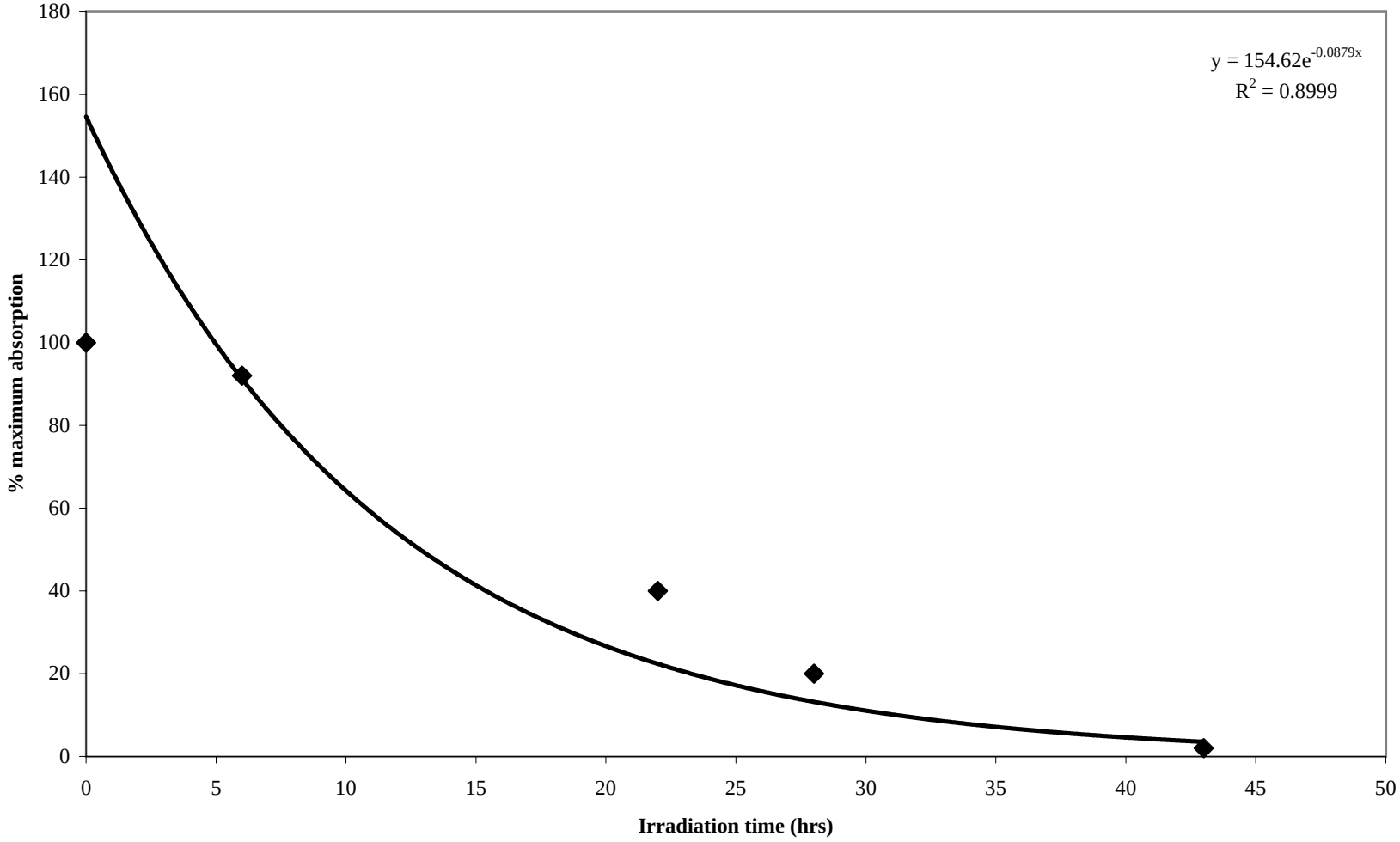

Degradation of Red PNO in Silica Particle Matrix

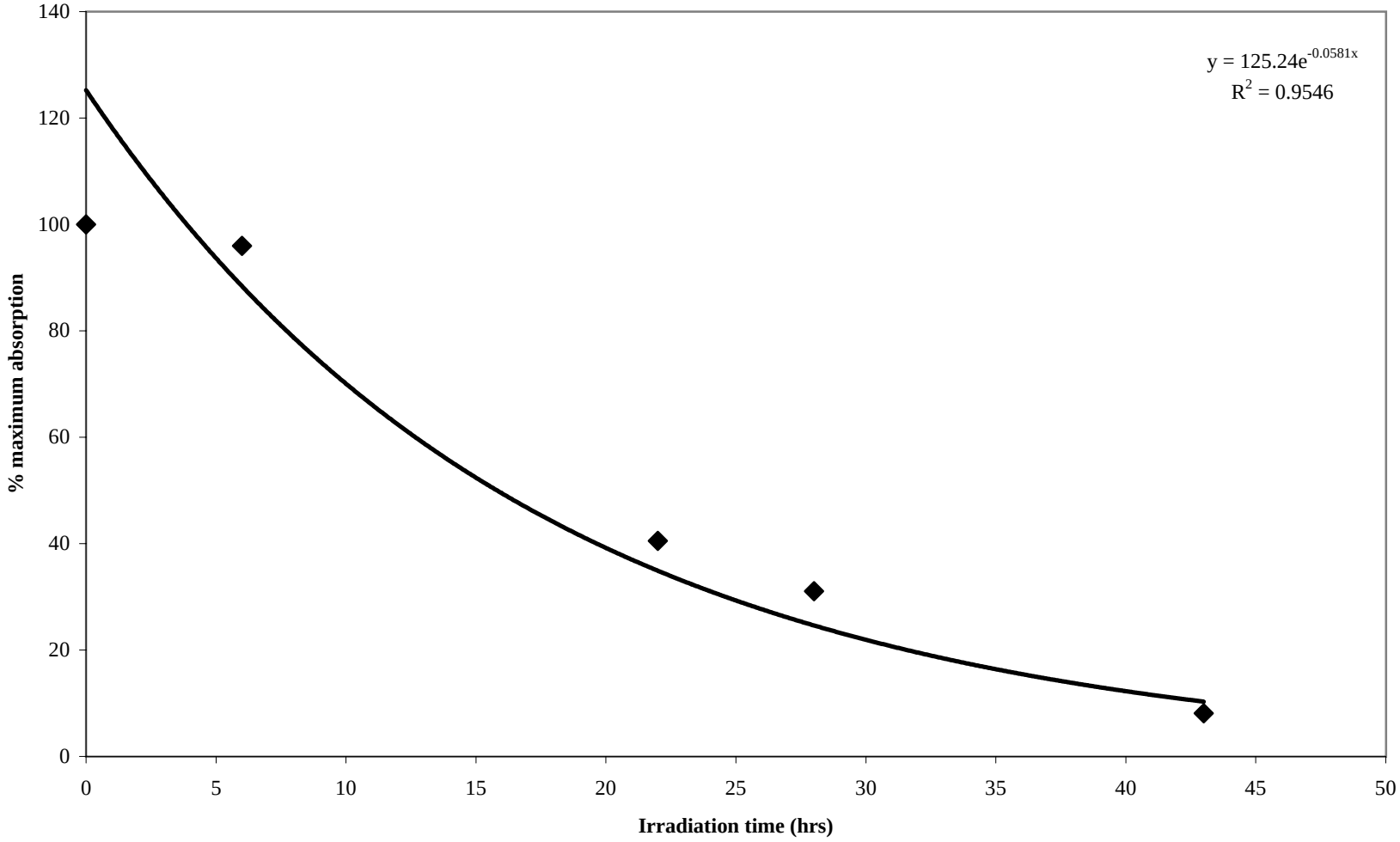

Degradation of Photosol 7-49 in 0% TMOS Matrix

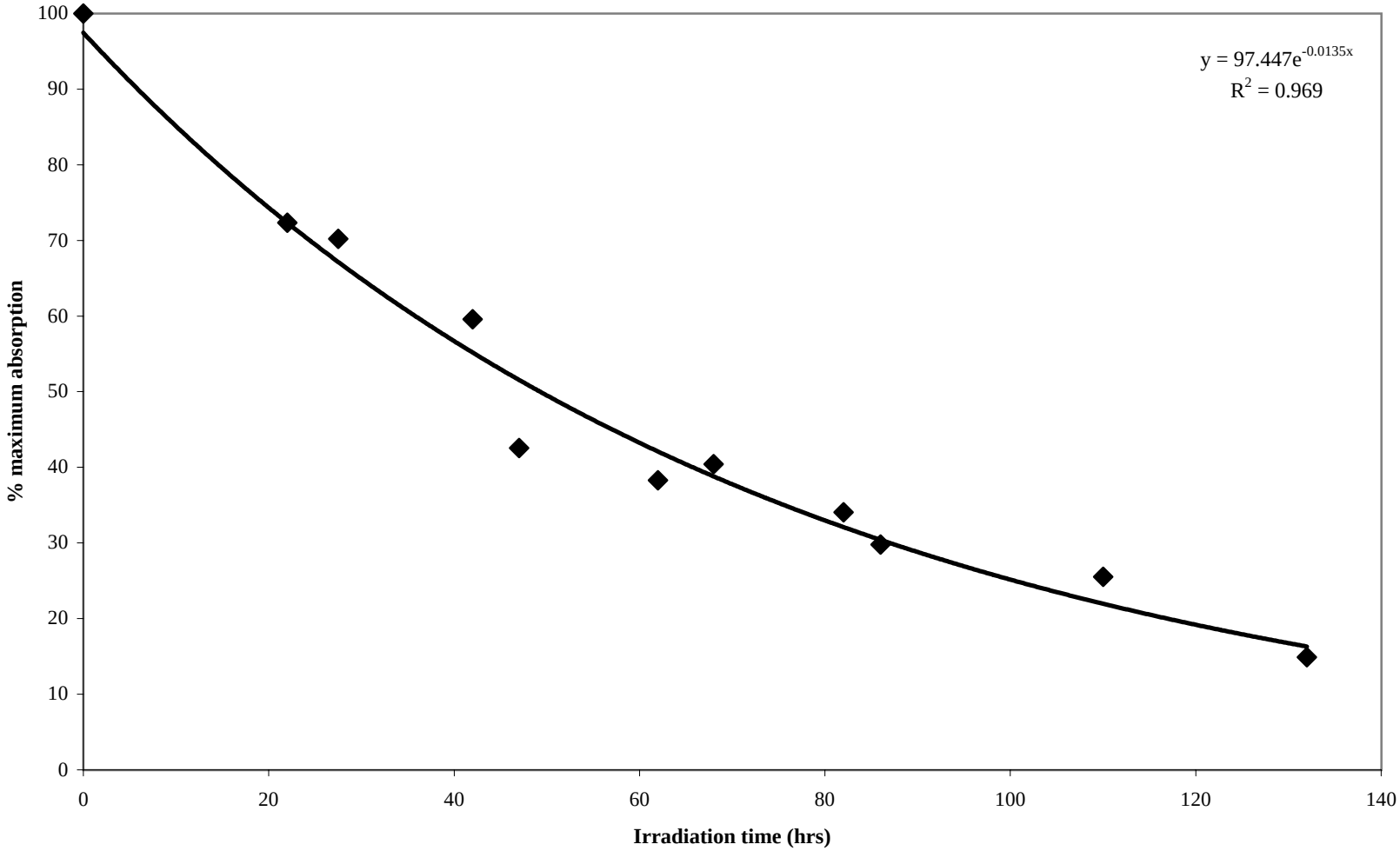

Degradation of Photosol 7-49 in 10% TMOS Matrix

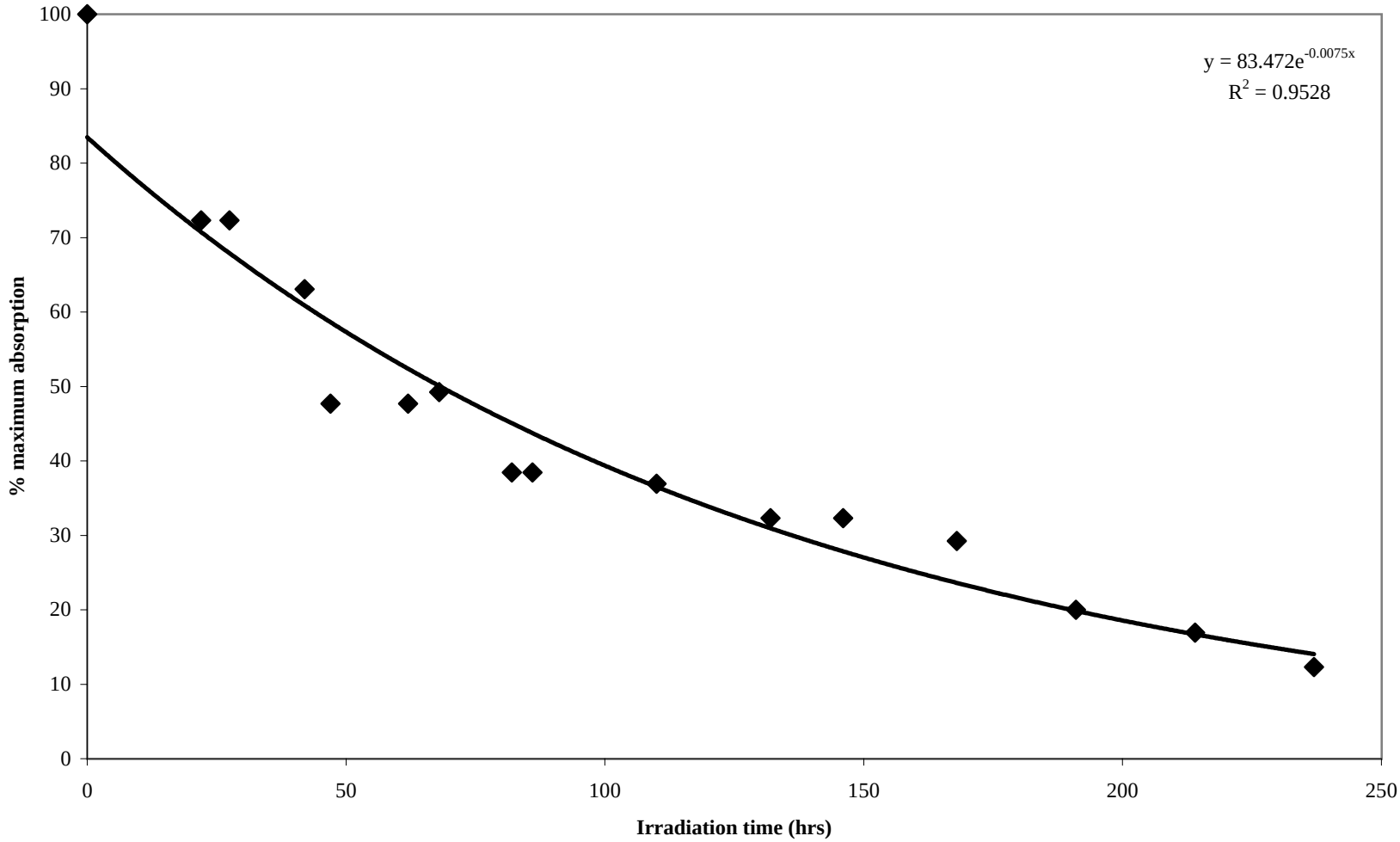

Degradation of Photosol 7-49 in 25% TMOS Matrix

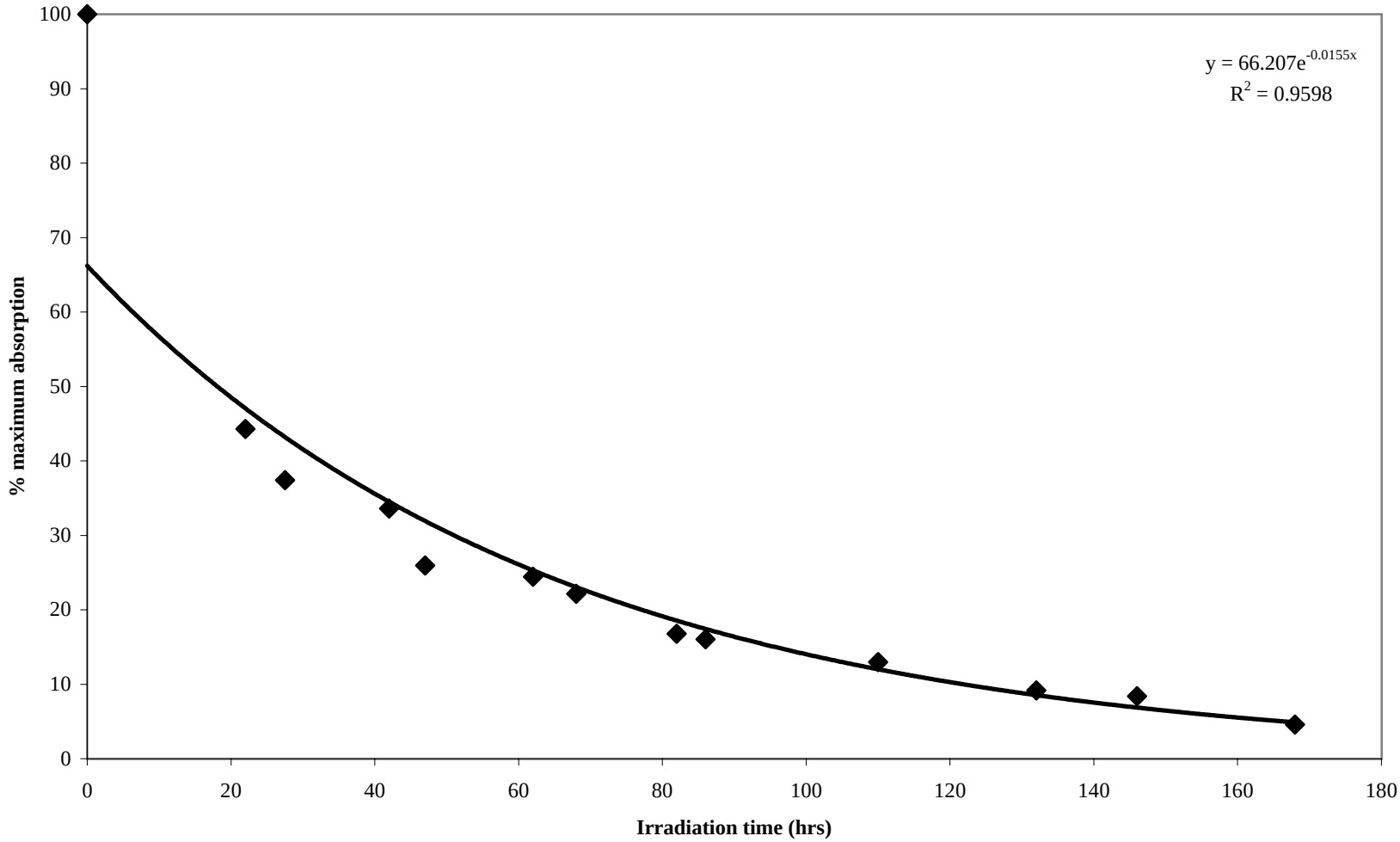

Degradation of Photosol 7-49 in 40% TMOS Matrix

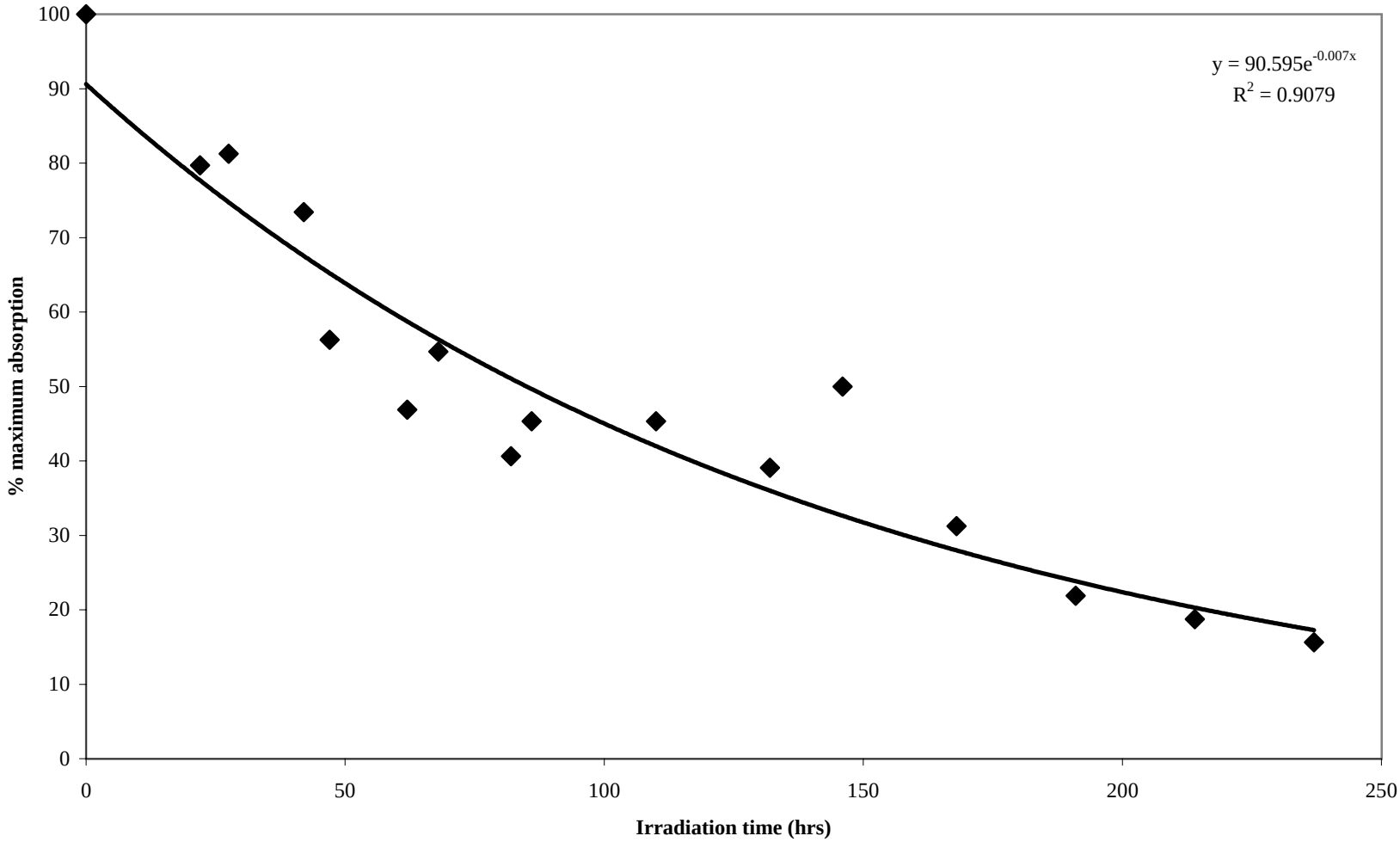

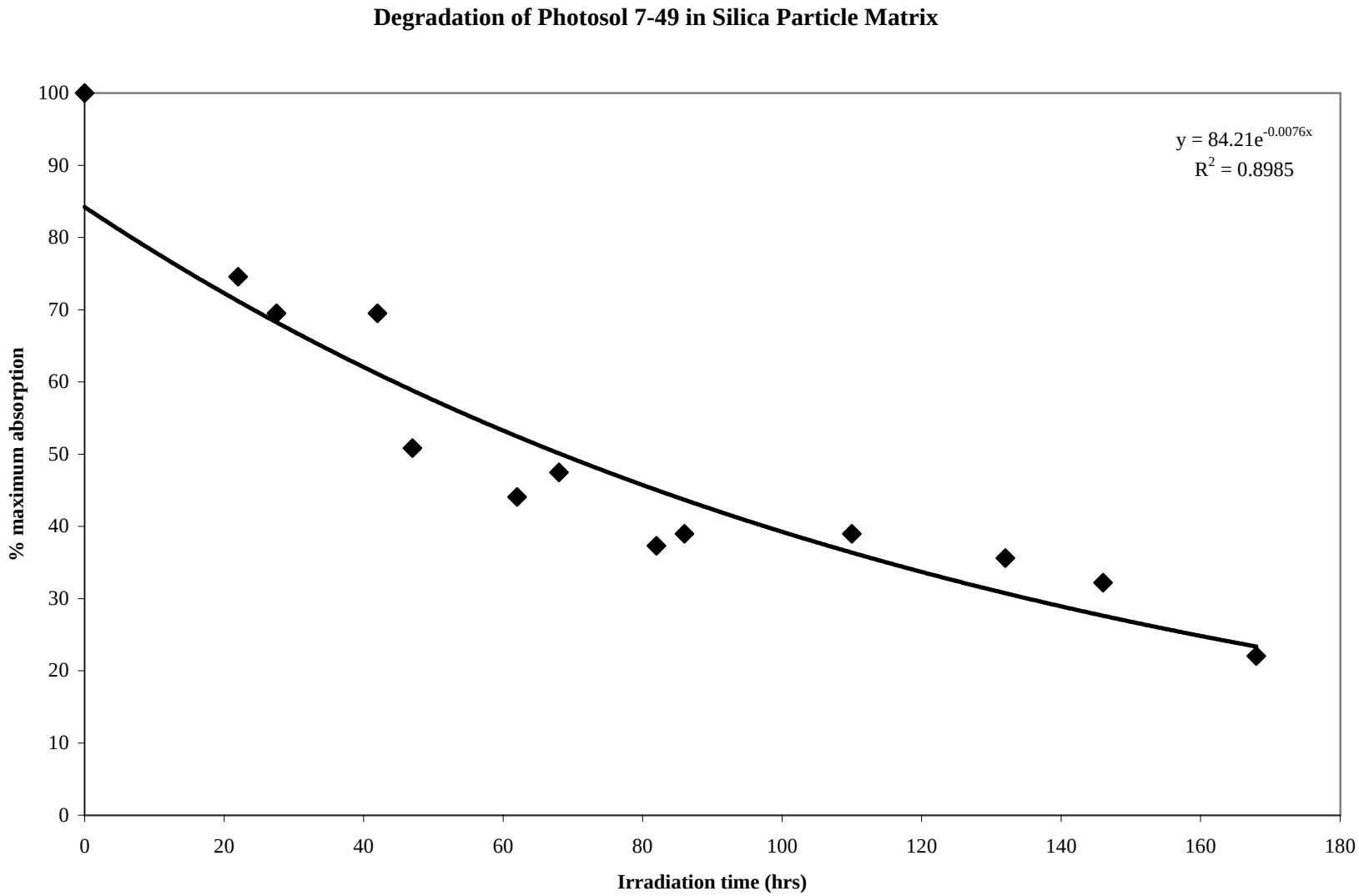
Degradation of Photosol 7-49 in Silica Particle Matrix
y = 84.21e-0.0076x
R2 = 0.8985
% maximum absorption
Irradiation time (hrs)
0
10
20
30
40
50
60
70
80
90
100
0
20
40
60
80
100
120
140
160
180

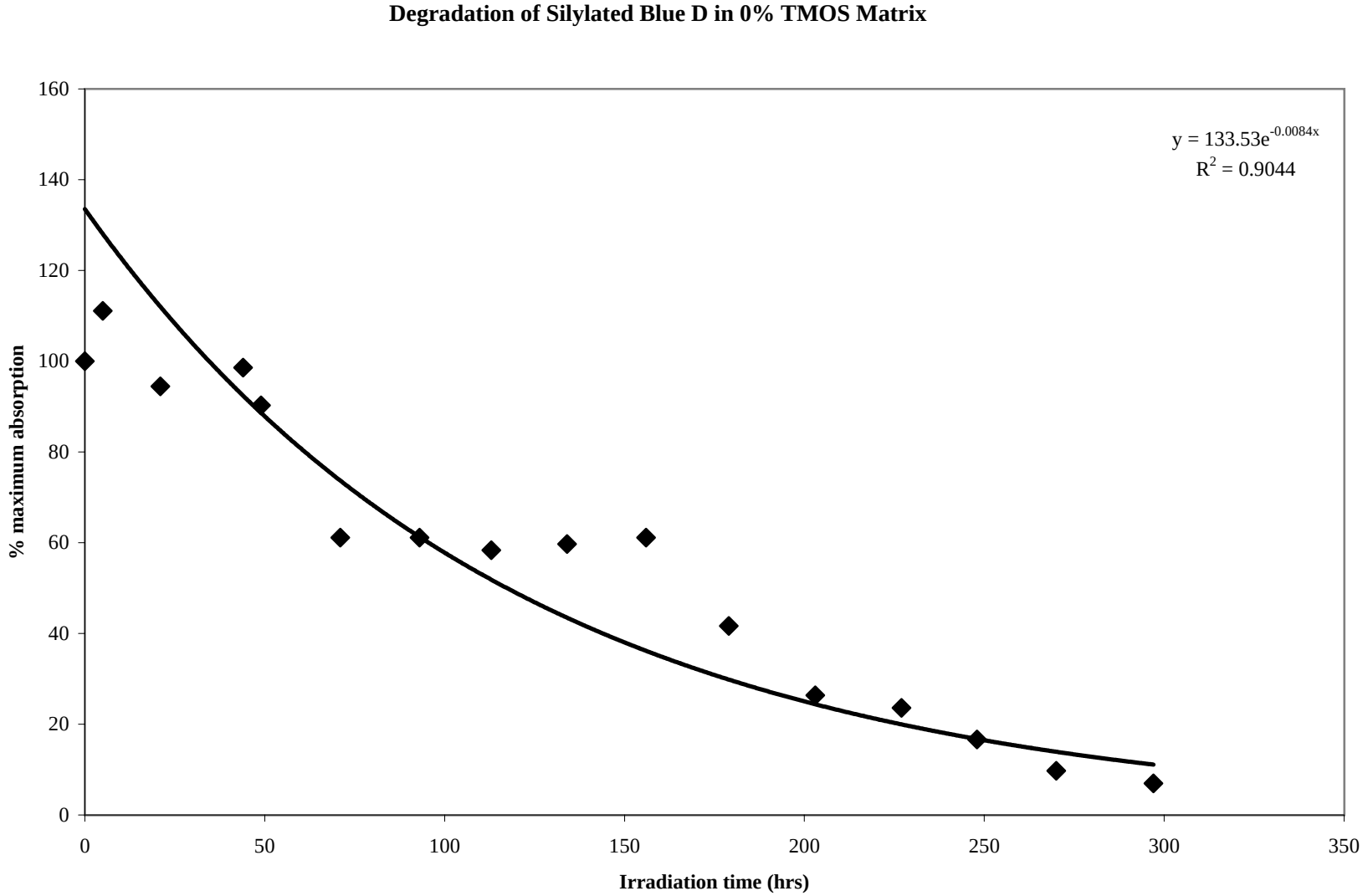
Degradation of Silylated Blue D in 0% TMOS Matrix
y = 133.53e-0.0084x
R2 = 0.9044
% maximum absorption
Irradiation time (hrs)
0
20
40
60
80
100
120
140
160
0
50
100
150
200
250
300
350

Degradation of Silylated Blue D in Silica Particle Matrix

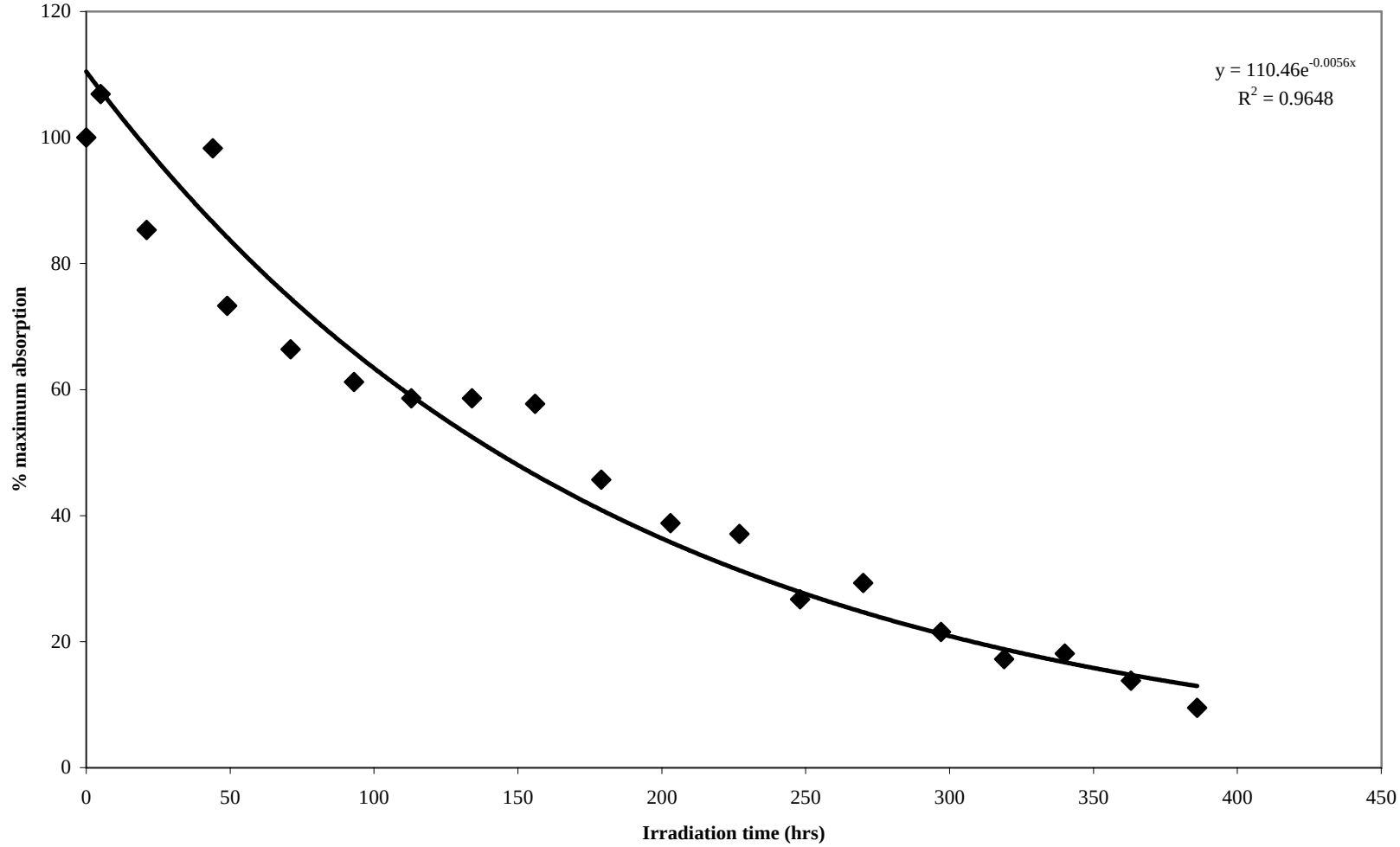

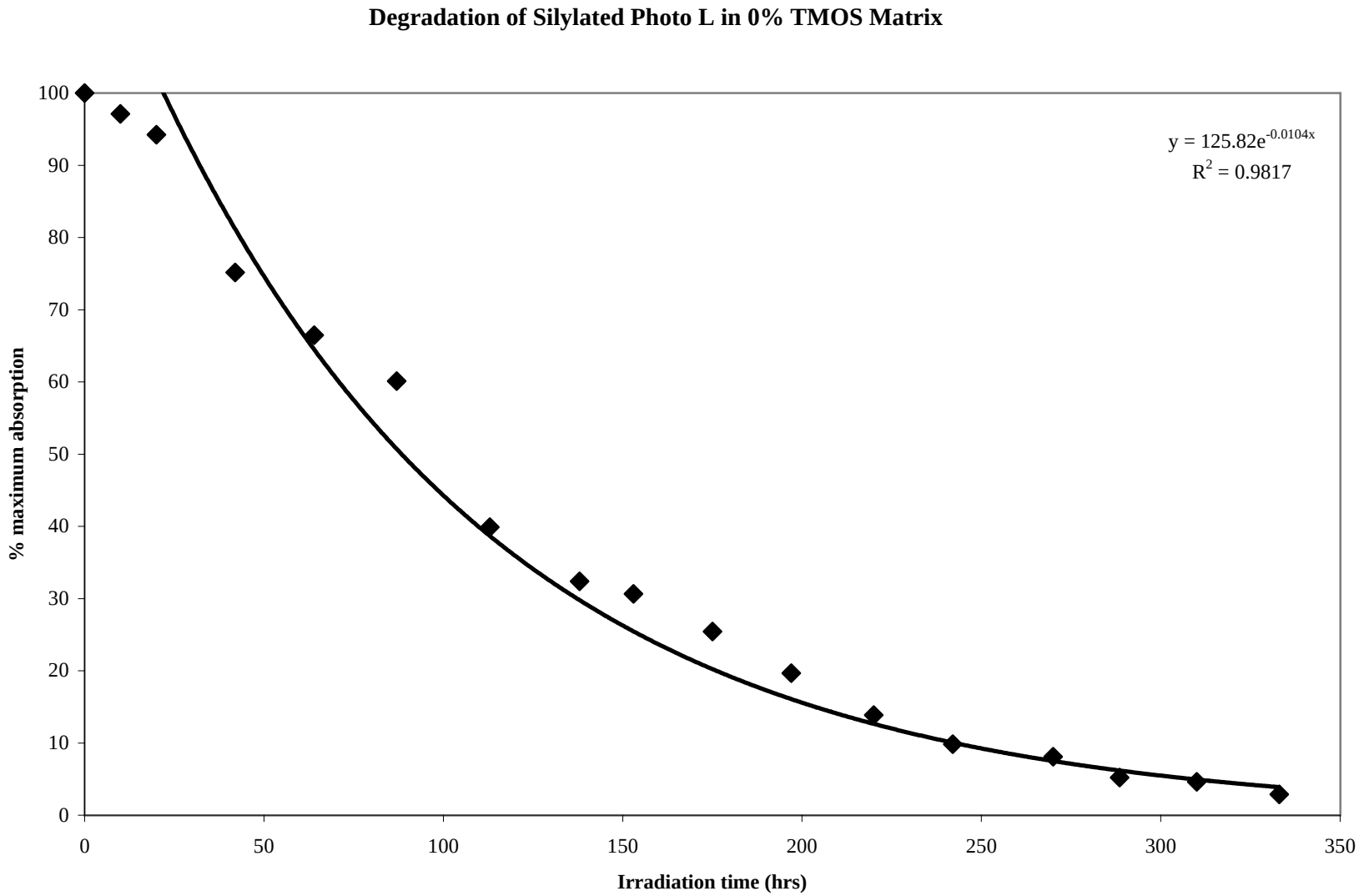
Degradation of Silylated Photo L in 0% TMOS Matrix
y = 125.82e-0.0104x
R2 = 0.9817
% maximum absorption
Irradiation time (hrs)
0
10
20
30
40
50
60
70
80
90
100
0
50
100
150
200
250
300
350

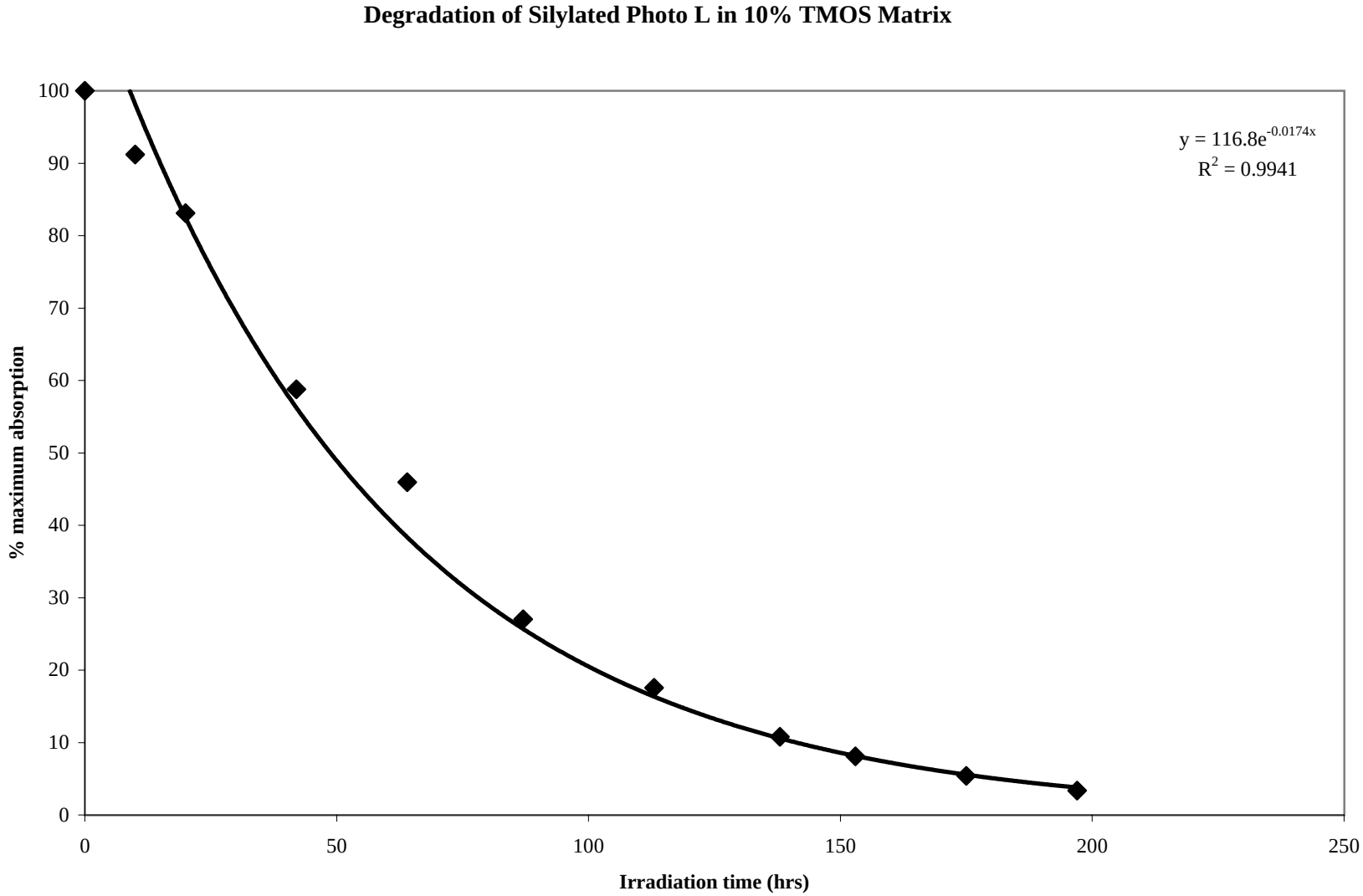
Degradation of Silylated Photo L in 10% TMOS Matrix
y = 116.8e-0.0174x
R2 = 0.9941
% maximum absorption
Irradiation time (hrs)
0
10
20
30
40
50
60
70
80
90
100
0
50
100
150
200
250

Degradation of Silylated Photo L in Silica Particle Matrix

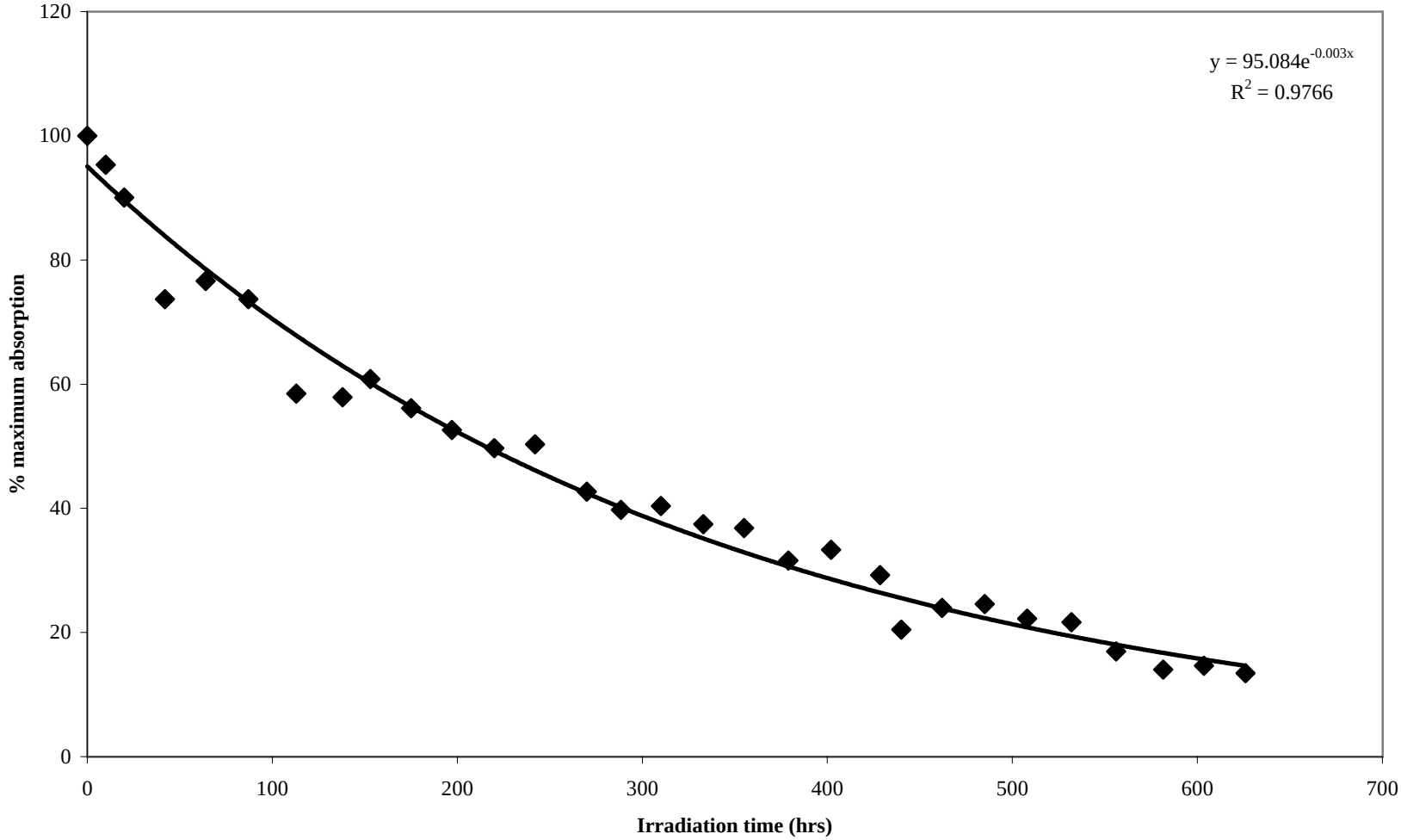

Appendix 2

Blue A in 0% TMOS Matrix at 29.1° C - First Order Kinetic Plot

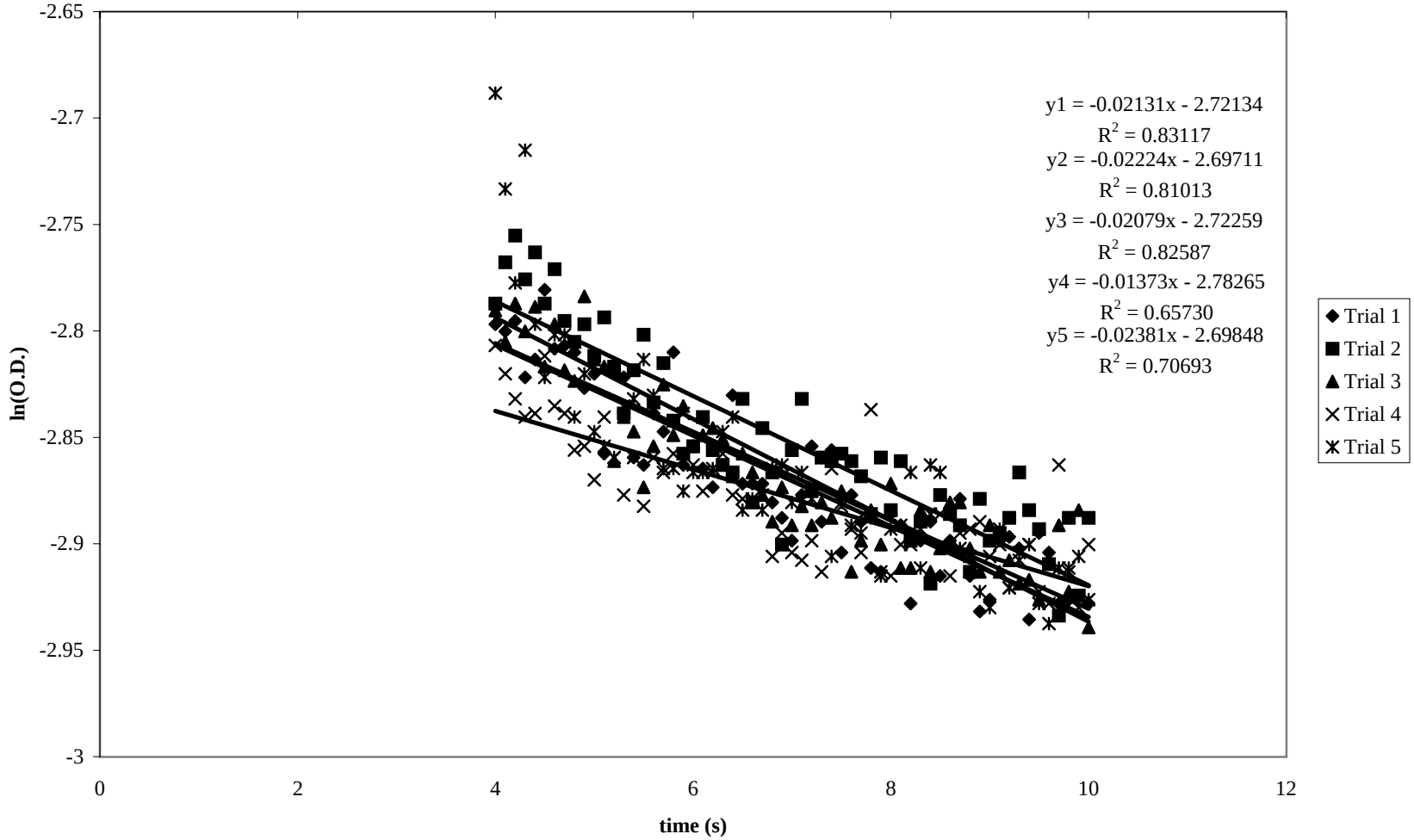

Blue A in 0% TMOS at 24.7° C - First Order Kinetic Plot

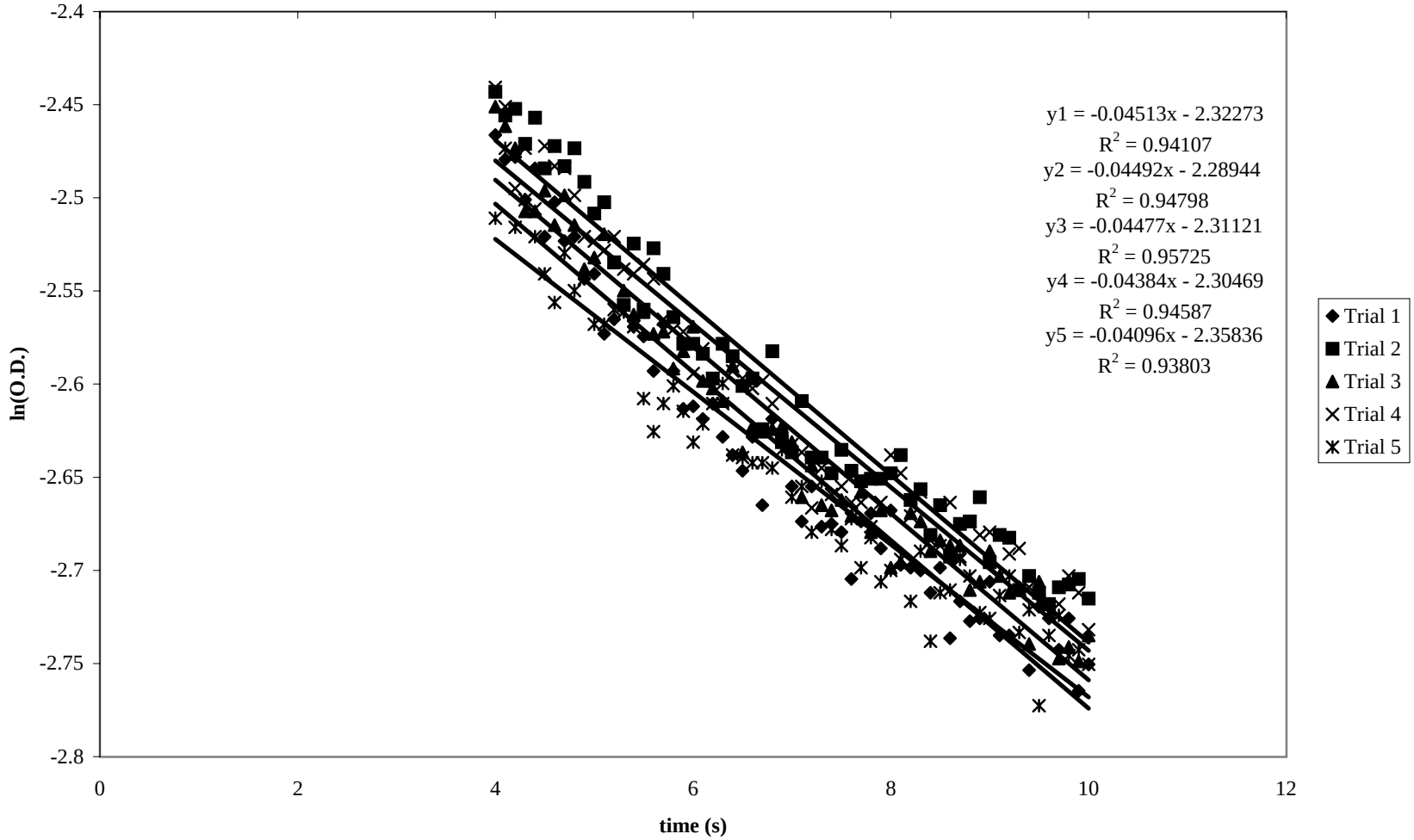

Blue A in 0% TMOS Matrix at 20.2° C - First Order Kinetic Plot

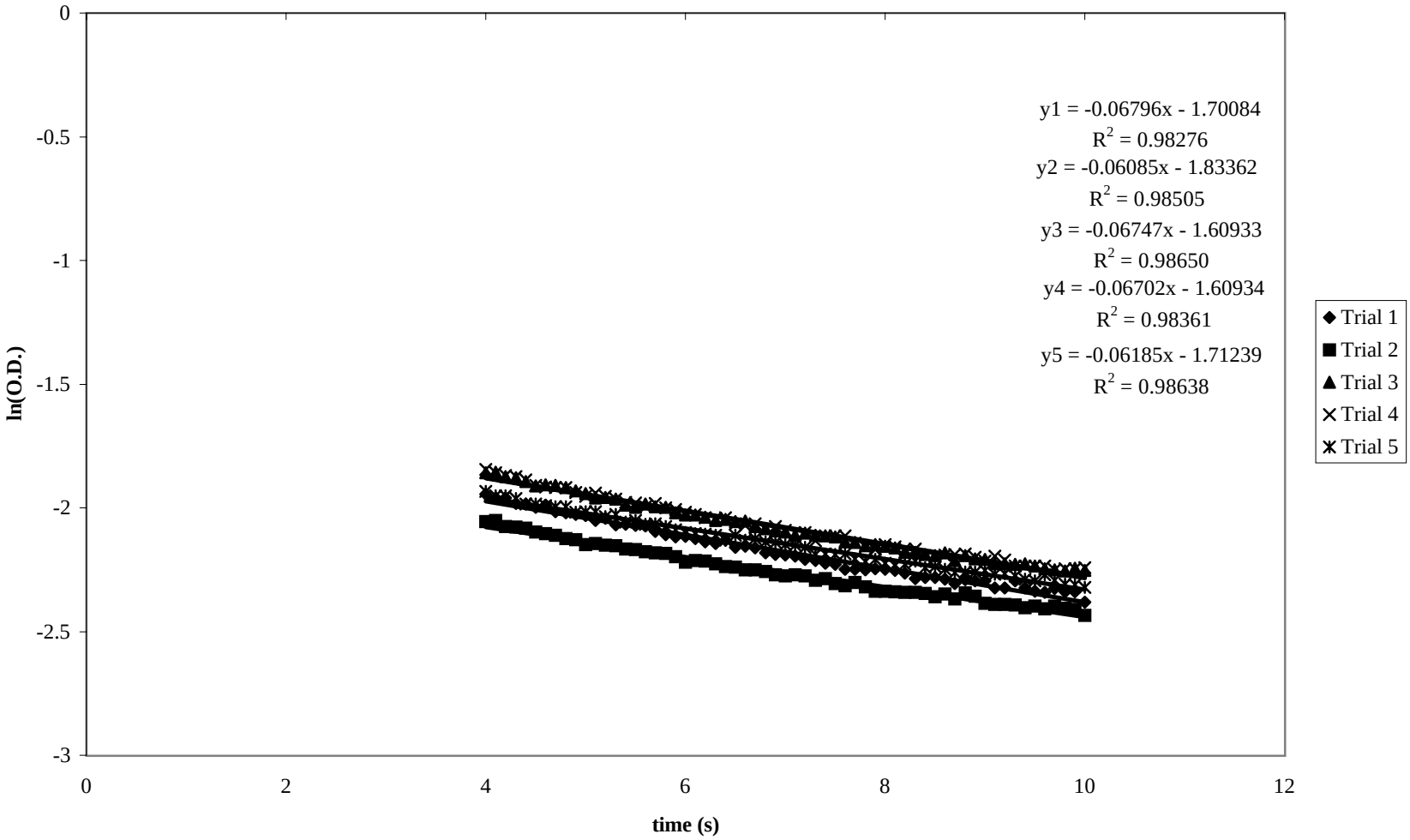

A2-3

Blue A in 0% TMOS Matrix at 15.1° C - First Order Kinetic Plot

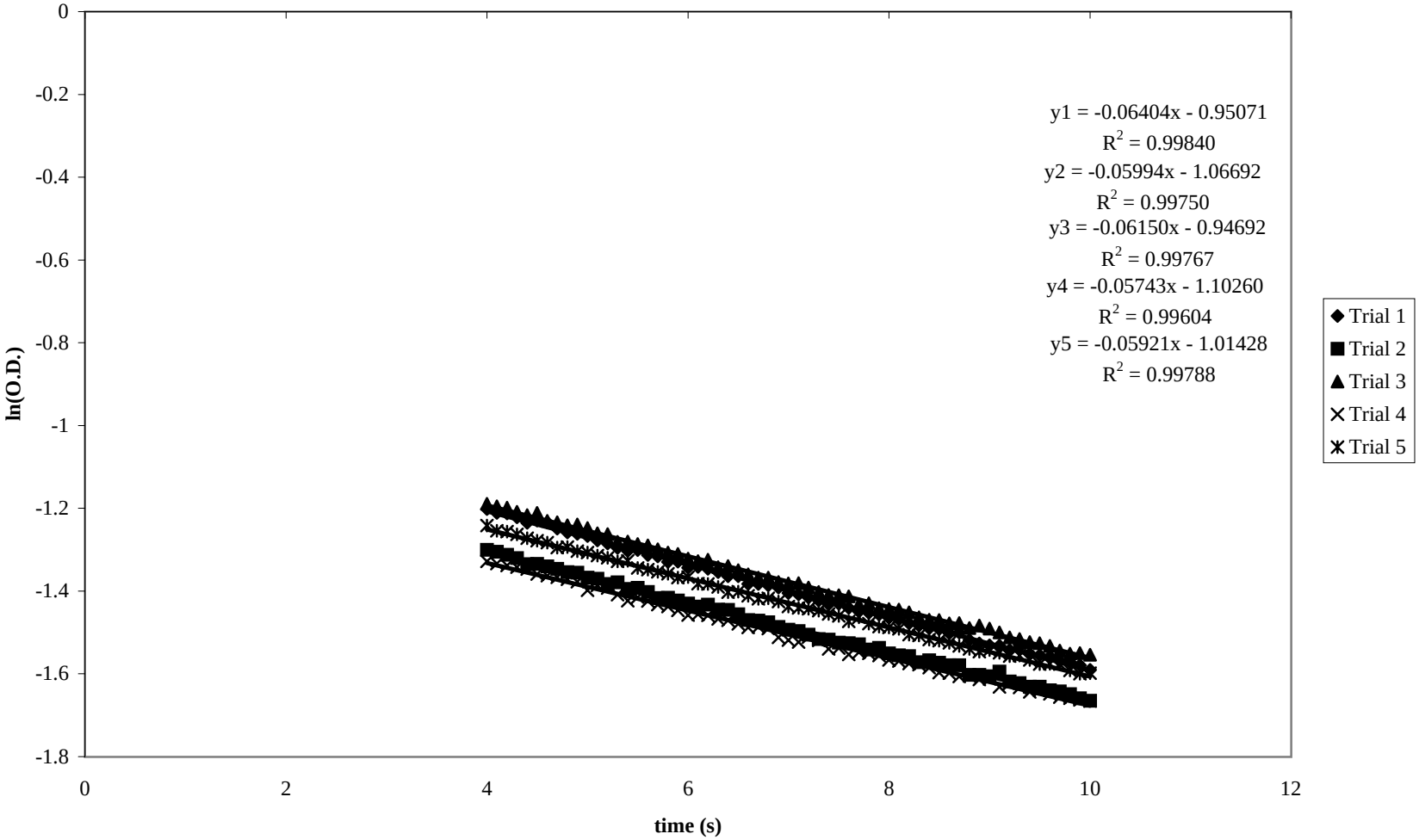

Blue A in 0% TMOS Matrix at 10.3° C - First Order Kinetic Plot

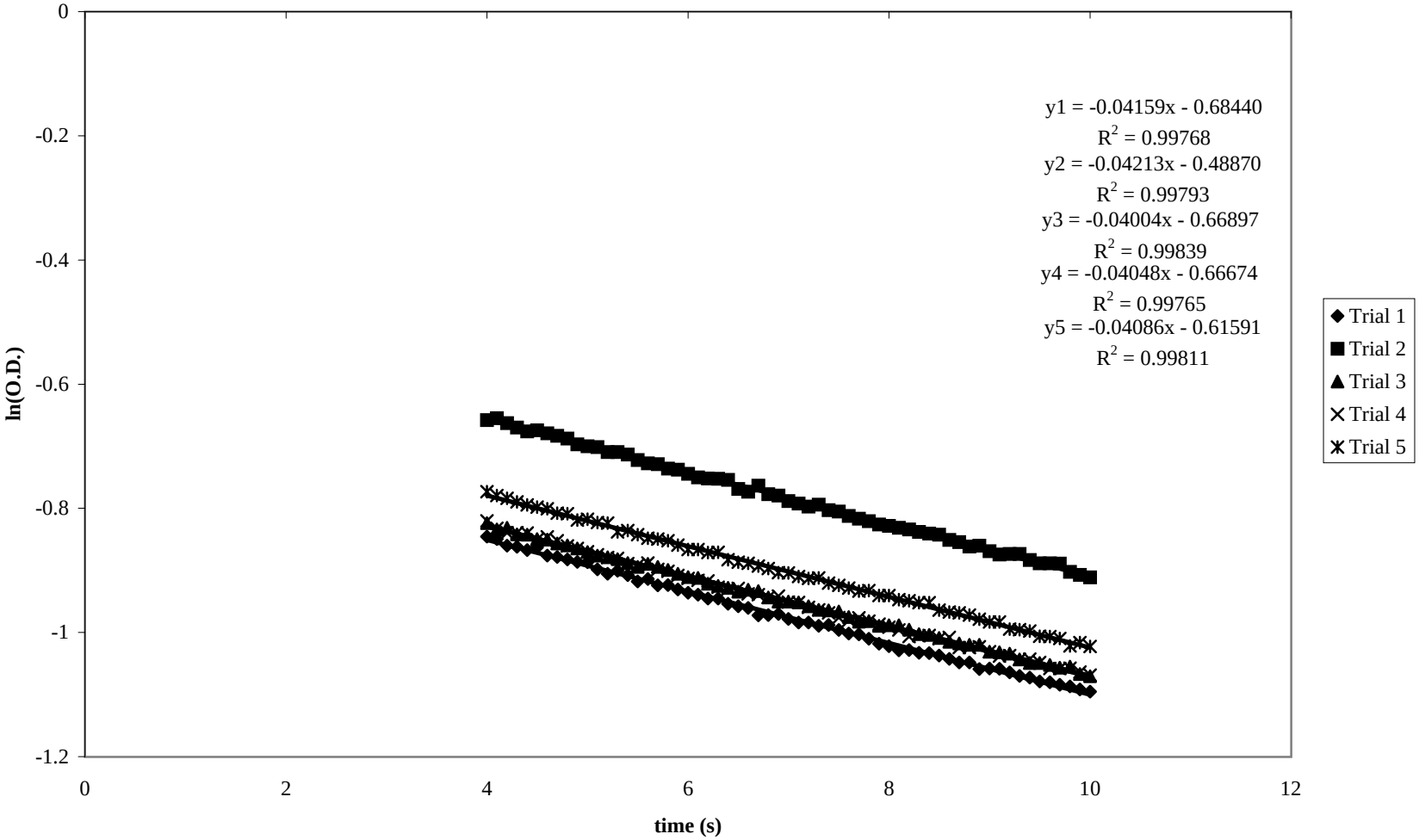

Blue A in 0% TMOS at 5.6° C - First Order Plot

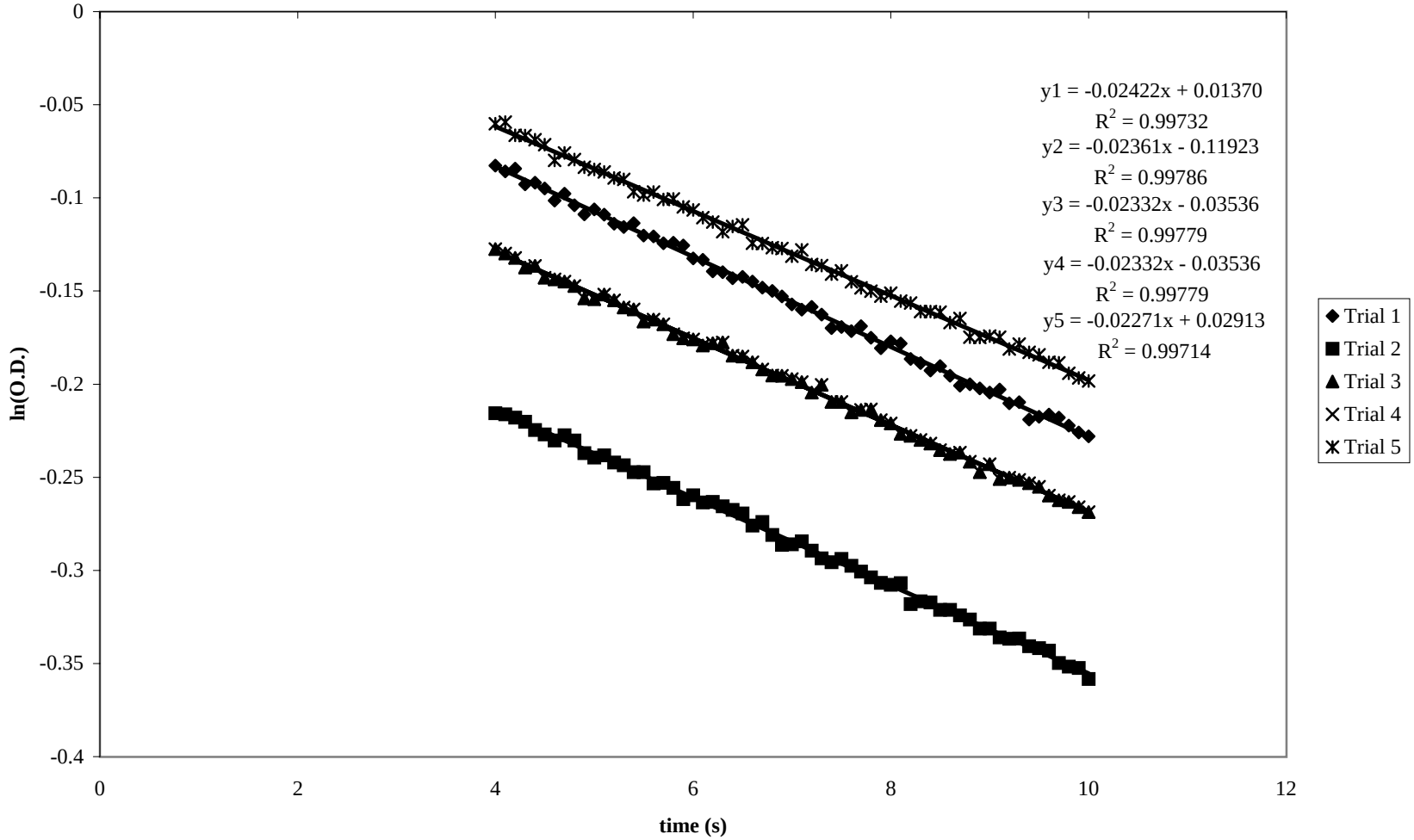

Blue A in 10% TMOS Matrix at 29.1° C - First Order Kinetic Plot

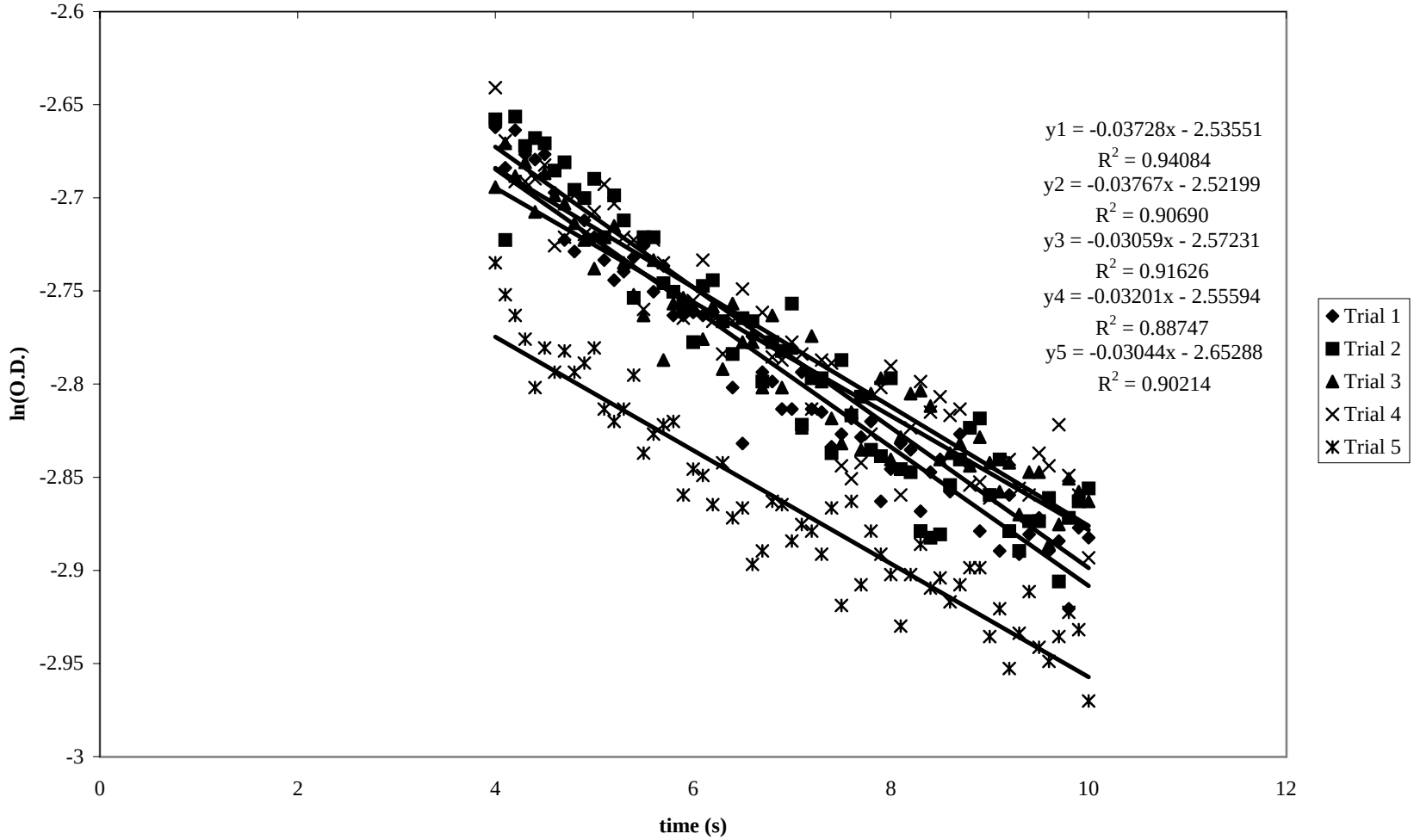

Blue A in 10% TMOS at 24.7° C - First Order Kinetic Plot

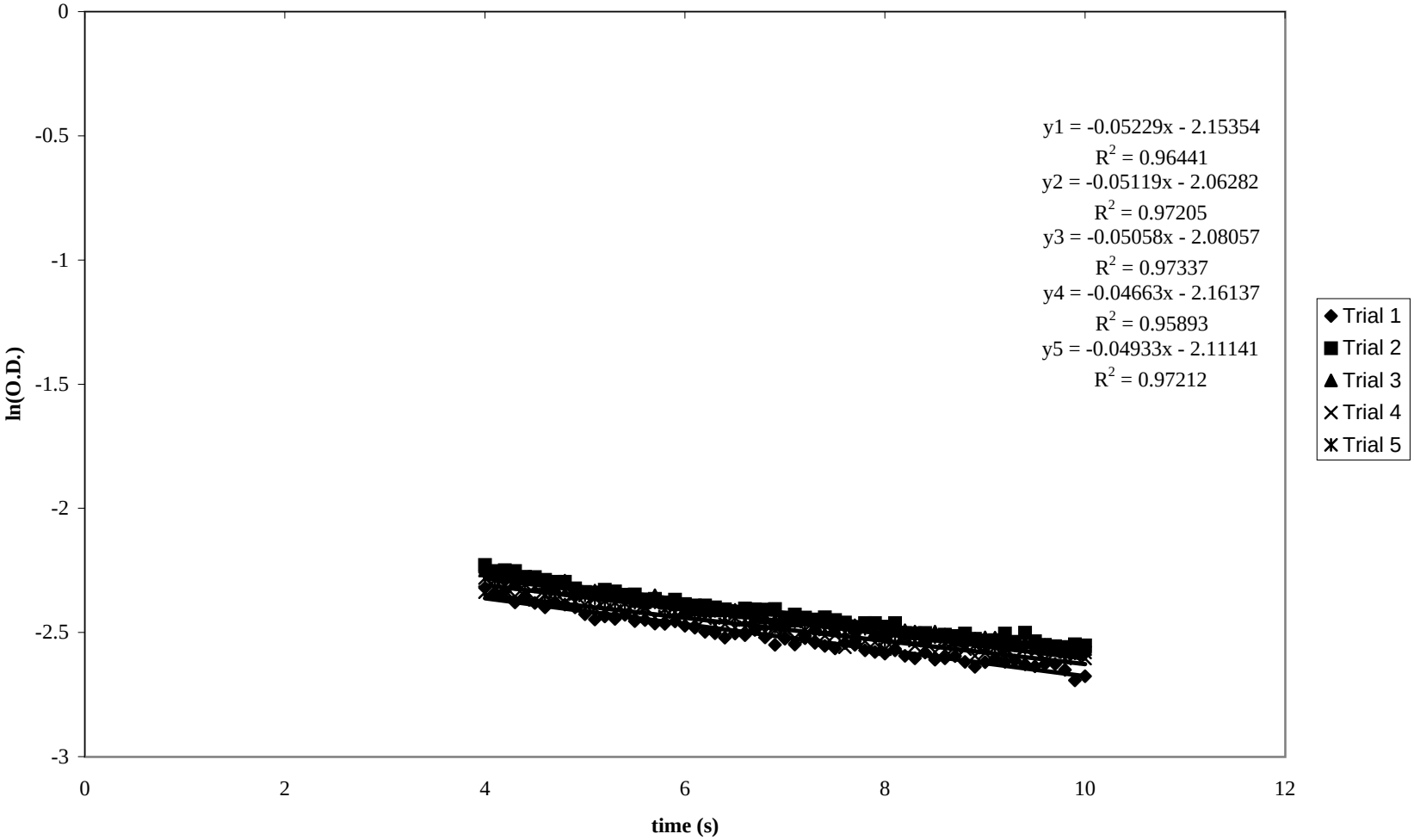

Blue A in 10% TMOS at 20.4° C - First Order Kinetic Plot

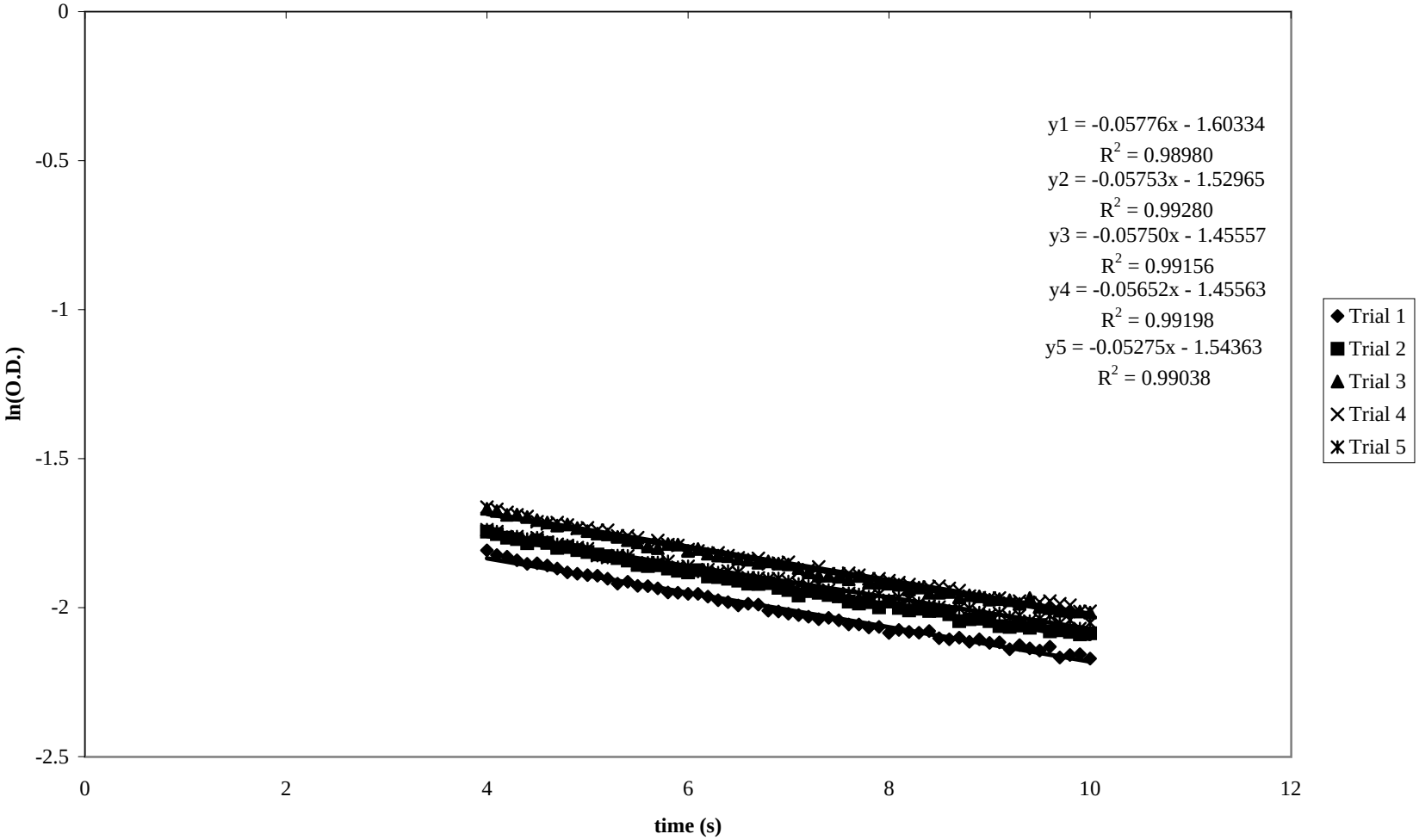

Blue A in 10% TMOS Matrix at 15.2° C - First Order Kinetic Plot

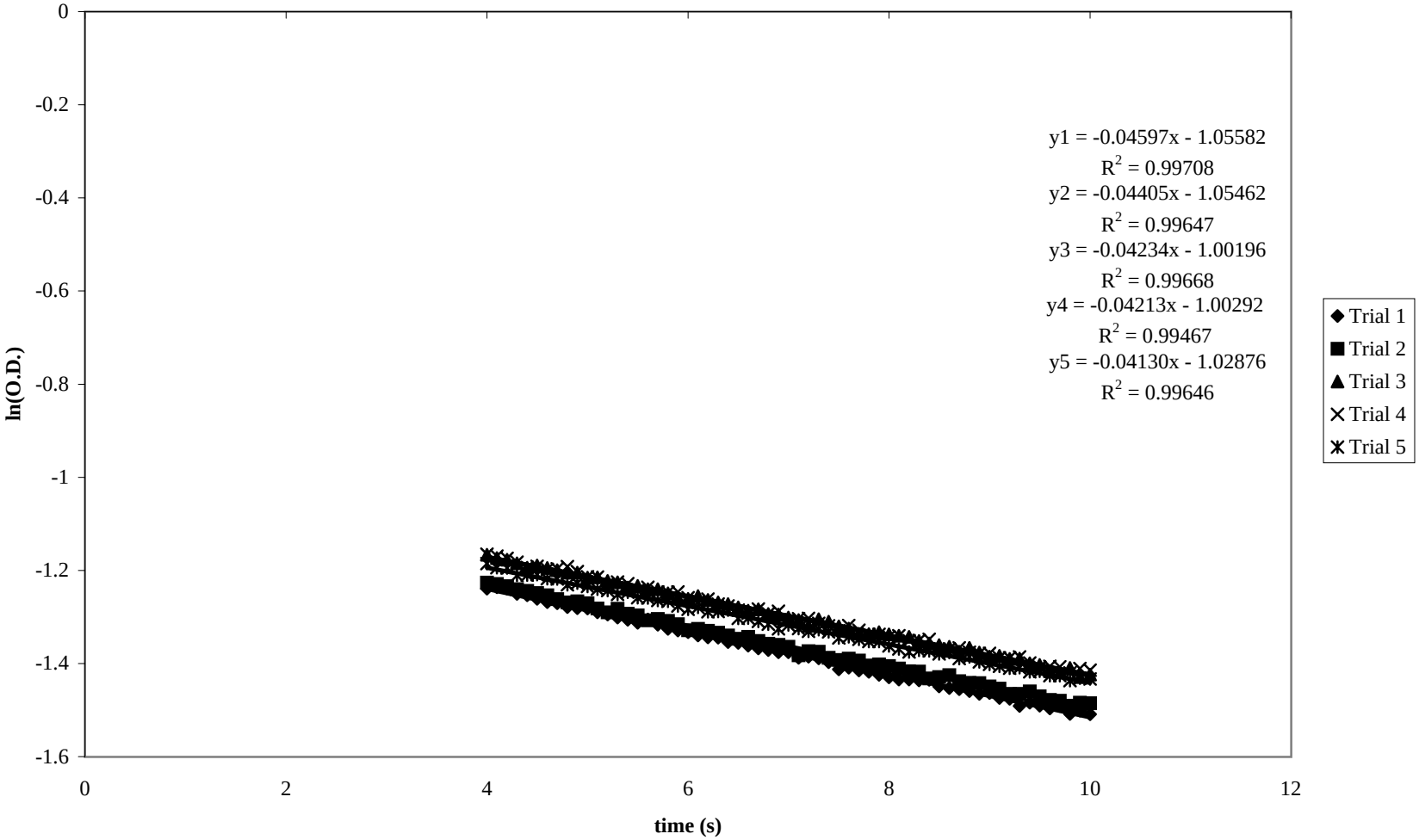

Blue A in 10% TMOS at 10.6° C - First Order Kinetic Plot

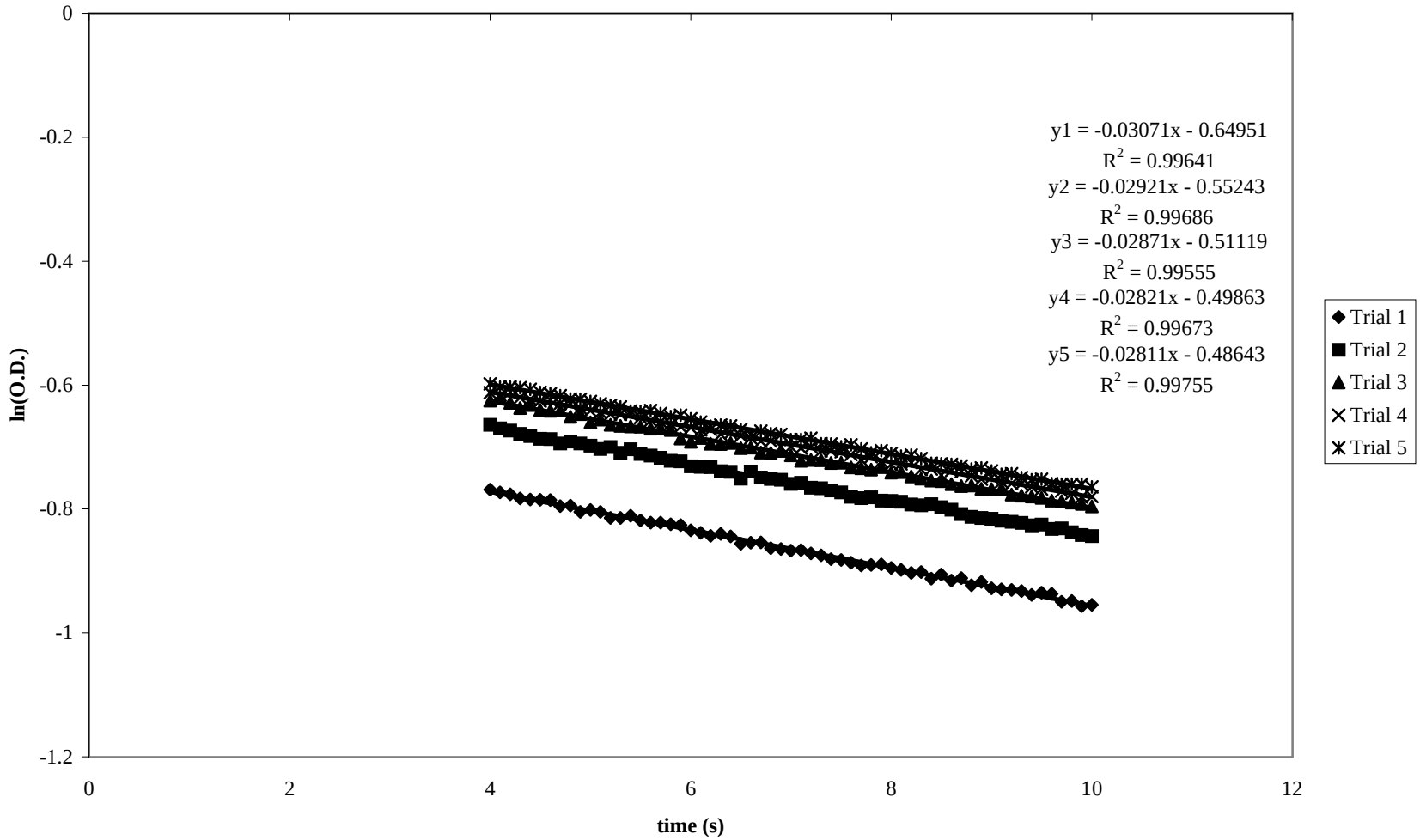

Blue A in 10% TMOS at 6.4° C - First Order Kinetic Plot

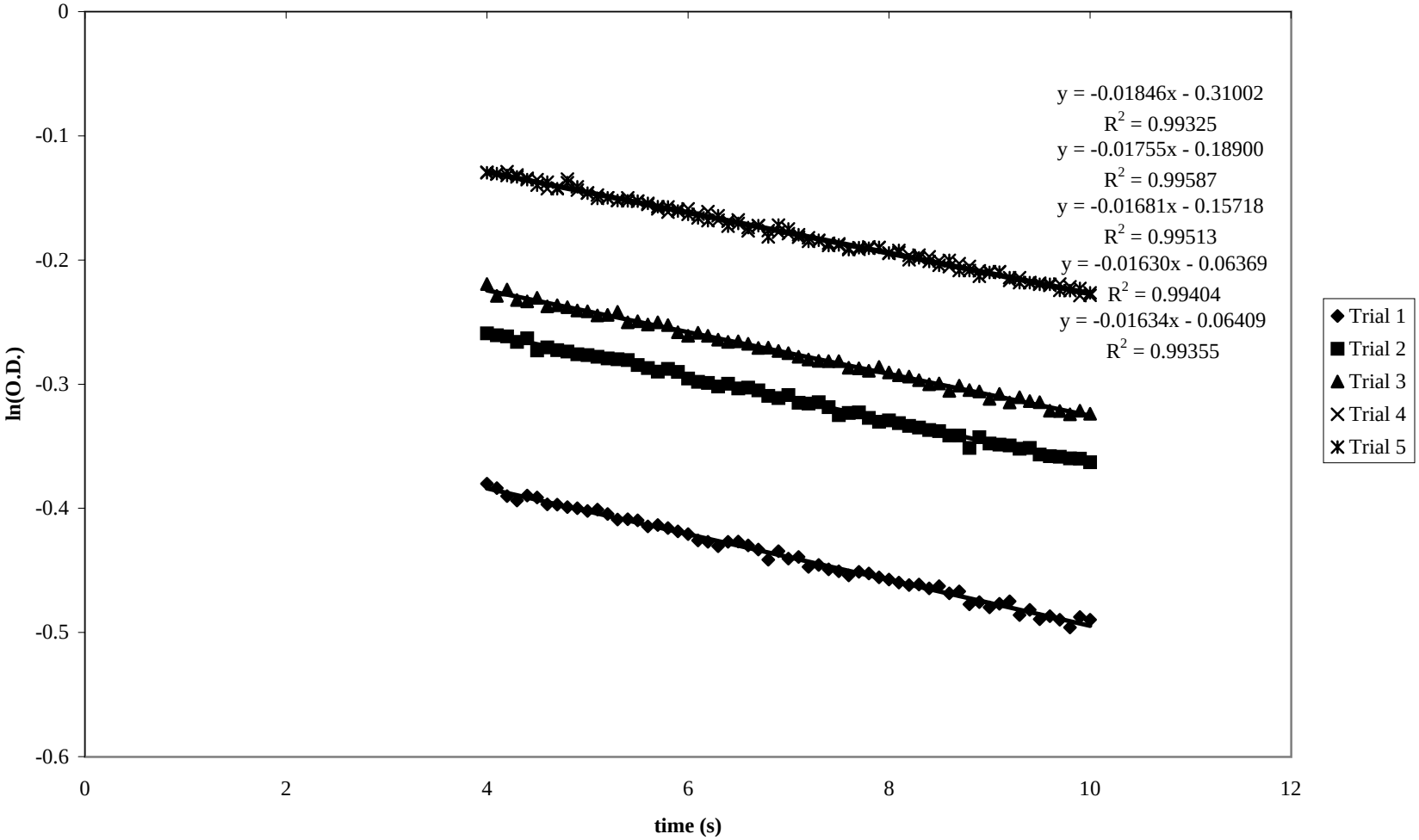

Blue A in 25% TMOS Matrix at 29.1° C - First Order Kinetic Plot

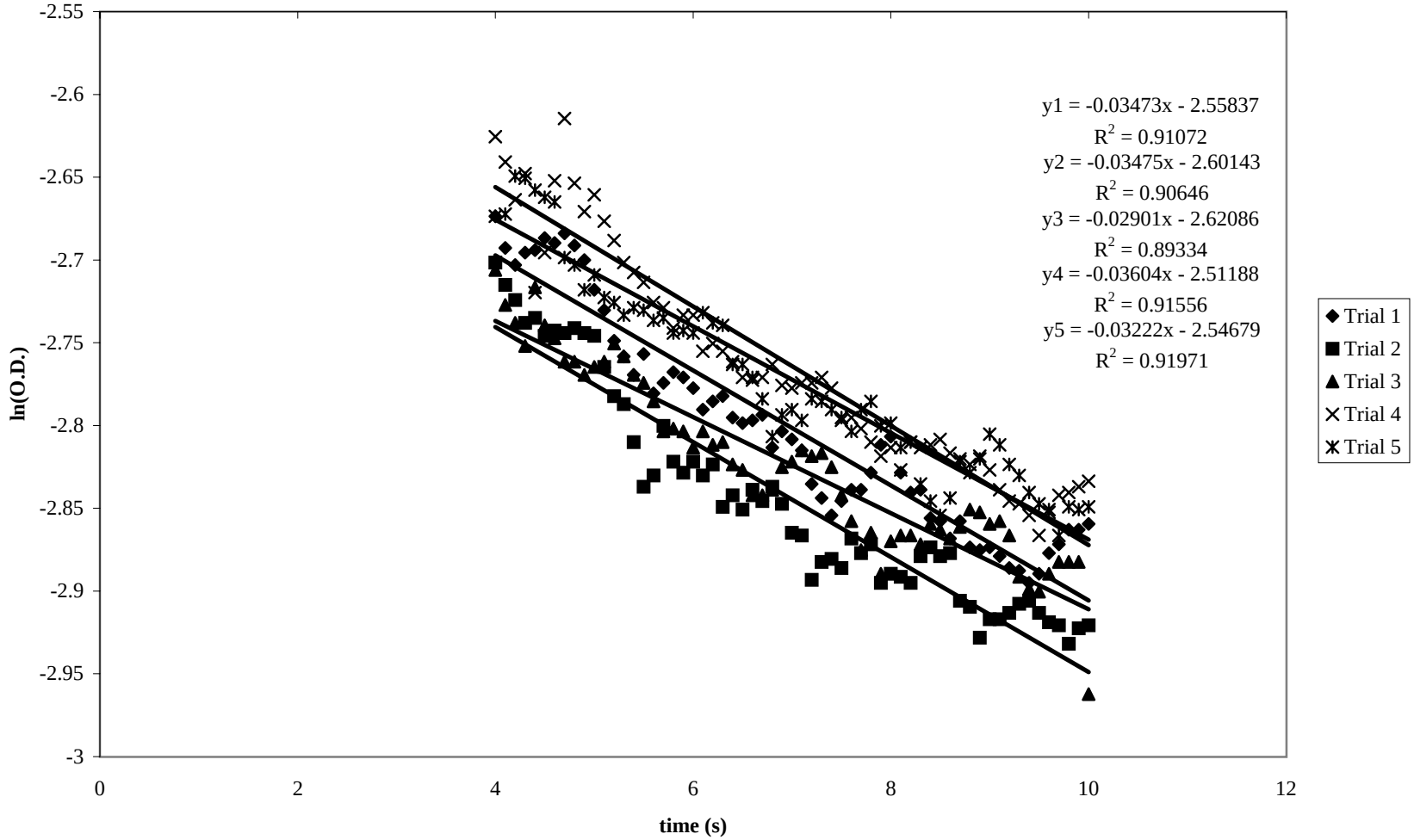

Blue A in 25% TMOS Matrix at 24.7° C - First Order Kinetic Plot

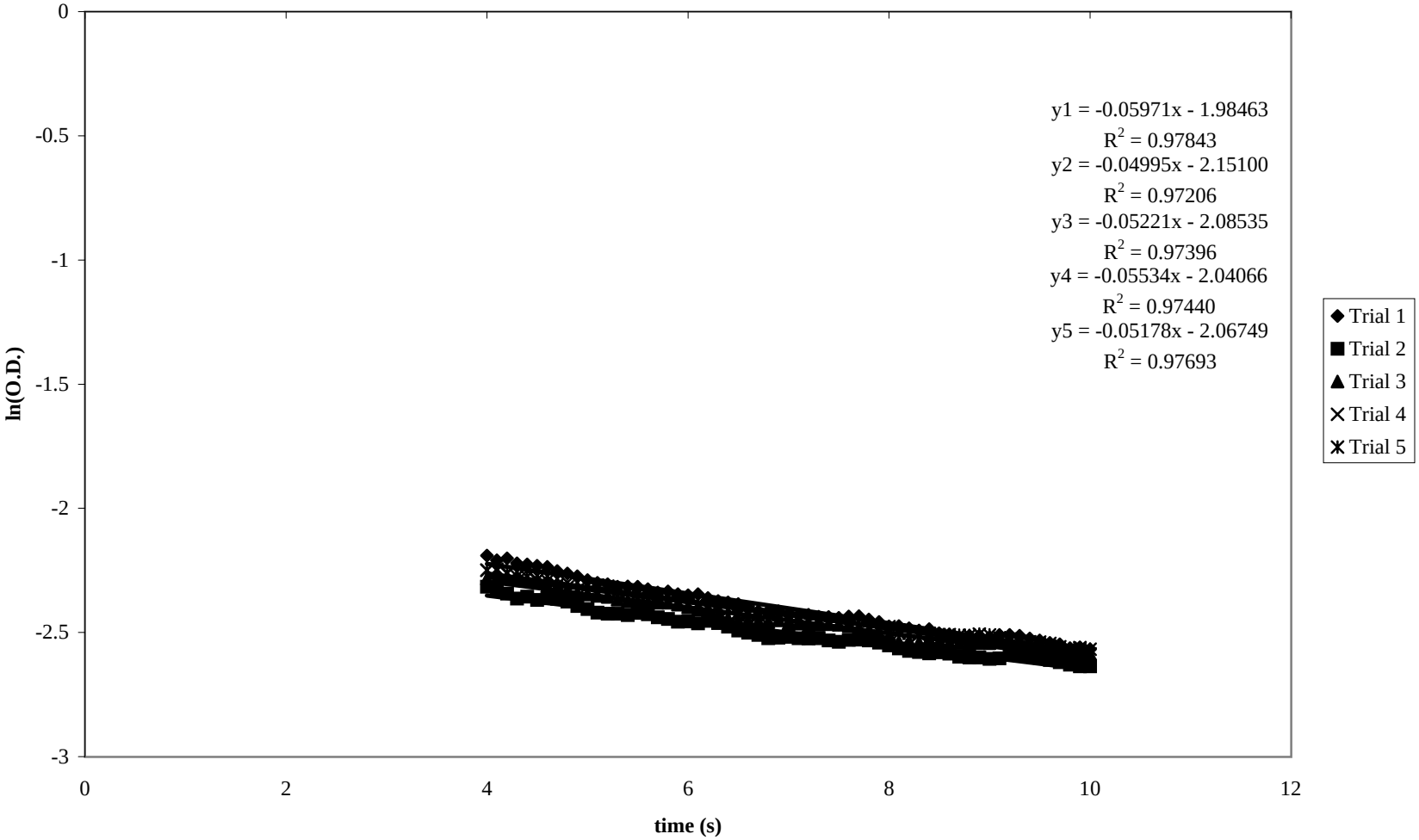

Blue A in 25% TMOS at 20.2° C - First Order Kinetic Plot

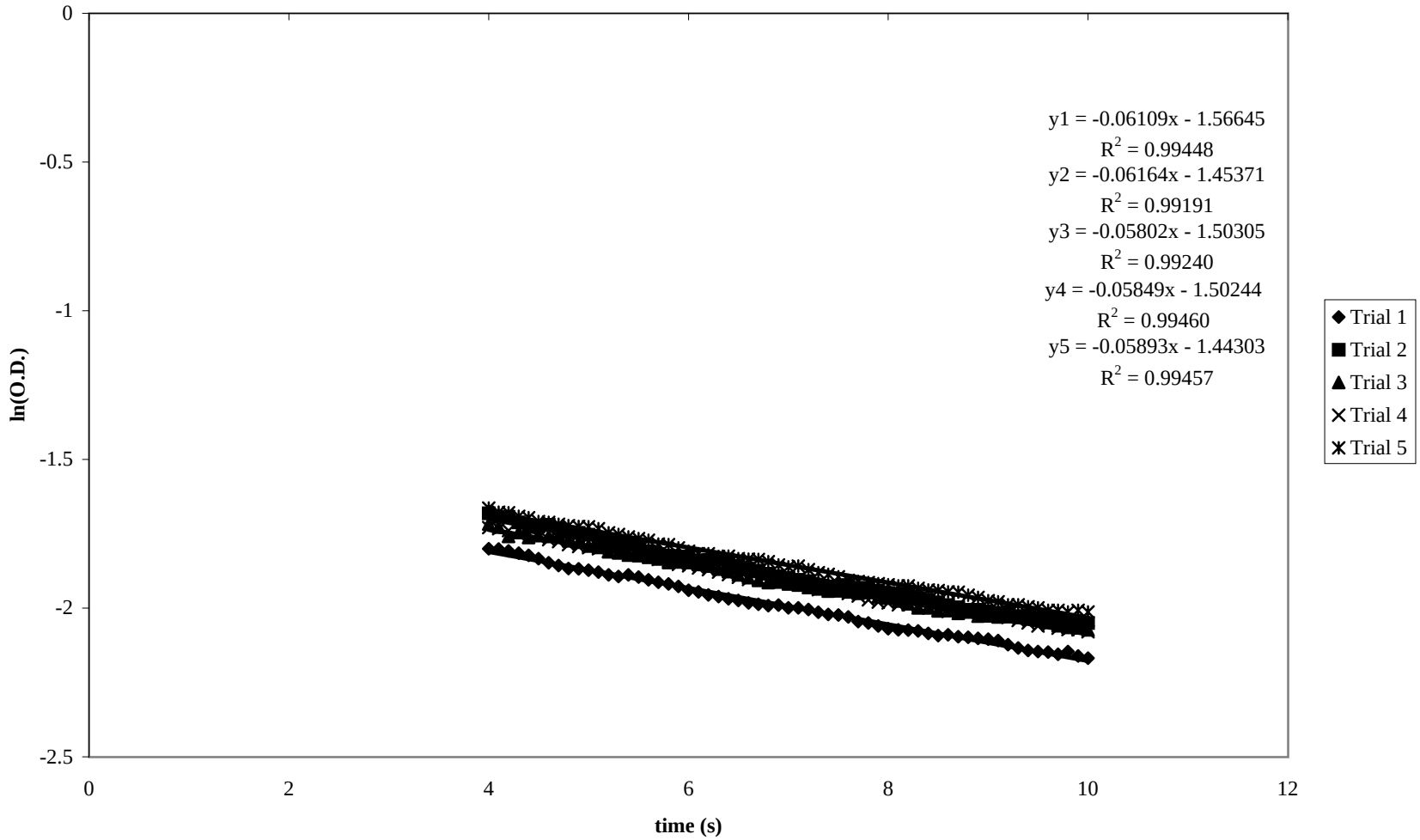

Blue A in 25% TMOS at 15.2° C - First Order Kinetic Plot

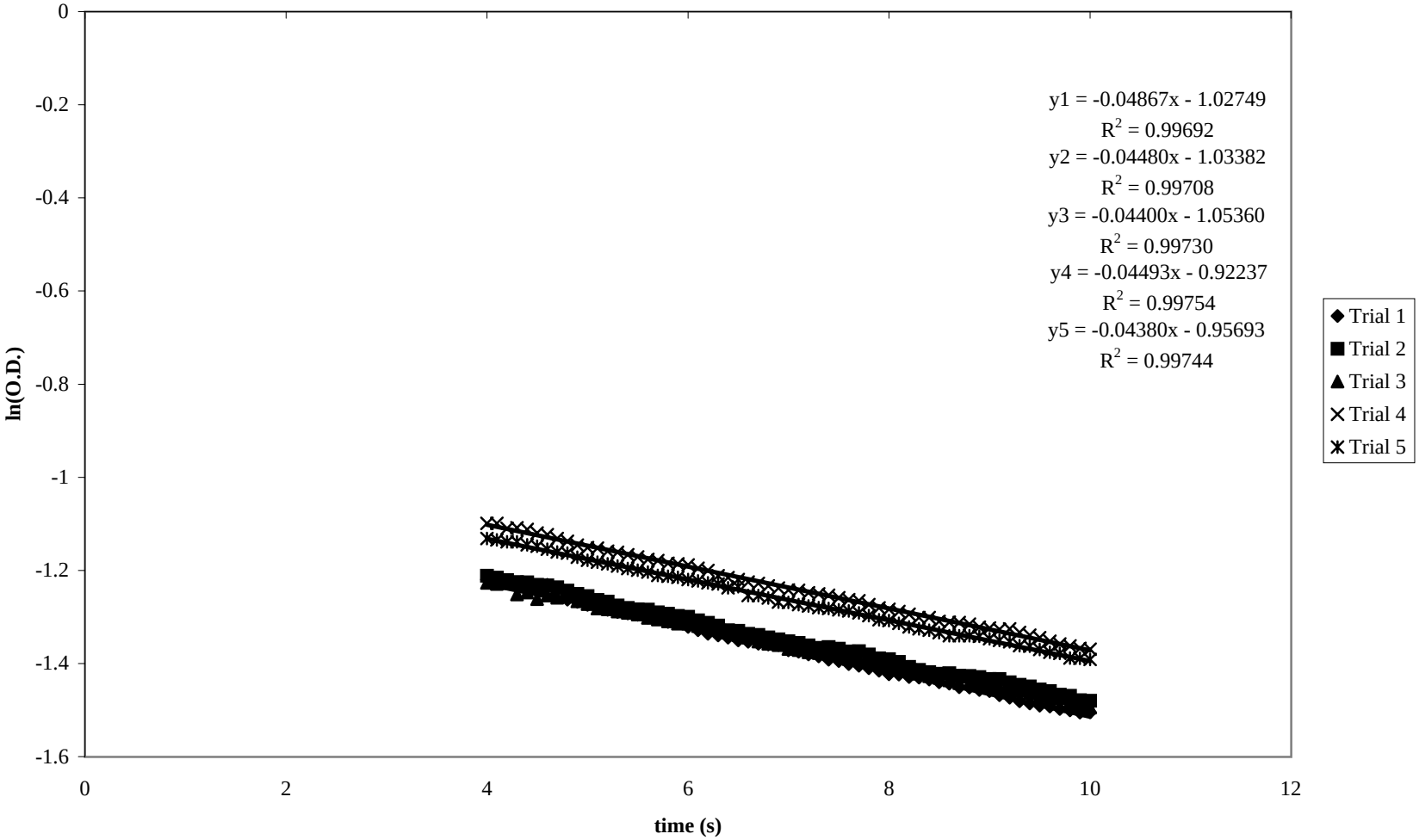

Blue A in 25% TMOS at 10.3° C - First Order Kinetic Plot

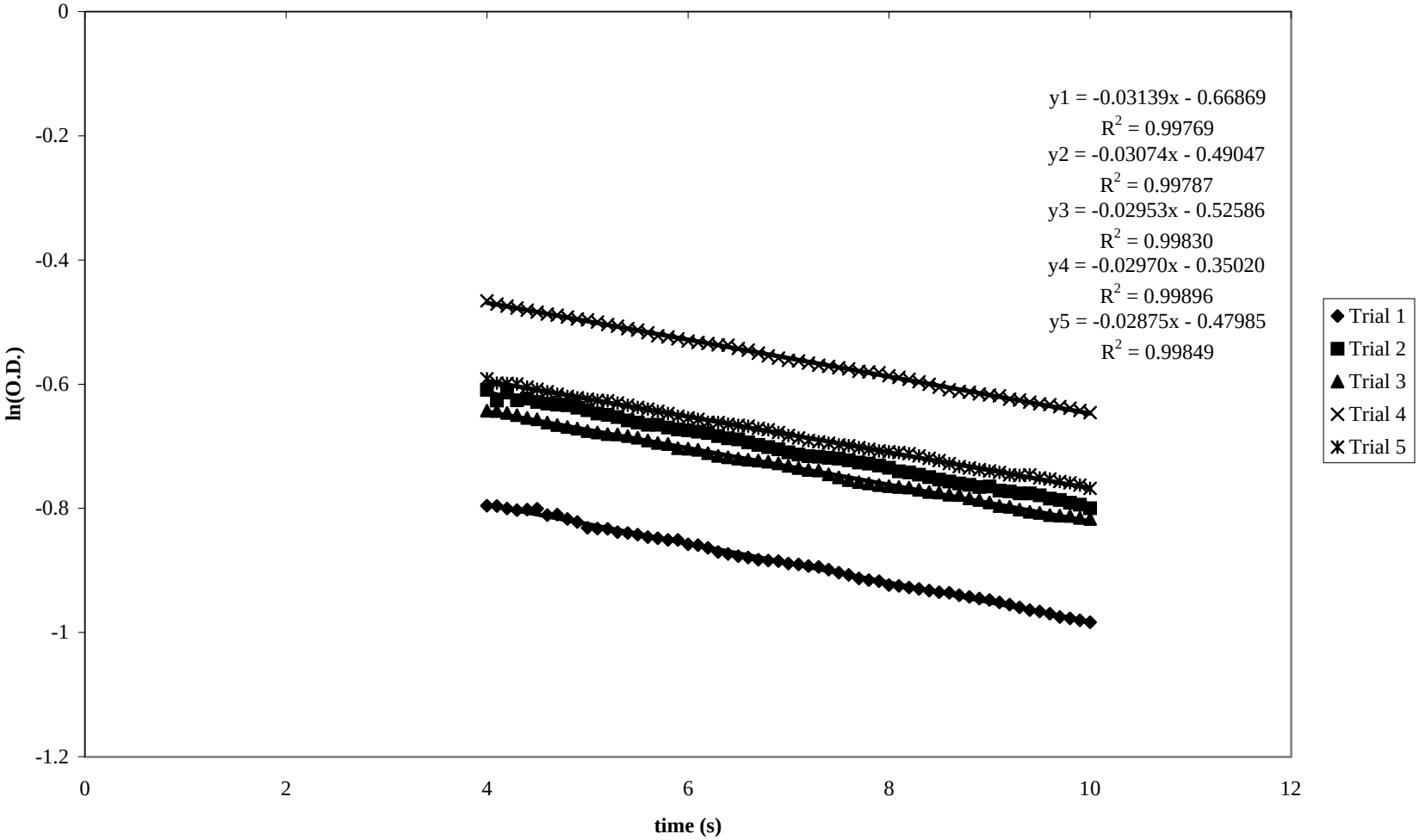

Blue A in 25% TMOS Matrix at 5.3° C - First Order Kinetic Plot

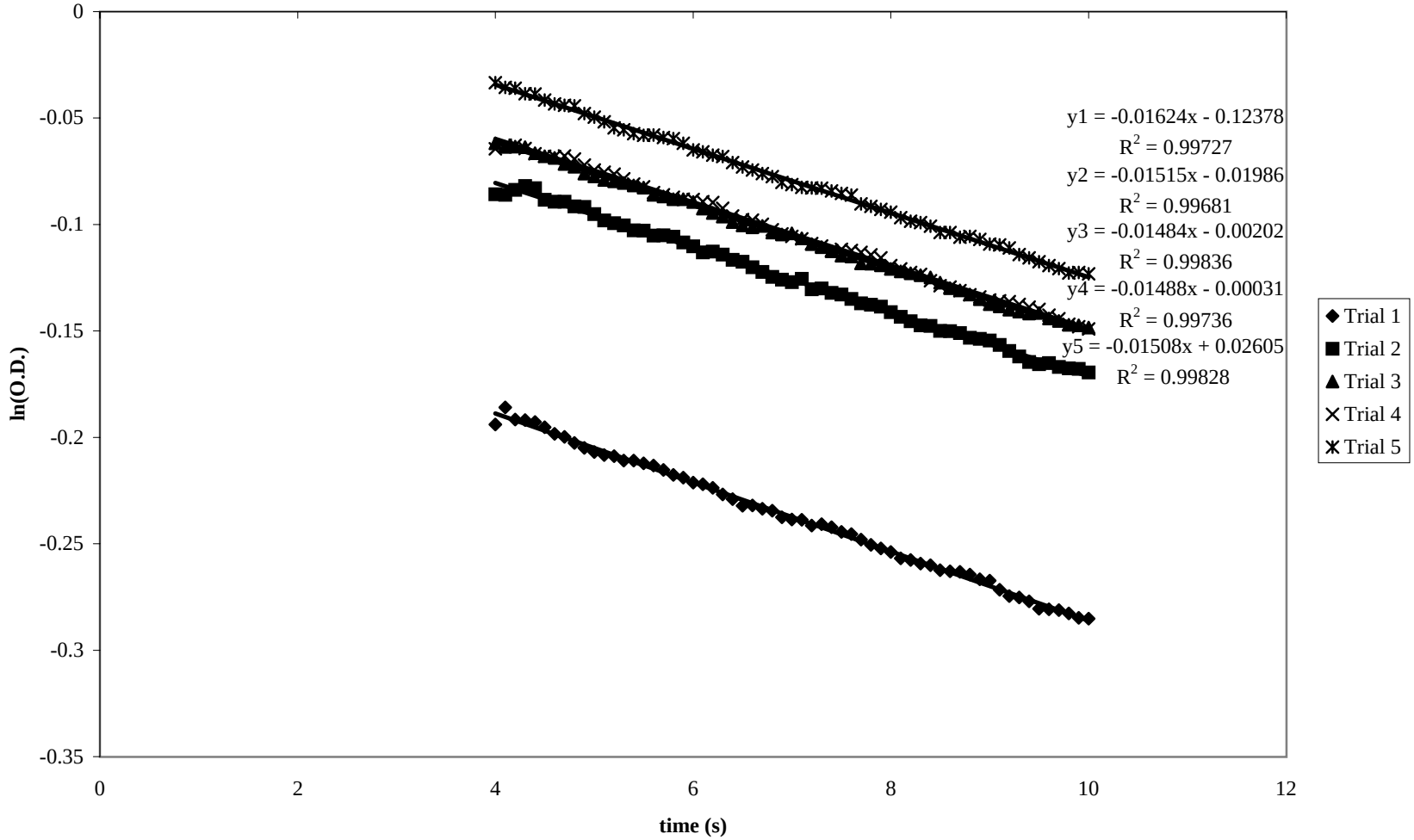

Blue A in 40% TMOS Matrix at 29.1° C - First Order Kinetic Plot

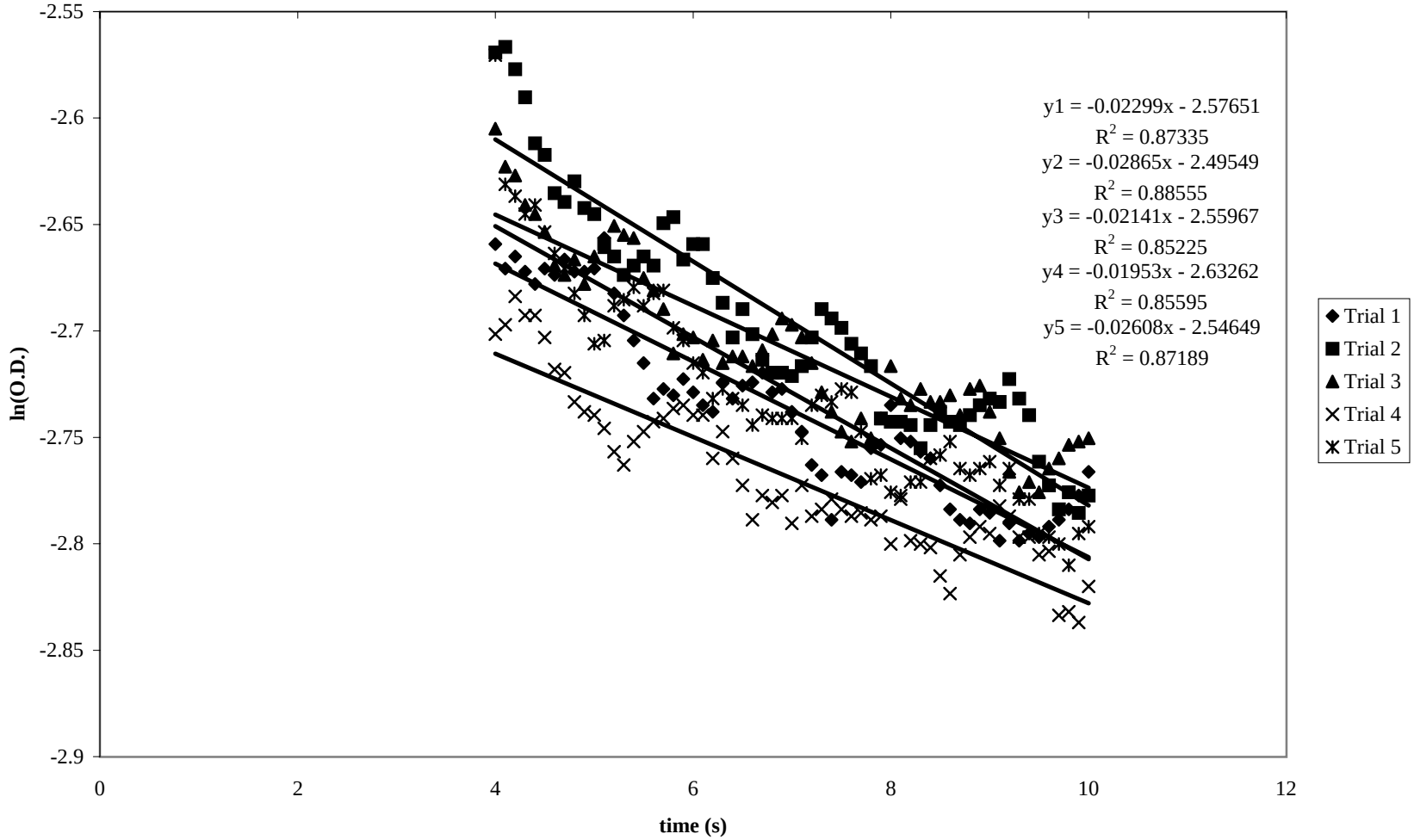

Blue A in 40% TMOS Matrix at 24.8° C - First Order Kinetic Plot

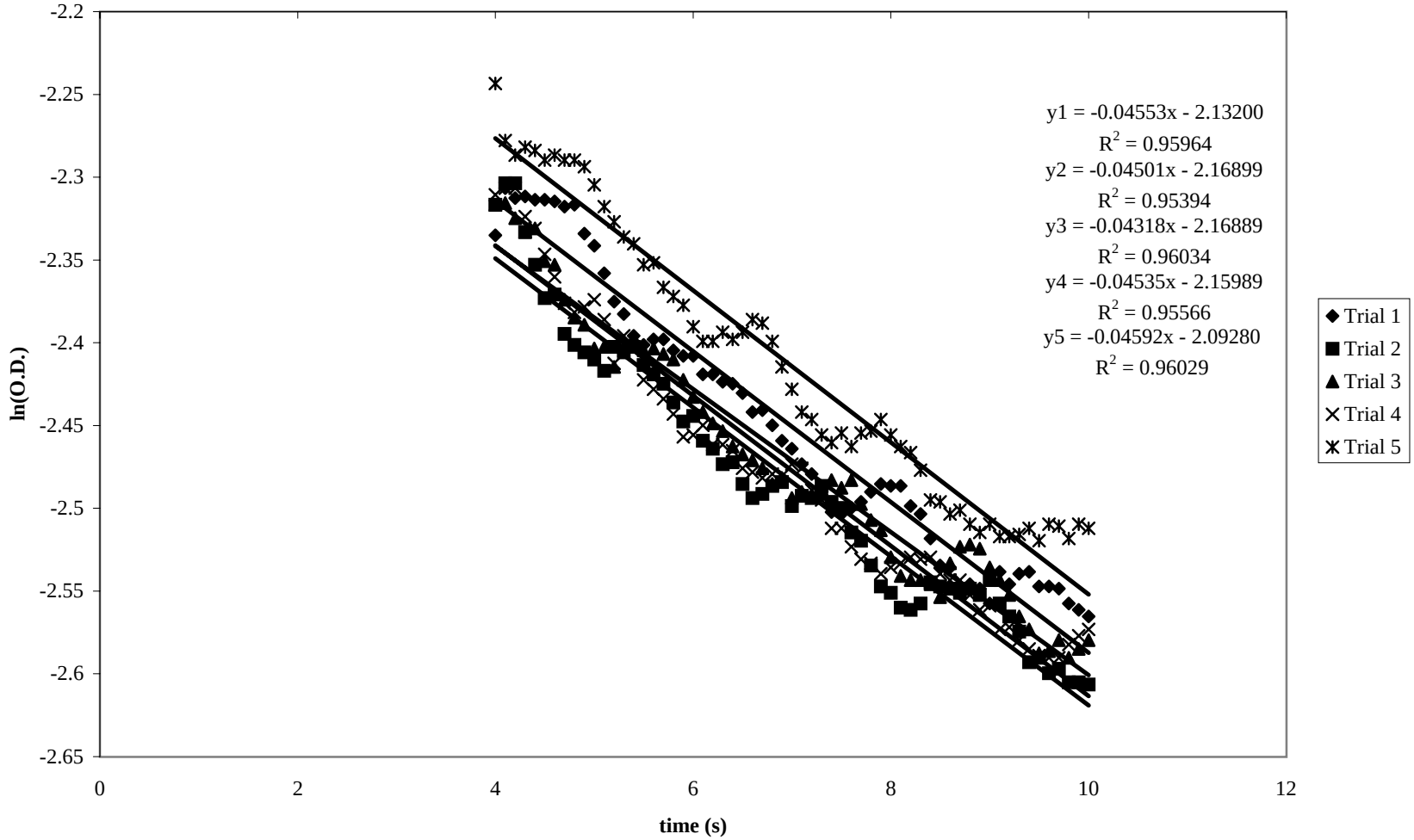

Blue A in 40% TMOS Matrix at 20.4° C - First Order Kinetic Plot

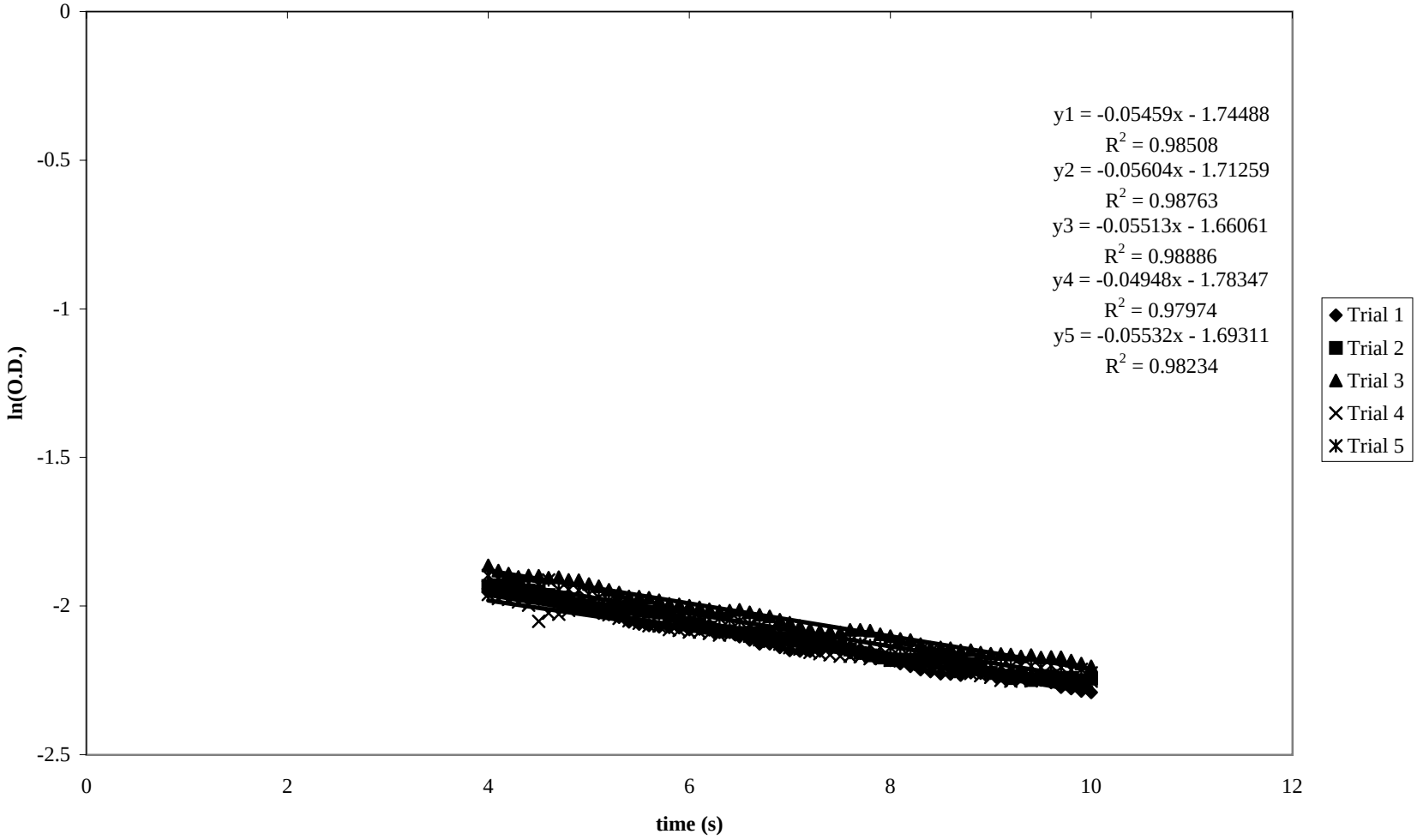

Blue A in 40% TMOS at 15.1° C - First Order Kinetic Plot

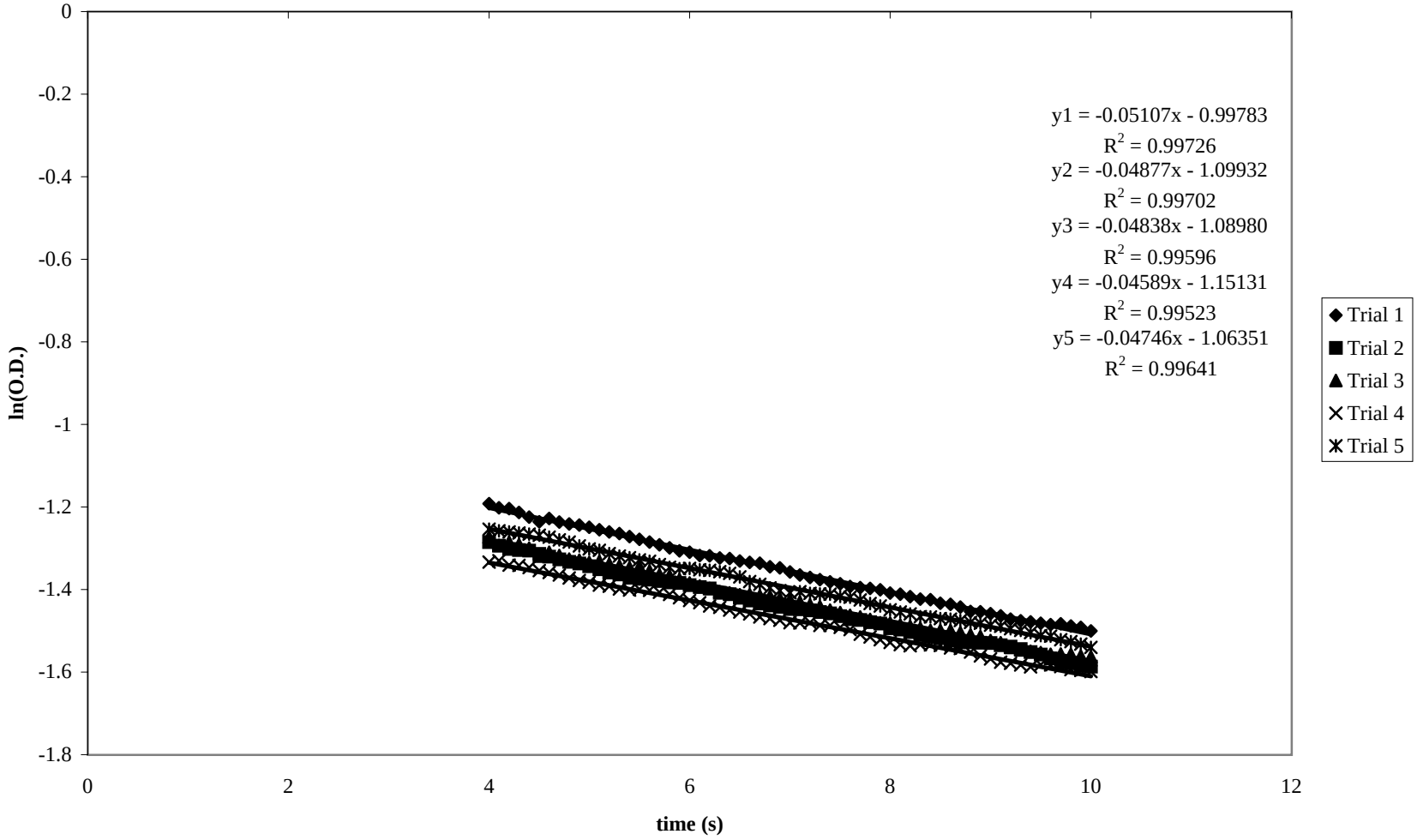

Blue A in 40% TMOS at 10.6° C - First Order Kinetic Plot

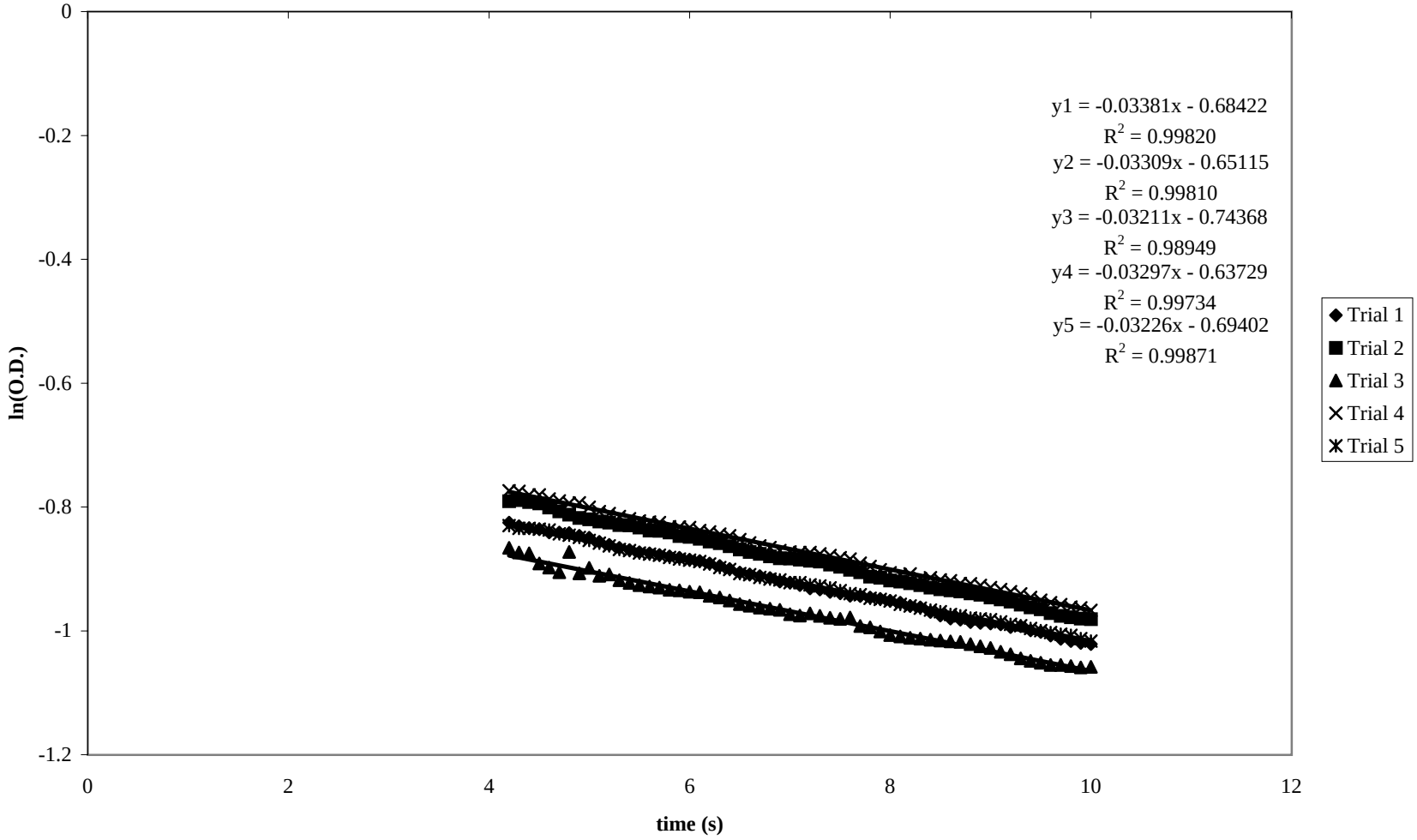

Blue A in 40% TMOS at 6.0° C - First Order Kinetic Plot

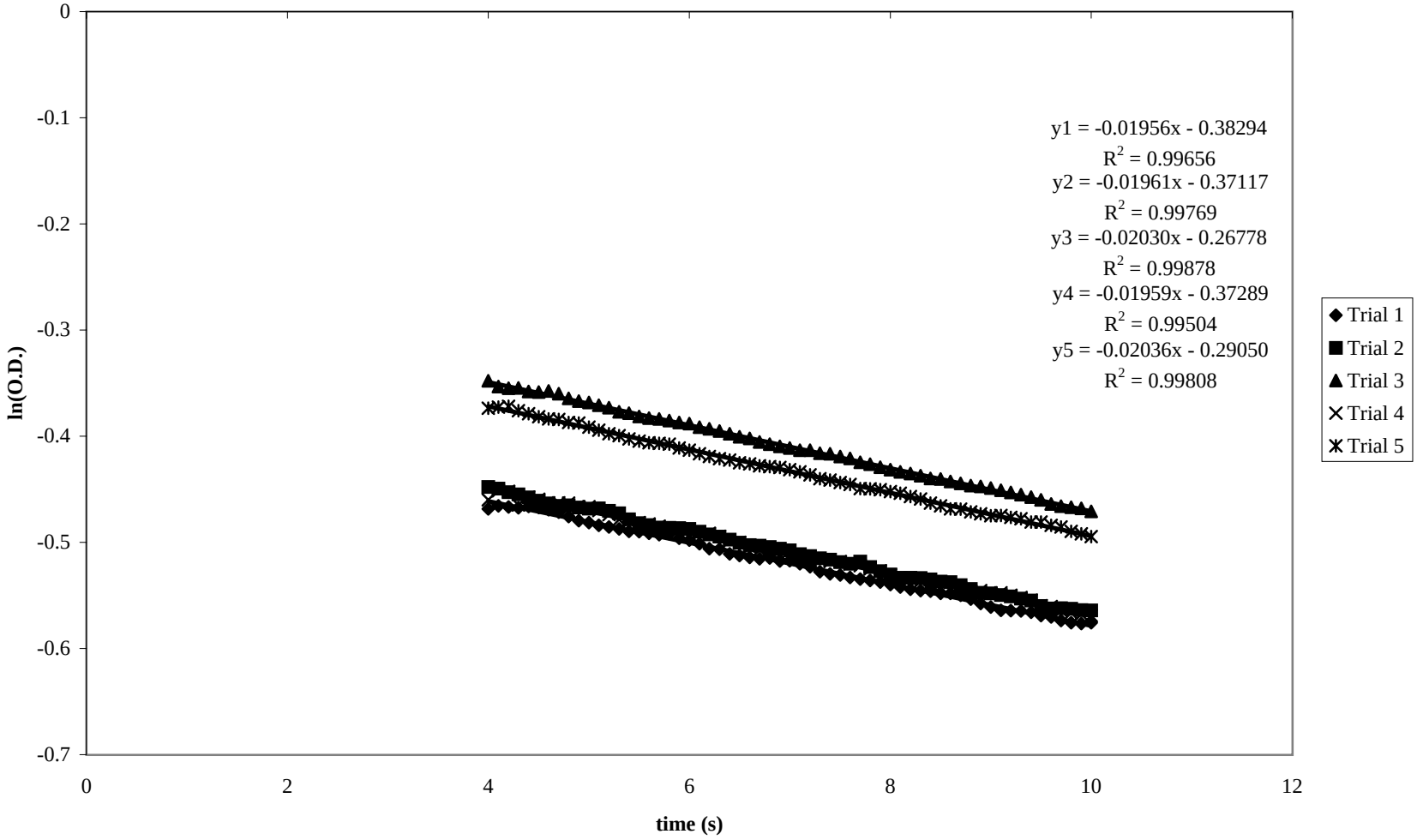

Blue A in Silica Particle Matrix at 29.1° C - First Order Kinetic Plot

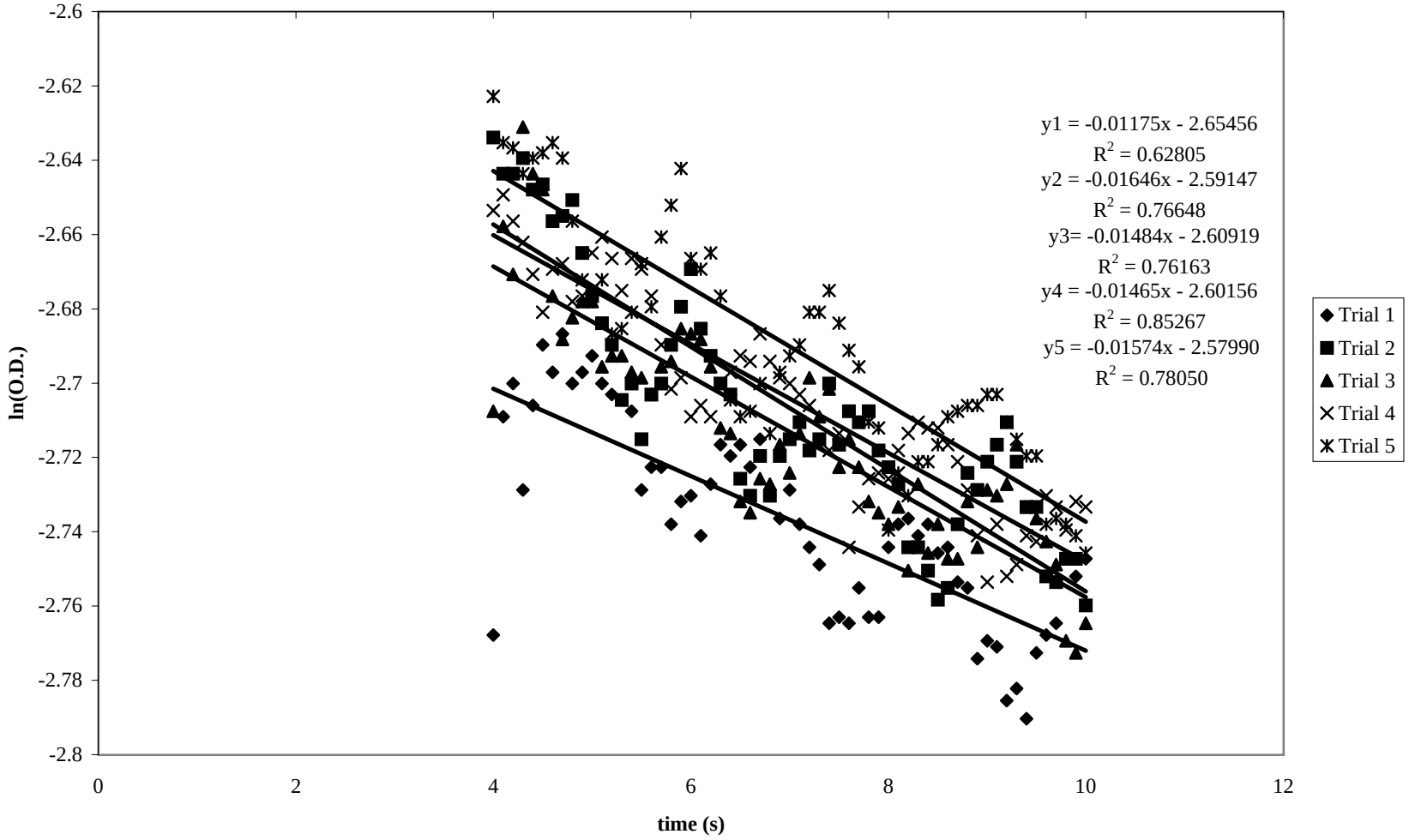

Blue A in Silica Particle Matrix at 24.7° C - First Order Kinetic Plot

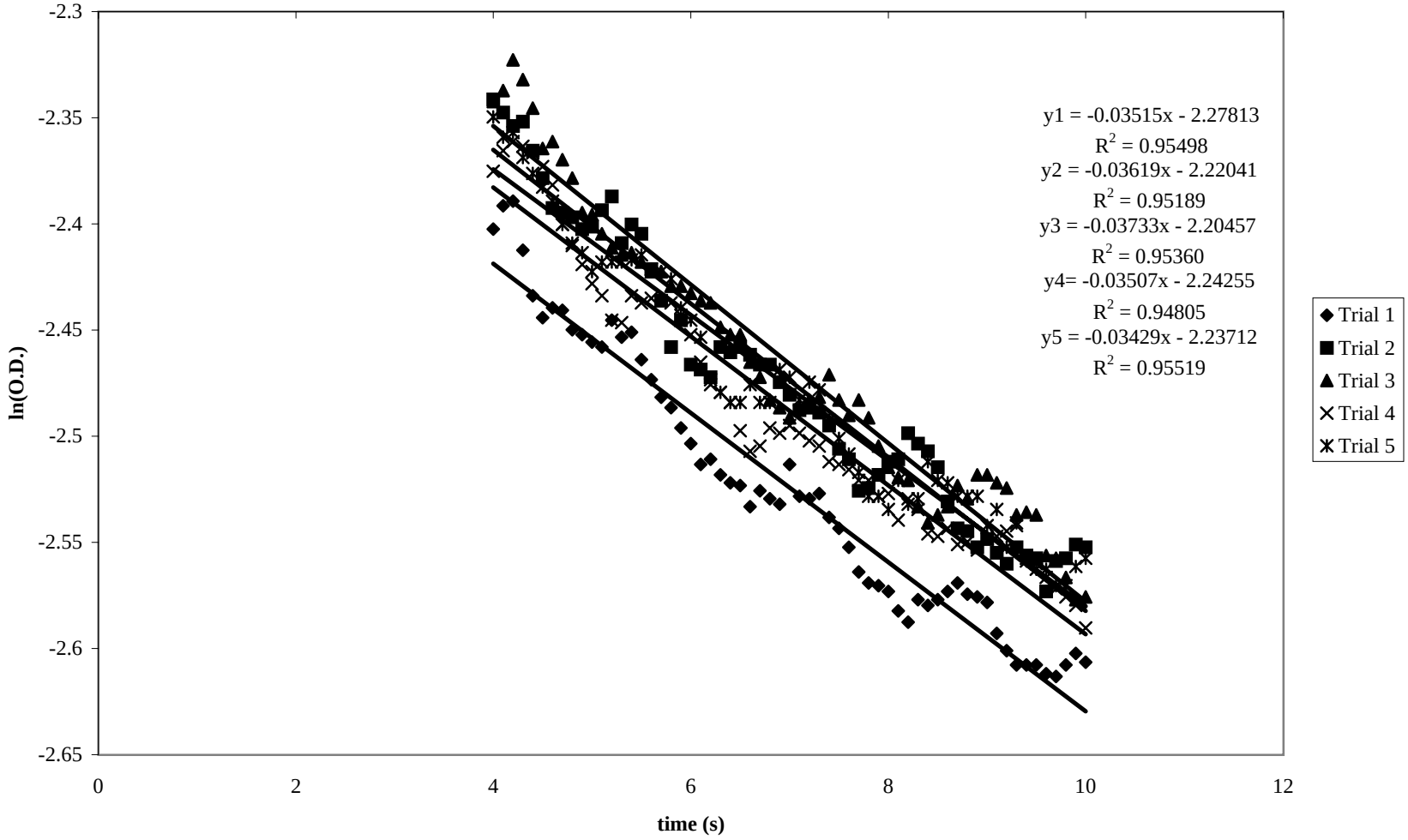

Blue A in Silica Particle Matrix at 20.3° C - First Order Kinetic Plot

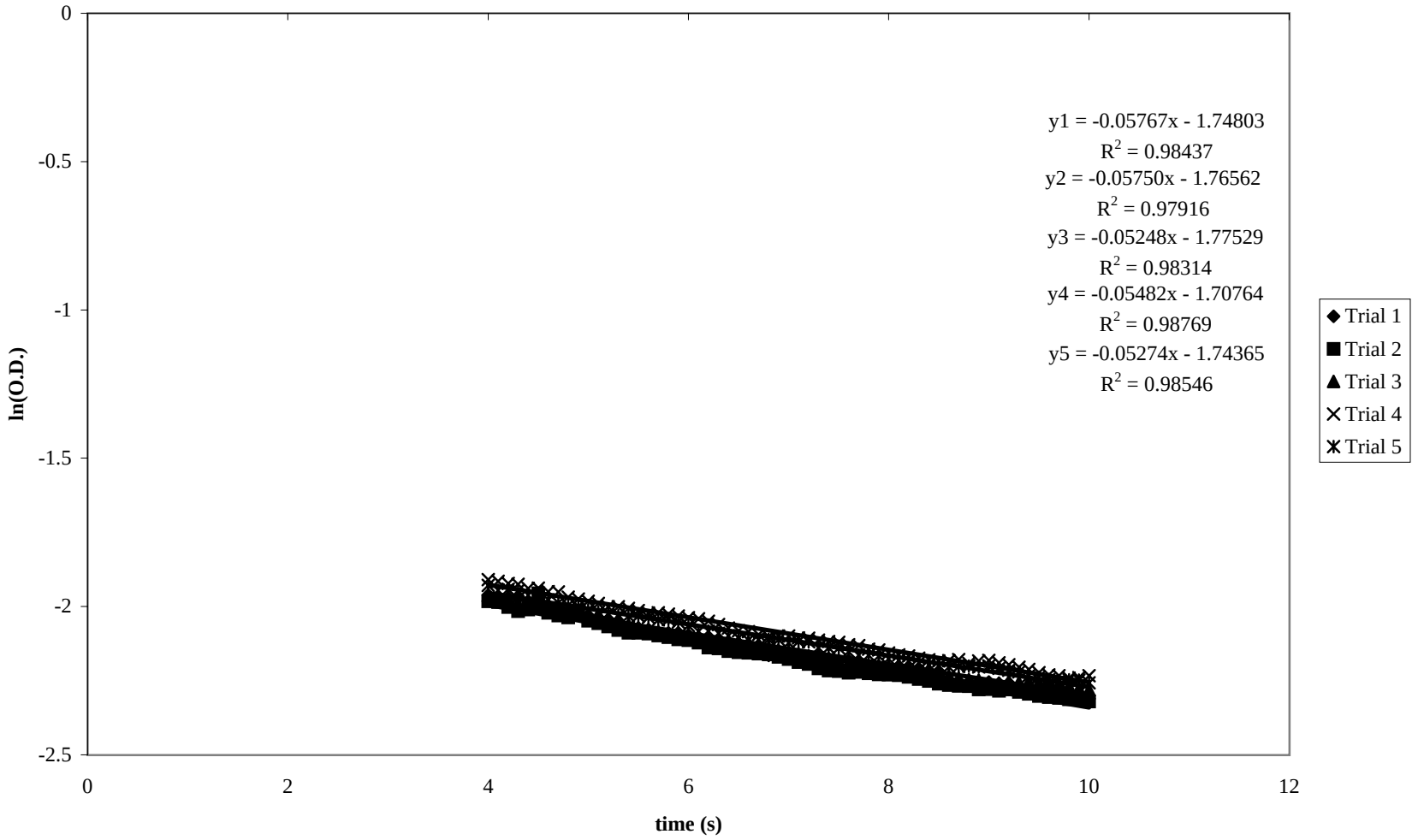

Blue A in Silica Particle Matrix at 15.2° C - First Order Kinetic Plot

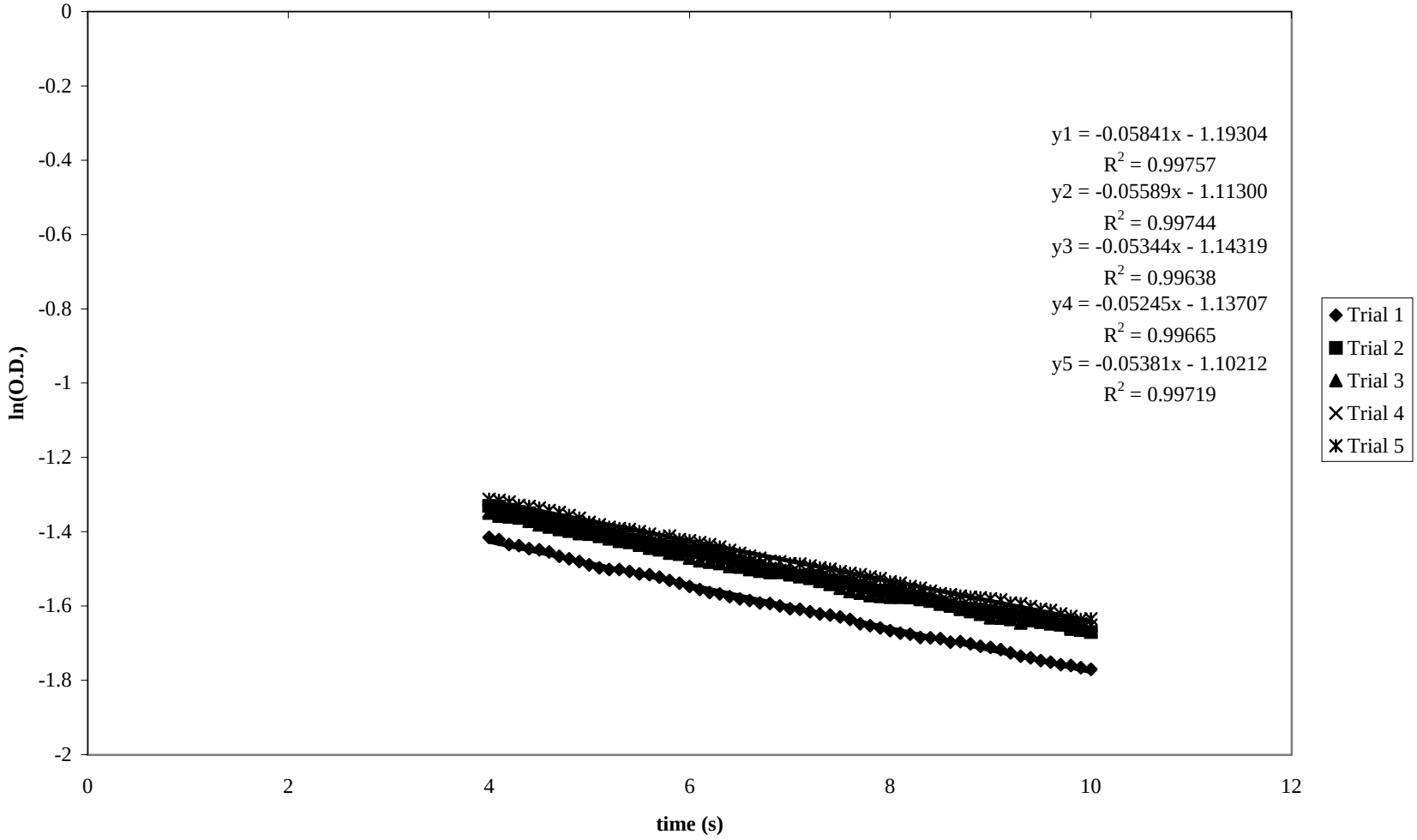

Blue A in Silica Particle System at 10.1° C - First Order Kinetic Plot

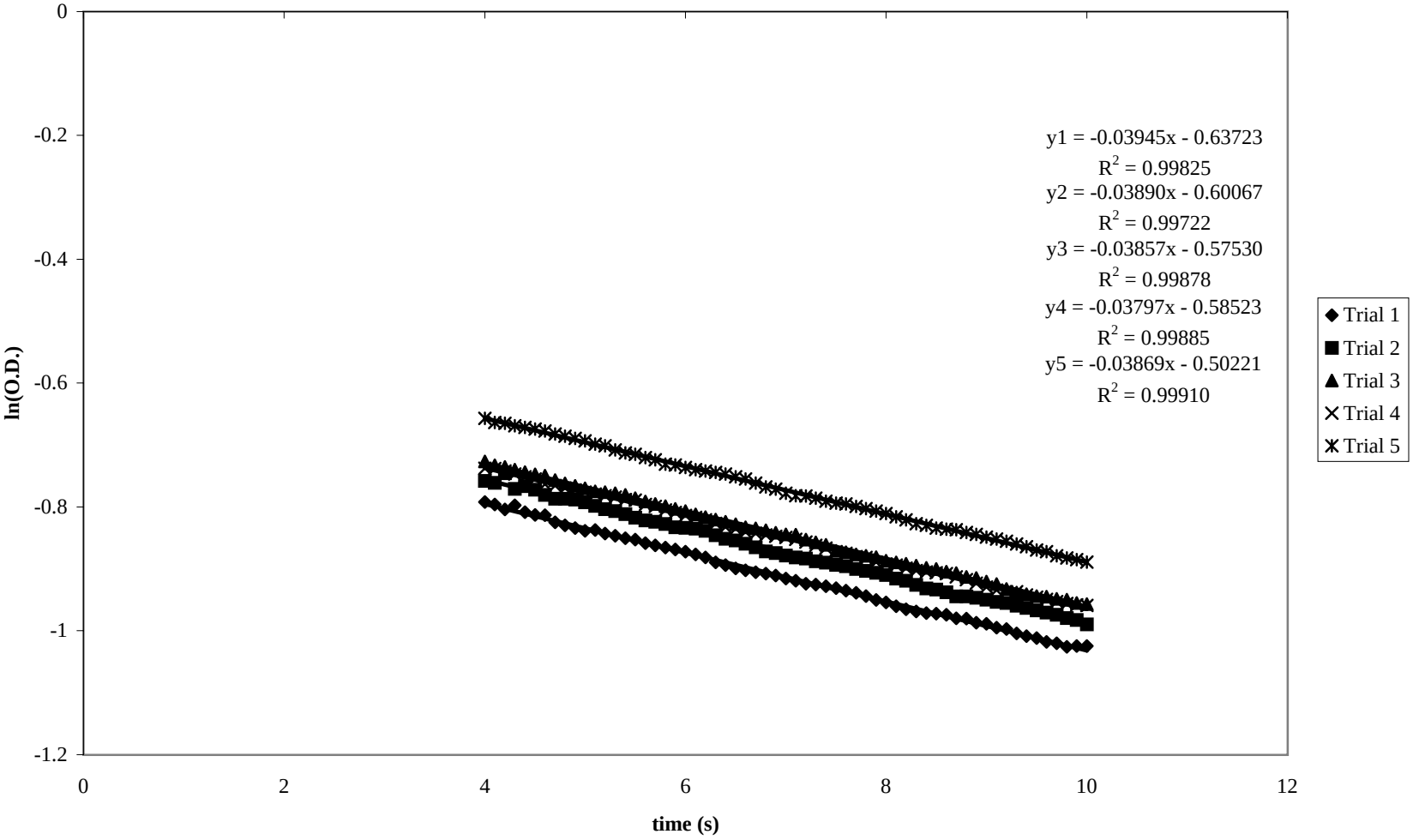

Blue A in Silica Particle Matrix at 4.7° C - First Order Kinetic Plot

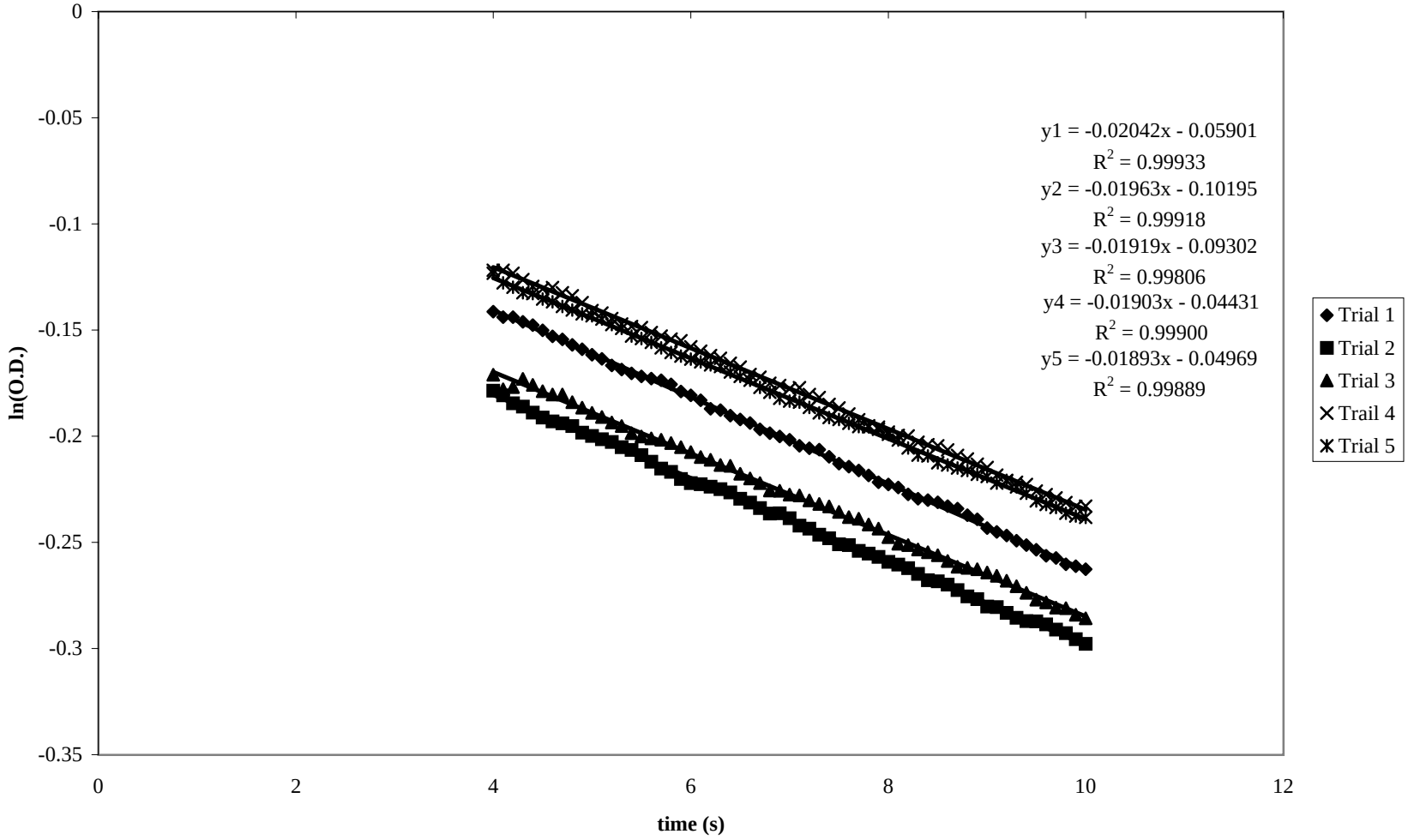

Blue A in Methanol at 19.9° C - First Order Kinetic Plot

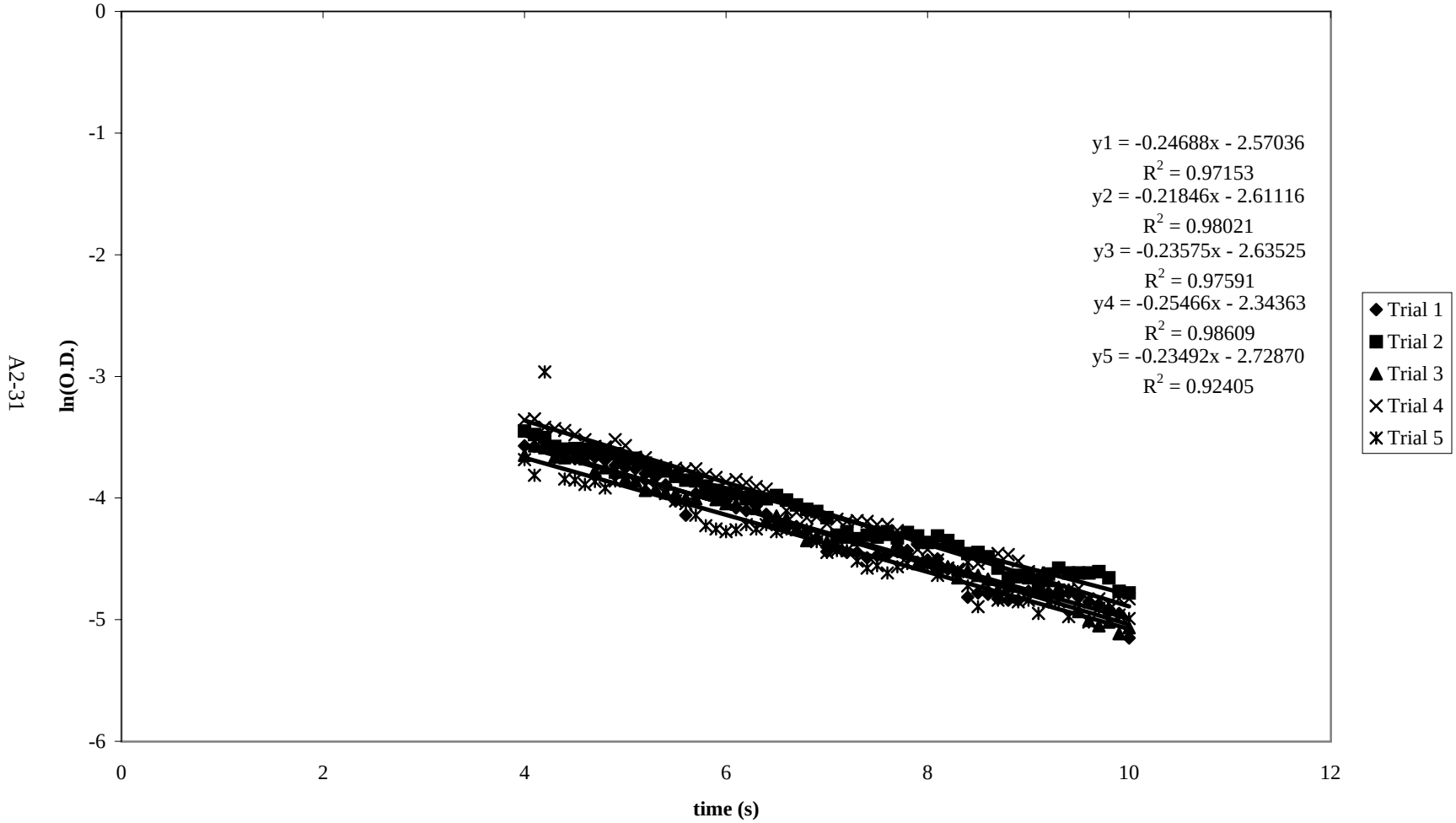

Blue A in Methanol at 15.9° C - First Order Kinetic Plot

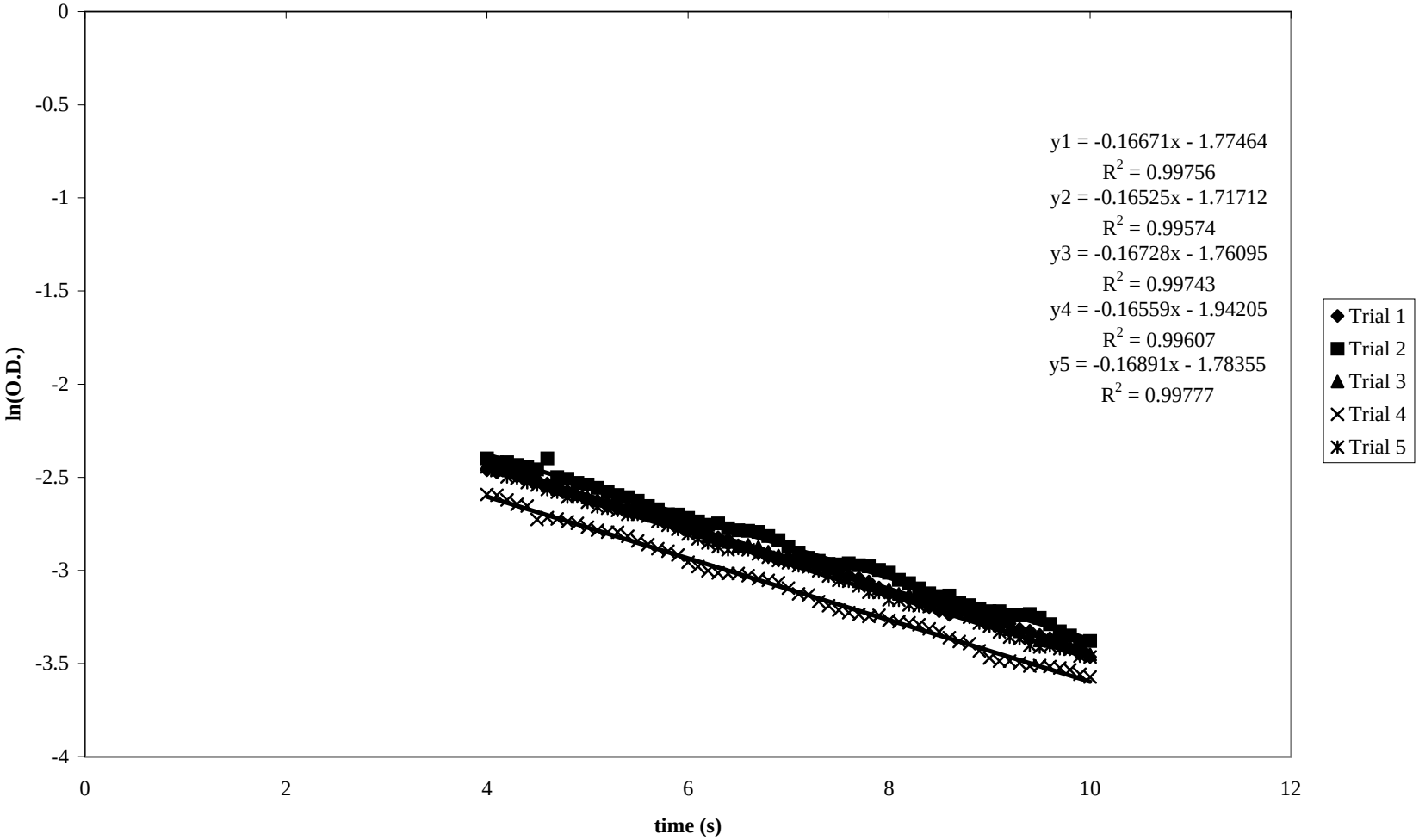

Blue A in Methanol at 11.6° C - First Order Kinetic Plot

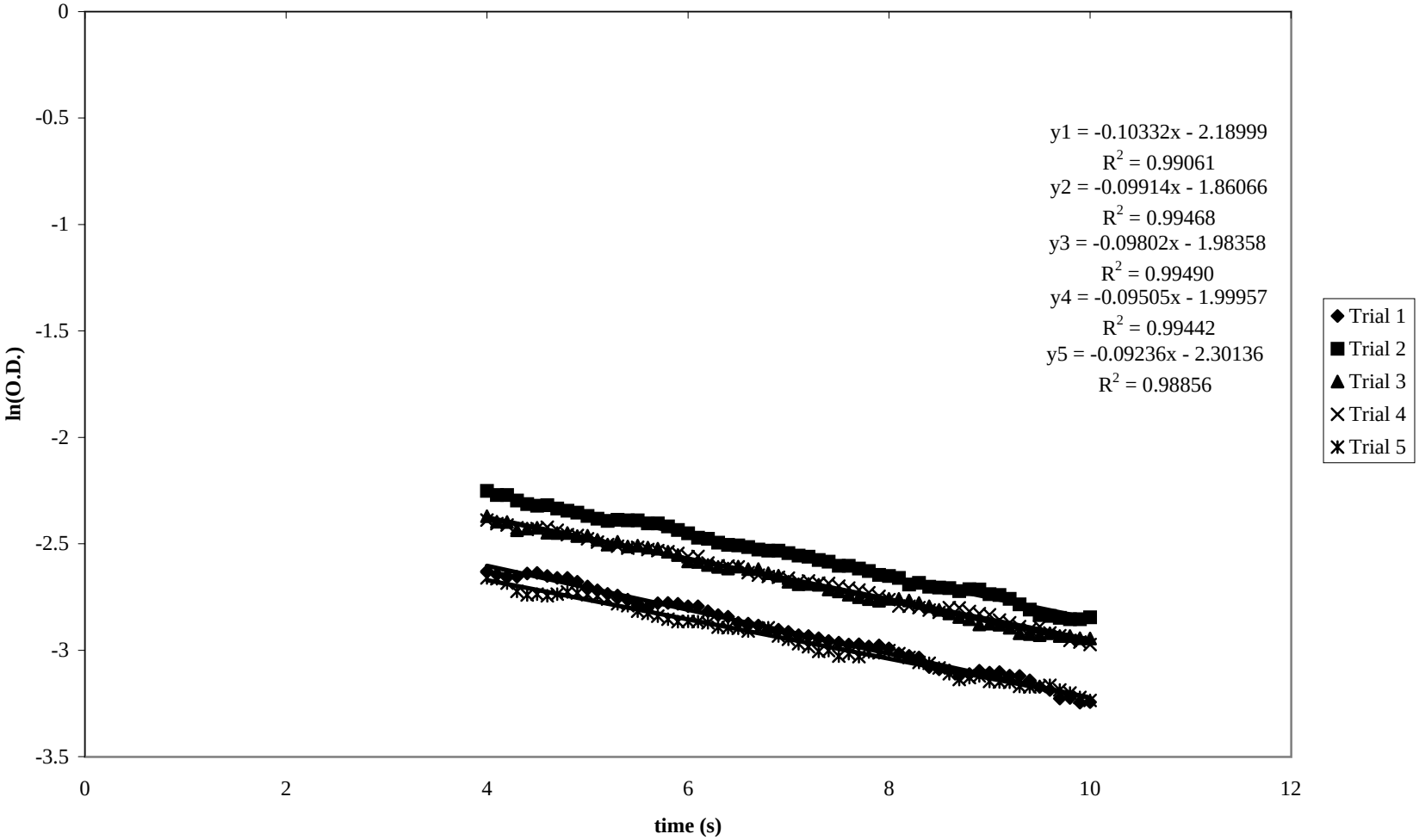

Blue A in Methanol at 8.3° C - First Order Kinetic Plot

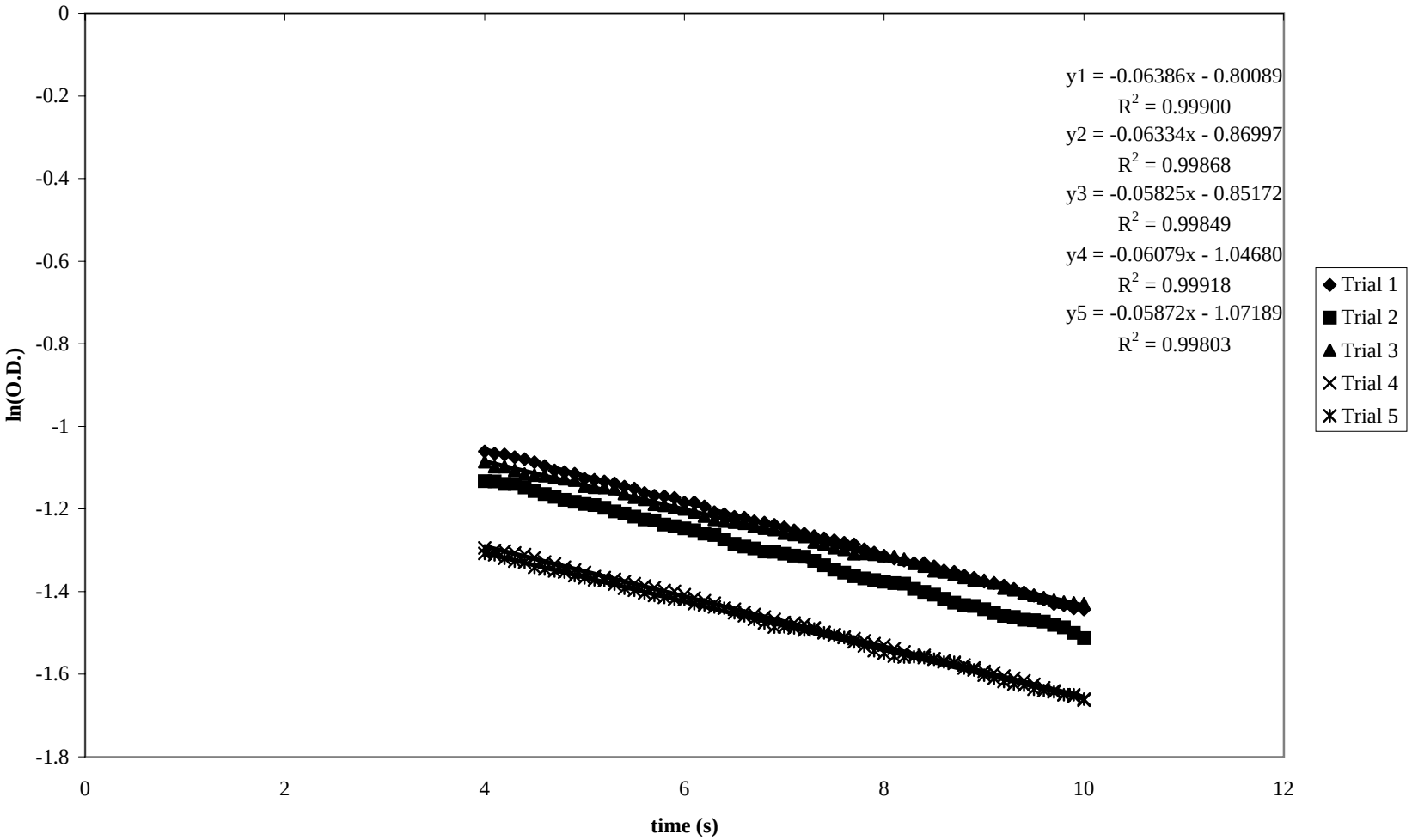

Blue A in Methanol at 3.9° C - First Order Kinetic Plot

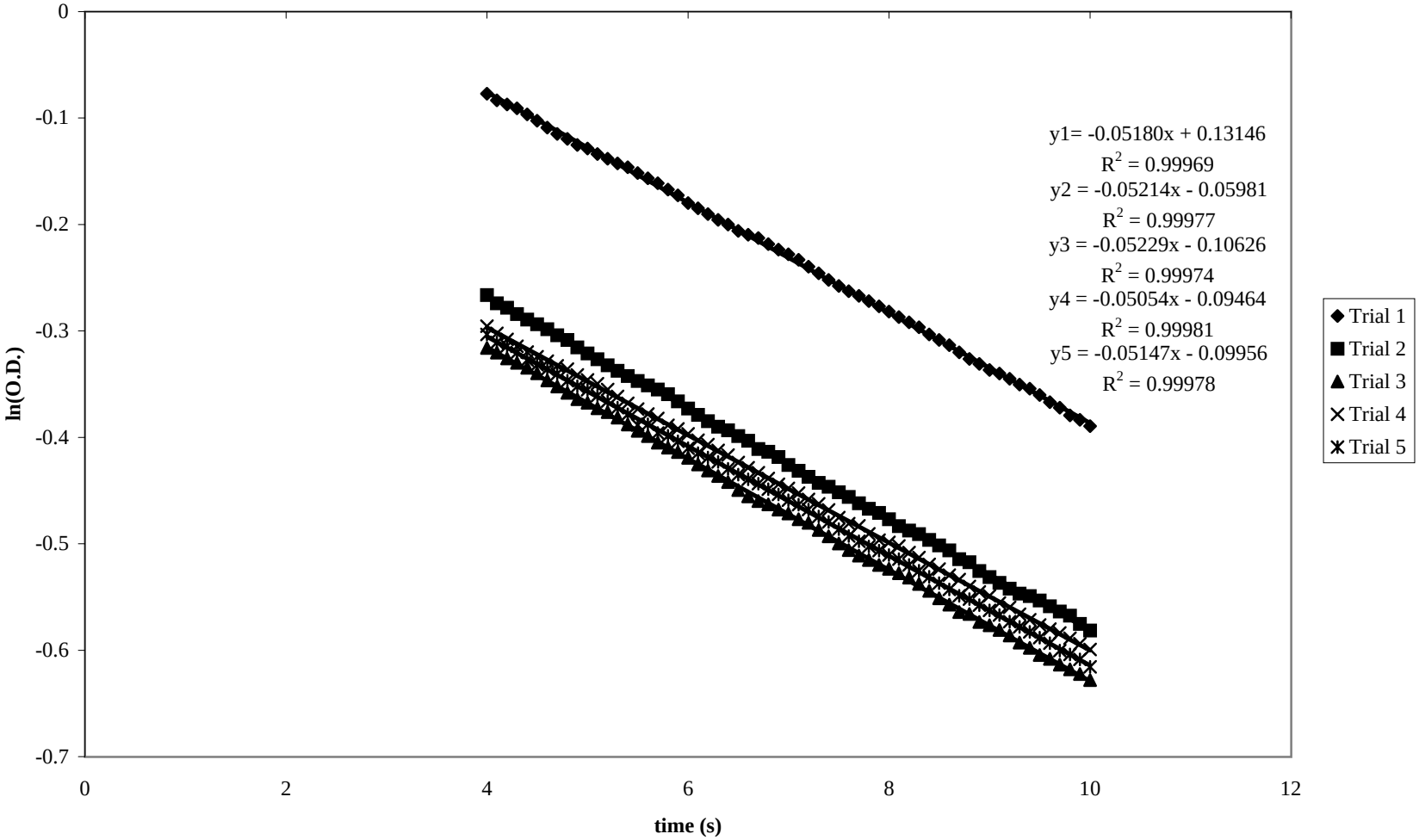

Blue A in 30% ETES / 70% GPTMS Matrix at 15.9° C - First Order Kinetic Plot

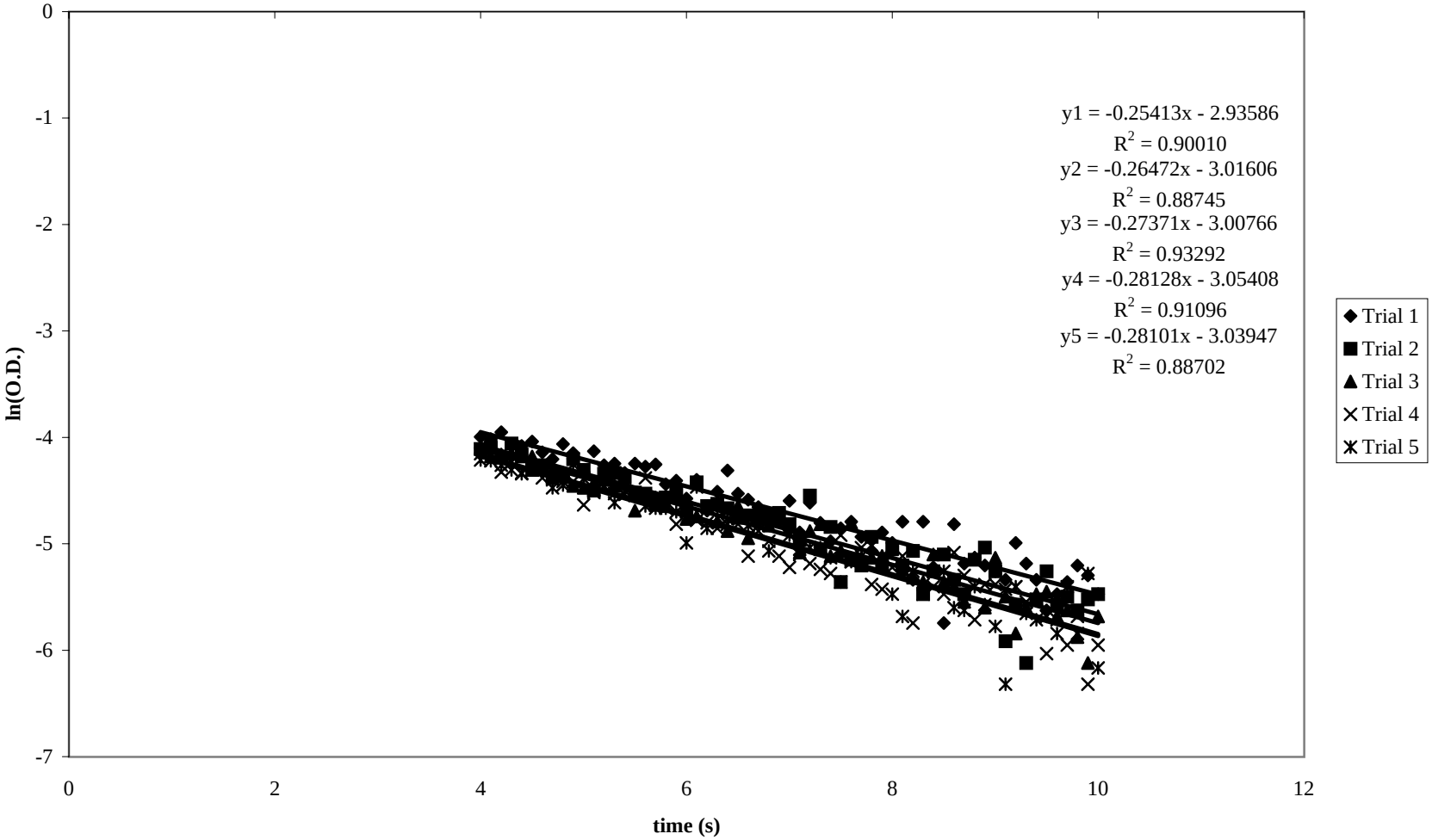

Blue A in 30% ETES / 70% GPTMS at 14.0° C - First Order Kinetic Plot

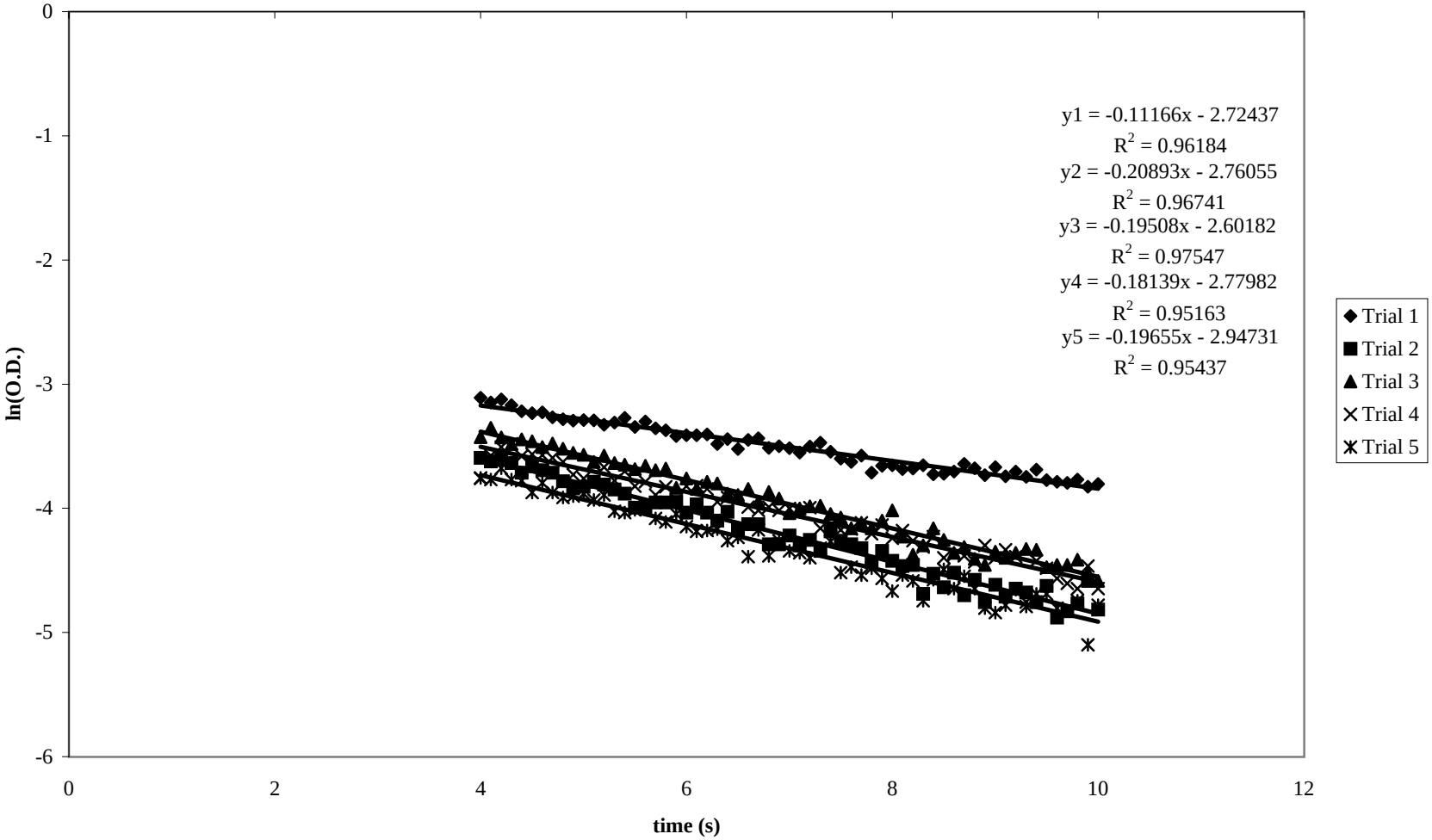

Blue A in 30% ETES / 70% GPTMS Matrix at 12.1° C - First Order Kinetic Plot

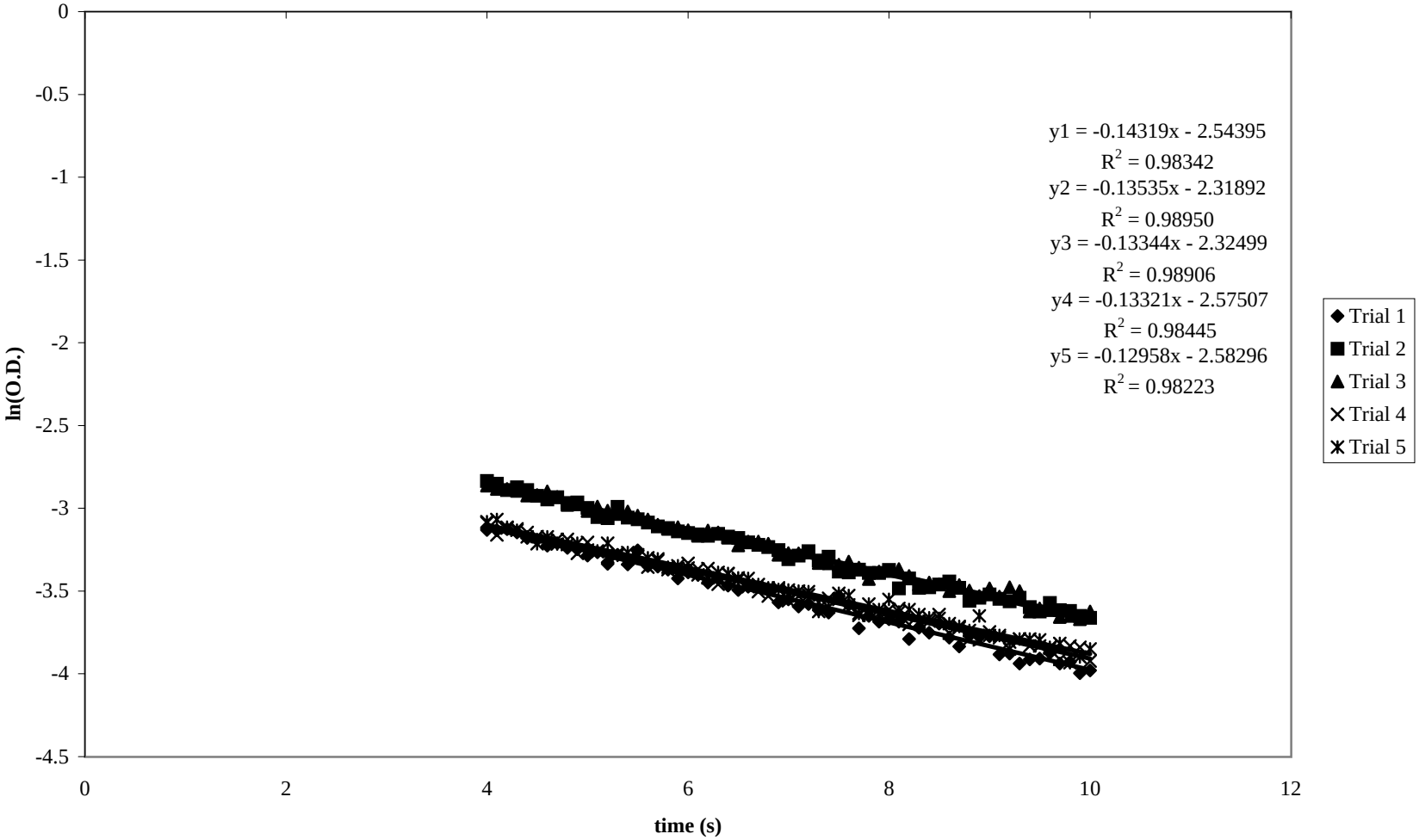

Blue A in 30% ETES / 70% GPTMS Matrix at 8.3° C - First Order Kinetic Plot

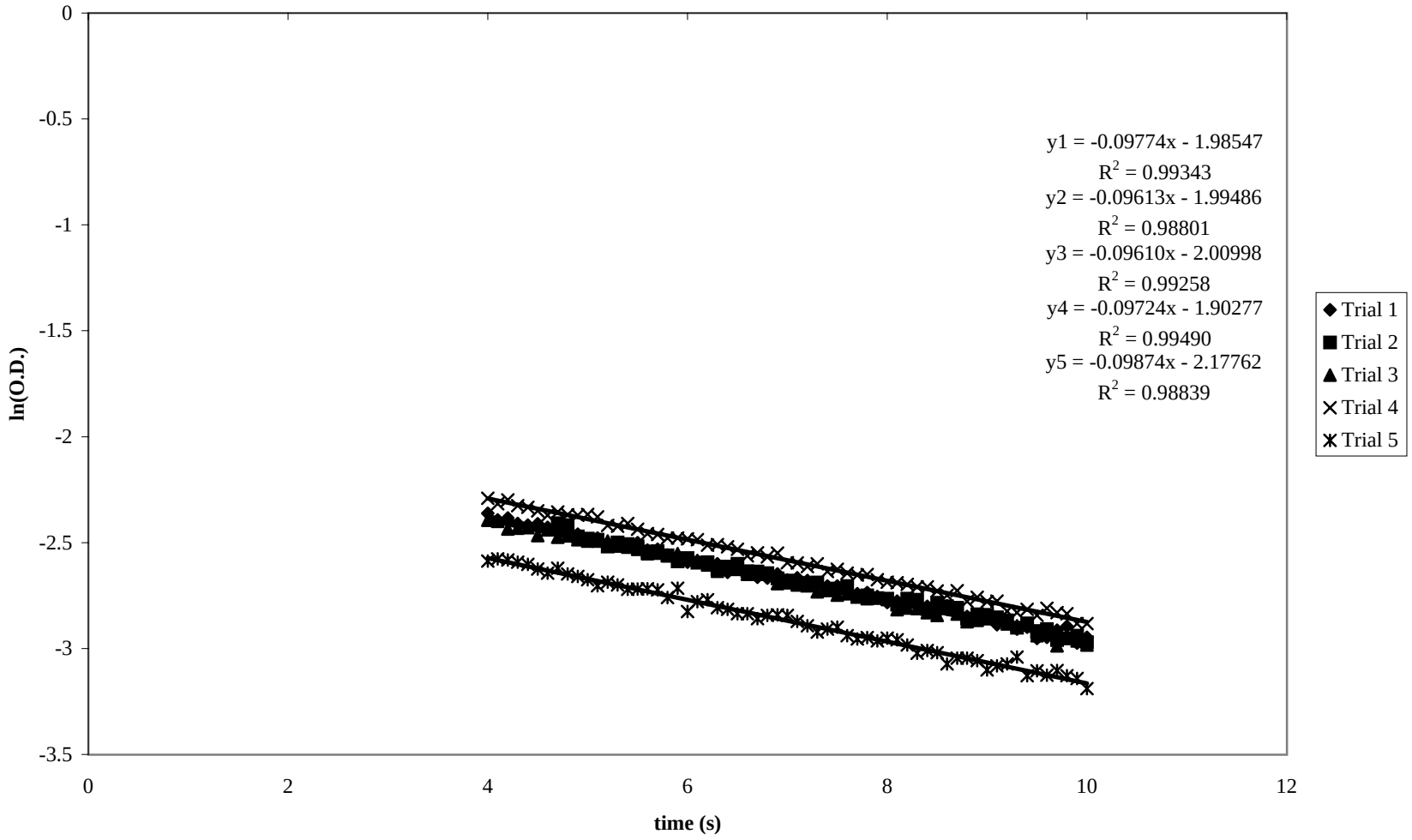

Blue A in 30% ETES / 70% GPTMS Matrix at 4.7° C - First Order Kinetic Plot